Effects of astrocyte-targeted production of either **IL-6 or IL-10** after facial nerve axotomy in the adult mouse

Nàdia Villacampa Pérez

PhD Dissertation

Universitat Autònoma de Barcelona

INc Institut de Neurociències

Bellaterra, 2016

Annex I. Scientific publications

i. Effects of Astrocyte-Targeted Production of Interleukin-6 in the Mouse on the Host Response to Nerve Injury

ii. Astrocyte-Targeted Production of IL-10 Induces Changes in Microglial Reactivity and Reduces Motor Neuron Death After Facial Nerve Axotomy

iii. Purine signaling and microglial wrapping

iv. Astrocyte-targeted IL-6 or IL-10 production alters expression of TREM2 in microglia after peripheral nerve injury

Effects of Astrocyte-Targeted Production of Interleukin-6 in the Mouse on the Host Response to Nerve Injury

Beatriz Almolda,[1] Nàdia Villacampa,[1] Peter Manders,[2] Juan Hidalgo,[1] Iain L. Campbell,[2] Berta González,[1] and Bernardo Castellano[1]

Interleukin-6 (IL-6) is a pleiotropic cytokine with a key role in the control of inflammatory/immune responses. In the central nervous system (CNS), an increase in IL-6 occurs in a wide range of pathological conditions such as excitotoxicity and traumatic brain injury. We evaluated the effects of astrocyte-targeted production of IL-6 in the CNS in the sterile-nerve injury model of facial nerve axotomy. To accomplish this, facial nerve transection was performed in transgenic mice (glial fibrillary acidic protein [GFAP]-IL6Tg) with IL-6 production under the GFAP promoter. Neuronal death, glial activation, lymphocyte recruitment, and integrin expression were evaluated by immunohistochemistry and flow cytometry from 3 to 28 days postinjury. Our findings revealed an increase in motor neuron cell death in GFAP-IL6Tg mice correlating with changes in the microglial activation pattern, characterized principally by less attachment to neurons and reduced expression of both CD11b and CD18. We also found a higher $CD4^+$ T-lymphocyte recruitment in GFAP-IL6Tg mice. In addition, changes in the expression pattern of different integrins and their receptors were observed in transgenic animals. Specifically, alterations in osteopontin expression in motor neurons and its receptors CD44 and CD49e in lymphocytes and microglia, respectively, which may account for the variations related to glial reactivity and lymphocyte infiltration. In conclusion, our results indicated that forced local production of IL-6 has a direct impact on the outcome of nerve injury in the CNS inducing an increase in neurodegeneration, changes in glial response, and lymphocyte recruitment as well as in the expression of different integrins and their receptors.

GLIA 2014;62:1142–1161

Key words: microglia, transgenic animal, lymphocytes, osteopontin, CD44, facial nerve axotomy

Introduction

Interleukin-6 (IL-6) is a pleiotropic and multifunctional cytokine involved in the regulation of inflammatory and immunological responses in the periphery (Kishimoto et al., 1995; Taga and Kishimoto, 1997; Kishimoto, 2006). In the central nervous system (CNS), IL-6 is low in normal conditions but increased significantly in neurons, astrocytes, and microglial cells, under acute and chronic injury and in certain diseases including excitotoxicity, traumatic brain injury, ischemia, multiple sclerosis, and neurodegenerative diseases like Alzheimer and Parkinson (Benveniste, 1998; Erta et al., 2012; Gadient and Otten, 1997; Gruol and Nelson, 1997; Nakamura et al., 2005; Spooren et al., 2011; Suzuki et al., 2009; Van Wagoner and Benveniste, 1999). However, the exact role played by this cytokine in these harmful circumstances is not yet well established, and both detrimental as well as beneficial functions have been proposed in different clinical as well as experimental neuropathologies.

The detrimental role attributed to IL-6 production is based on evidence that, together with TNF-α and IL-1β, this IL can be considered as a major modulator of the inflammatory response in the CNS (Benveniste, 1998; Erta et al., 2012; Gadient and Otten 1997). Although whether neuroinflammation is protective or detrimental remains the subject of

View this article online at wileyonlinelibrary.com. DOI: 10.1002/glia.22668

Published online April 2, 2014 in Wiley Online Library (wileyonlinelibrary.com). Received Dec 10, 2013, Accepted for publication Mar 14, 2014.

Address correspondence to Beatriz Almolda, Unitat d'Histologia, Torre M5, Universitat Autònoma de Barcelona, 08193 Bellaterra, Spain. E-mail: beatriz.almolda@uab.cat

From the [1]Department of Cell Biology, Physiology and Immunology, Institute of Neuroscience, Autonomous University of Barcelona, Bellaterra, 08193, Spain; [2]School of Molecular Bioscience, University of Sydney, Sydney, NSW 2006, Australia.

Beatriz Almolda and Nàdia Villacampa contributed equally to the work.

Additional Supporting Information may be found in the online version of this article.

intense discussion, classically it has been associated with glial activation and the consequent production of deleterious reactive oxygen species and inflammatory mediators, such as cytokines, chemokines, and prostaglandins, which may, among others, induce blood brain barrier disruption, lymphocyte recruitment, and promote neurodegeneration. Studies *in vitro* support the view that IL-6 is able to induce glial activation (Krady et al., 2008) and neuronal death (Conroy et al., 2004). Moreover, in agreement with work *in vivo* showing glial activation after IL-6 administration (Tilgner et al., 2001), chronic production of IL-6 achieved in transgenic animals has been linked to neurodegeneration (Campbell et al., 1993), increased astrocyte and microglial activation (Brunello et al., 2000; Campbell et al., 1993; Chiang et al., 1994) and impaired higher order brain function (Heyser et al., 1997). Other studies showed a decrease in axonal regrowth in hyper-IL-6-administered rats after spinal cord injury (Lacroix et al., 2002). Furthermore, an improvement of neuronal survival has been reported in IL-6 deficient mice after optic nerve crush (Fisher et al., 2001) and blocking of IL-6 signaling by anti-IL-6 receptor treatment induced a significant increase in functional recovery together with decreased gliosis in spinal cord-injured mice (Mukaino et al., 2010; Okada et al., 2004).

In contrast, anti-inflammatory and neuroprotective functions have been attributed to IL-6 due to the capacity of this cytokine to increase axonal regeneration in spinal cord-injured rats when administered intrathecally (Cao et al., 2006), the decrease in lesion volume reported in ischemic rats after intracerebroventricular IL-6 treatment (Loddick et al., 1998) and the reduction of motor neuronal loss described after sciatic nerve transection in intraperitoneally IL-6-treated rats (Ikeda et al., 1996). Furthermore, some studies conducted in IL-6 deficient mice support a role for IL-6 in neuroprotection, as these animals showed an increase in neuronal loss after both cryolesion (Swartz et al., 2001) and sciatic nerve axotomy (Murphy et al., 1999) and a reduction in functional recovery in axotomized animals (Zhong et al., 1999).

Altogether, these studies clearly indicate that the effects derived from IL-6 production are complex and may depend on several factors including the time-point and the specific microenvironment where this cytokine is produced or administered in the CNS. In this context, and in an attempt to better understand the function of IL-6 in CNS pathologies, this study focused on the analysis of the effects that local IL-6 production in the brain may exert following nerve injury in the facial nerve axotomy paradigm. For this purpose, we used the glial fibrillary acidic protein (GFAP)-IL6 transgenic (Tg) mouse model in which production of this cytokine was selectively targeted to astrocytes within the CNS of mice (Campbell, 1998; Campbell et al., 1993).

Materials and Methods

Animals and Facial Nerve Axotomy

A total of 47 transgenic animals with astrocyte-targeted production of IL-6 (GFAP-IL6Tg) and their corresponding wild-type (WT) littermates ($n = 36$) were used in this study. Characterization of the GFAP-IL6Tg mice was described previously (Campbell et al., 1993). In these animals, astrocyte-targeted production of IL-6 has been demonstrated under basal conditions in several CNS areas including the brainstem (Giralt et al., 2013). Animals were maintained with food and water *ad libitum* in a 12 h light/dark cycle during all the experiment.

After being anaesthetized by an intraperitoneal injection of ketamine 80 mg/kg and xylazine 20 mg/kg at dose of 0.01 mL/g, the right facial nerve was resected at the level of the stylomastoid foramen in both WT and GFAP-IL6Tg animals.

All experimental animal work was conducted according to Spanish regulations (Ley 32/2007, Real Decreto 1201/2005, Ley 9/2003, y Real Decreto 178/2004) in agreement with European Union directives (86/609/CEE, 91/628/CEE i 92/65/CEE) and was approved by the Ethical Committees of the Autonomous University of Barcelona and the University of Sydney.

Experimental Groups

Axotomized animals were distributed in different groups and euthanized at different days, ranging from 1 to 28 days postinjury (dpi), and tissue samples appropriately processed for flow cytometry, histochemistry, and immunohistochemistry (for details see later). A total of 10 WT and 8 GFAP-IL6Tg animals were used for flow cytometry studies; 23 WT and 36 GFAP-IL6Tg were processed for histochemistry and immunohistochemistry and 3 WT and 3 GFAP-IL6Tg animals were used for neuronal quantification.

Flow Cytometry Analysis

The percentage of infiltrated $CD3^+CD4^+$ cells was analyzed by flow cytometry at two specific time-points: 14 and 21 dpi following the protocol previously described (Almolda et al., 2009, 2011). For details of specific protocol, see Supporting Information 1.

Tissue Processing for Histochemistry and Immunohistochemistry Analysis

Under deep anaesthesia (0.015 mL/g) of ketamine (80 mg/kg)/xylazine (20 mg/kg) animals were perfused intracardially for 10 min with either 4% paraformaldehyde in 0.1 M cacodylate buffer (pH 7.4) + 5% sucrose for vibratome sectioning or 4% paraformaldehyde in 0.1M PBS (pH 7.4) for cryostat sections. Brainstems containing the facial nucleus (FN) were immediately dissected out, postfixed for 4 h at 4°C in the same fixative, and then a series of parallel sections were obtained using a VT 1000S Leica vibratome (40-μm thick) or a CM 3050s Leica cryostat (30-μm thick). Vibratome and cryostat series were stored at −20°C in Olmos antifreeze solution and used for immunohistochemistry, with the exception of one of the vibratome series that was processed for the histoenzymatic demonstration of nucleoside diphosphatase (NDPase) as described later.

A set of axotomized WT ($n = 3$) and GFAP-IL6Tg ($n = 3$) animals were perfused at 21 dpi as described earlier and coronal

sections (16 μm) of the entire brainstem were obtained using a CM 3050s Leica cryostat. The sections were mounted on gelatin-coated slides and used for toluidine blue staining.

Toluidine Blue Staining and Neuronal Survival Quantification

Toluidine blue staining was performed with a solution containing 0.1% toluidine blue diluted in Wallpole buffer (0.05 M, pH 4.5). After staining, sections were dehydrated in graded alcohols, N-butyl alcohol and after xylene treatment, coverslipped in DPX.

The nonlesioned (contralateral) and lesioned (ipsilateral) sides of every section through the FN were examined, photographed using a DXM1200F Nikon digital camera mounted on a Nikon Eclipse 80i brightfield microscope and photographs were analyzed using analySIS® software. In addition to the total number of neurons in each side, maximum and minimum diameters of cell profiles were recorded to calculate the mean diameter for each profile. To compensate for double counting of neurons in adjacent sections, the Abercrombie correction factor (Abercrombie et al., 1946) was applied: $N = n \times T/T + D$ where N corresponds to the actual number of neurons, n the total number of counted profiles, T the sections thickness, and D the mean diameter of each profile.

Histoenzymatic Demonstration of NDPase

Detection of NDPase, a microglial marker (Murabe and Sano, 1981), was performed by collecting one of the vibratome series in 0.1 M cacodylate buffer (pH 7.4) (C0250; Sigma, St Louis) with 5% sucrose as described earlier (Almolda et al., 2013; Castellano et al., 1991). See Supporting Information 1 for details of specific protocol.

Single Stain Immunohistochemistry

Parallel free-floating cryostat sections were processed for the visualization of Iba1, CD11b (αM integrin), CD18 (β2 integrin), GFAP, CD3, osteopontin (OPN) and its receptors CD44 and CD49e (α5 integrin) following the protocol previously described (Almolda et al., 2010, 2011). For detail see Supporting Information 1.

Double and Triple Stain Immunohistochemistry

As previously described parallel-free floating series were processed for double and triple immunostaining, following the protocol previously described (Almolda et al., 2010, 2011; Villacampa et al., 2013). For detail see Supporting Information 1.

Densitometric Analysis

Densitometric analysis was performed on sections immunolabeled with Iba1, CD11b, CD18, GFAP, OPN, CD44 and CD49e. For each target protein, both the ipsilateral and the contralateral side of at least three WT and three GFAP-IL6Tg animals per survival time were analyzed. A minimum of three different sections from the brainstem containing the central part of the FN were captured at 10× magnification with a DXM 1200F Nikon digital camera mounted on a Nikon Eclipse 80i brightfield microscope using the software ACT-1 2.20 (Nikon corporation). By means of NIH Image J® software (Wayne Rasband, National Institutes of Health), both the percentage of area occupied by the immunolabeling as well as the intensity of the immunoreaction (mean gray value) were recorded for each photograph.

For each animal, the gray grade quotient (GGQ) was obtained by dividing the mean gray value on the ipsilateral side by the mean gray value on the contralateral side. The intensity grade (IG) was calculated by multiplying the percentage of the immunolabeled area by the GGQ. In the case of GFAP, CD44 and CD49e, in which expression of these molecules was absent or very low in the contralateral FN, the AI index (% area immunolabeled multiplied by the mean gray value) was used.

Quantification of microglial clusters was performed, at 14 and 21 dpi, on sections stained for Iba1. At least three WT and three GFAP-IL6Tg animals per survival time were analyzed. A minimum of three different sections from the brainstem containing the central part of the FN of each animal were captured at 10× magnification with a DXM 1200F Nikon digital camera mounted on a Nikon Eclipse 80i brightfield microscope using the software ACT-1 2.20 (Nikon corporation). The number of microglial clusters per section was obtained using "cell counter" plug-in from NIH Image J® software (Wayne Rasband, National Institutes of Health).

Quantification of microglial cell density was performed, at 3 and 7 dpi, on sections stained with Iba1 and counterstained with toluidine blue. At least, five WT and five GFAP-IL6Tg animals per survival time were analyzed. A minimum of three different sections from the brainstem containing the central part of the FN of each animal were photographed at 40× magnification with a DXM 1200F Nikon digital camera mounted on a Nikon Eclipse 80i brightfield microscope using the software ACT-1 2.20 (Nikon corporation). All the nucleated Iba1$^+$ cells were counted in each photograph (0.0037 mm^2 frame), averaged and converted to cells/mm^2.

Statistical Analysis

All results were expressed as mean ± standard error. Statistics were performed using the Graph Pad Prism® software. Either standard two-tailed or unpaired Student's *T*-test were used to determine statistically significant differences between WT and GFAP-IL6Tg animals, and one-way ANOVA with Bonferroni's analysis as a *post hoc* test to determine differences among time-points postinjury.

Results

Neuronal Survival

After facial nerve axotomy, there is a proportion of FN motor neurons that degenerate (Dauer et al., 2011; Ha et al., 2008). To determine if IL-6 alters the ratio of neuronal death, we quantified the surviving neurons at 3 weeks postaxotomy. Our analysis revealed that the total number of motor neurons in the contralateral side of the FN of both WT (Fig. 1A) and GFAP-IL6Tg (Fig. 1C) animals was similar being around 2,000 neurons. Facial nerve axotomy resulted in a loss of 30.51% of motor neurons in the ipsilateral FN of WT animals (1,291 ± 10.54) while in the GFAP-IL6Tg animals, a greater loss of motor neurons was observed (37.3%, 1,138 ± 16.34; Fig. 1D,E).

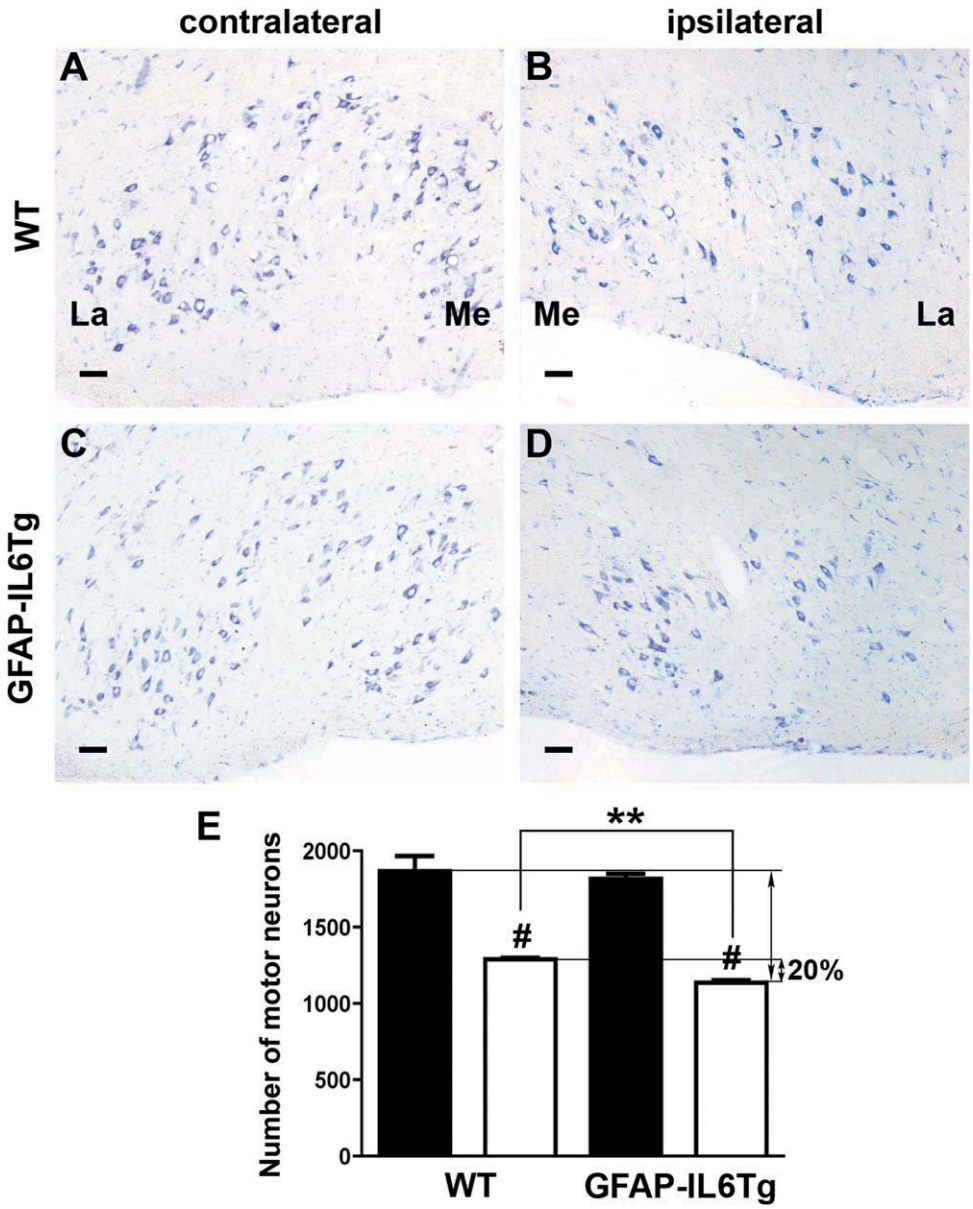

FIGURE 1: Neuronal death. Toluidine blue staining in the nonlesioned (contralateral) and lesioned (ipsilateral) FN of both WT (A and B) and GFAP-IL6Tg animals (C and D) at 21 dpi. La indicates the lateral area, whereas Me indicates the medial area of the brainstem. Note the decrease in the number of motor neurons in the ipsilateral side of both groups of animals in comparison to their corresponding contralateral side. Scale bar = 50 μm. (E) The histogram shows the quantification of the total number of motor neurons in the contralateral (black columns) and ipsilateral sides (white columns) of both experimental groups of animals (#$P \leq 0.05$ with respect to the corresponding contralateral side; **$P \leq 0.0015$). Note that motor neuron survival in GFAP-IL6Tg animals was reduced by a further 20% when compared with WT mice. [Color figure can be viewed in the online issue, which is available at wileyonlinelibrary.com.]

Glial Reactivity

Facial nerve axotomy provokes strong microglial activation in the FN that was characterized by the microglial attachment to motor neurons in the so-called mechanism of synaptic stripping (Blinzinger and Kreutzberg, 1968; Kreutzberg, 1996). To characterize the effects that IL-6 induces in the activation pattern of this glial population, microglial cells were visualized using the histochemical demonstration of NDPase, a purine-related enzyme located in the microglial plasma membrane, commonly used for the study of "resting" and reactive microglial cells (Castellano et al., 1991; Murabe and Sano, 1981). This enzyme is also located in the blood vessels, allowing the study of the relationship between microglial cells and the vasculature. We also evaluated the expression of Iba1 and the CD11b and CD18 proteins, two subunits of the heterodimeric integrin Mac-1, constitutively expressed by microglial cells and whose upregulation has been commonly associated with the activation of these cells. In

addition to the qualitative evaluation, a quantitative analysis of Iba1, CD11b and CD18 staining was done by determining the IG of each immunolabeling. As specified below, notable differences in the microglial response were found in this study with the use of different microglial markers.

Analysis of NDPase histochemistry (Fig. 2) and Iba1 immunohistochemistry (Fig. 3) revealed that in the nonlesioned FN of WT and GFAP-IL6Tg animals, microglial cells exhibited a characteristic ramified morphology and were homogenously distributed throughout the FN without any overlap between them and without showing any specific relationship with the neuronal cell bodies or blood vessels (Figs. 2A,B,O,P and 3A,B,P,Q). No significant differences in microglial NDPase, Iba1, CD11b, and CD18 immunostaining were found in the nonlesioned FN for GFAP-IL6Tg when compared with WT animals (Figs. 2A,B, 3A,B, 4A,B and 5A,B). Nevertheless, a statistically significant increase in the density of $Iba1^+$ cells was observed in the nonlesioned FN of GFAP-IL6Tg animals (Fig. 3O). Throughout the course of the study, at the different survival times analyzed, no changes in either microglial cell morphology or the spatial distribution or NDPase, Iba1, CD11b, and CD18 expression were detected in the nonlesioned FN side of neither WT nor GFAP-IL6Tg animals (not shown).

In the ipsilateral FN of both groups of animals, progressive changes in microglial cell number and morphology, their pattern of NDPase, Iba1, CD11b, and CD18 labeling and their relationship with neuronal cell bodies were observed at the different time-points studied. Marked differences between WT and GFAP-IL6Tg mice were found. The first signs of microglial reactivity were evident in both WT and GFAP-IL6Tg animals at 1 dpi (Fig. 2C,D), when microglial cells showed an enlargement of the cell body and a thickening of the main branches, and began to migrate close to neuronal cells bodies (Fig. 2Q,R).

At 3 dpi, in WT animals, reactive microglial cells displayed branched morphology but with coarser processes and high levels of NDPase (Fig. 2E,S), Iba1 (Fig. 3C,R), CD11b (Fig. 4C,P), and CD18 (Fig. 5C,P) staining and were wrapping most neuronal cell bodies along the ipsilateral FN. Also the density of $Iba1^+$ cells increased at this time-point in comparison with the nonlesioned FN (Fig. 3O). Although in GFAP-IL6Tg animals, similar changes in microglial morphology and both NDPase (Fig. 2F,T) and Iba1 (Fig. 3D,S) expression was observed, the $Iba1^+$ cell density was higher (Fig. 3O) and the motor neuron perikaryon surface wrapped by microglial cell processes was lower than those observed in WT mice. Higher CD11b (Fig. 4D,M,Q) and CD18 (Fig. 5D,M,Q) IG were detected at this time-point in microglial cells of transgenic animals when compared with their WT littermates.

At 7 dpi, a marked increase in both the amount of $Iba1^+$ cells and motor neuron perikaryon surface covered by microglial cell projections was observed in both WT and GFAP-IL6Tg mice (Figs. 2U,V and 3O). In both groups, reactive microglia with high NDPase (Fig. 2G,H,U,V) and high Iba1 IG (Fig. 3E,F,M) showed numerous projections displaying, as well, high levels of both CD11b and CD18 (Figs. 4M and 5M, respectively) that, in addition to wrapping the major part of neuronal cell bodies, were widely distributed along the FN neuropil. No differences in the density of $Iba1^+$ cells were detected at this time-point when WT and GFAP-IL6Tg animals were compared (Fig. 3O).

Microglial reactivity remained high at 14 dpi in both groups of animals and, in addition to elevated microglial wrapping of neurons, characteristic clusters of highly $NDPase^+$ (Fig. 2W,X) and $Iba1^+$ (Fig. 3T,U) microglial cells were also observed scattered along the ipsilateral FN. Although, no significant differences in NDPase staining and Iba1 (Fig. 3M) or CD18 (Fig. 5M) IG were detected between WT and GFAP-IL6Tg animals, the neuronal wrapping was more frequent in the ipsilateral FN of WT than in GFAP-IL6Tg mice (Figs. 2W,X, 3T,U and 5R,S). In addition, the number of microglial clusters found in the FN of GFAP-IL6Tg mice was significantly lower than in WT animals (Fig. 3N). Noticeably at this time-point, significant changes in CD11b were detected between WT and GFAP-IL6Tg animals: whereas in WT animals, the IG for CD11b showed the highest level, in GFAP-IL6Tg animals, labeling of this integrin abruptly decreased at this time-point dropping lower than those observed at 3 dpi (Fig. 4R,S,M).

At 21 dpi, a reduction in the microglial expression of NDPase (Fig. 2K), Iba1 (Fig. 3I), CD11b (Fig. 4I), and CD18 (Fig. 5I) was observed in the ipsilateral FN of WT mice, although microglial cells still exhibited high reactive morphologies in specific FN subnucleus, such as the lateral and the ventral intermediate subnucleus. Moreover, both the number of neuronal cell bodies wrapped by microglial cells and the clusters of microglia began to decrease at this time-point in these animals. In contrast, NDPase (Fig. 2L) and Iba1 (Fig. 3J,M) staining remained significantly elevated and widely distributed along all the subnucleus of the ipsilateral FN in GFAP-IL6Tg mice, and the amount of FN motor neurons wrapped by microglial processes was comparatively higher than in WT. Also the number of microglial clusters found in the axotomized FN of transgenic animals was lower than in WT mice at this time-point (Fig. 3N). Similar to 14 dpi, the IG of both CD11b (Fig. 4J,M), and CD18 (Fig. 5J,M) in activated microglia was significantly lower in GFAP-IL6Tg animals than in their WT littermates.

At 28 dpi, there was a slight decrease in both NDPase (Fig. 2M,N) and Iba1 (Fig. 3K,L,M) staining in the FN of both WT and GFAP-IL6Tg animals although some areas of the FN neuropil still remained totally covered by highly reactive

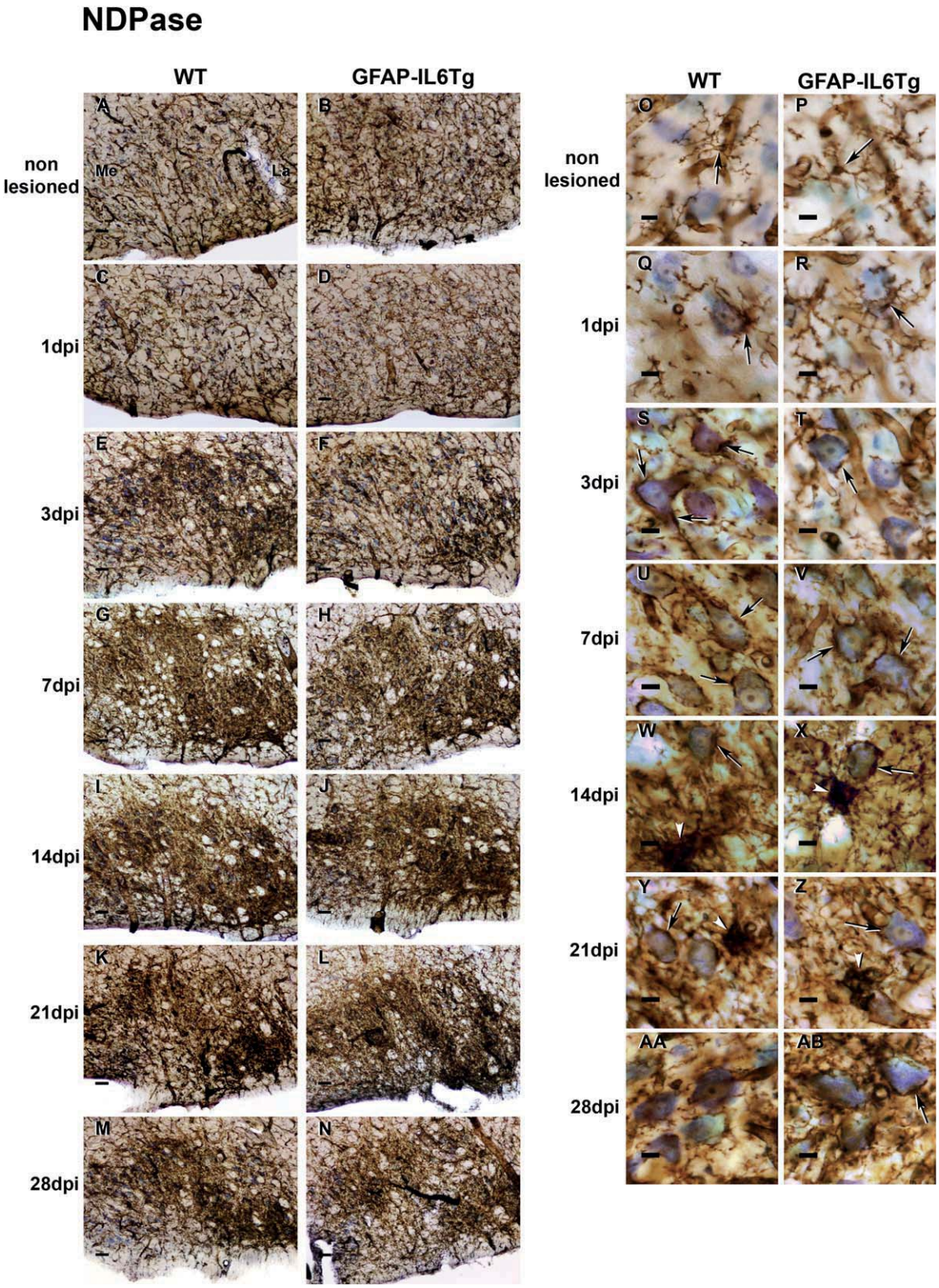

FIGURE 2: NDPase histochemistry. Representative images of the NDPase histochemistry in the nonlesioned FN (A and B) and in the ipsilateral side of both WT (C, E, G, I, K and M) and GFAP-IL6Tg animals (D, F, H, J, L and N) at the different survival times after facial nerve axotomy. Magnifications on the right hand (O to AB) show the progressive changes in the morphology of microglial cells and their association with neuronal cell bodies along the lesion progression. Arrows in O to AB point to individual microglial cells and arrowheads in W to Z to the so-called "microglial clusters." In A, La indicates the lateral area, whereas Me indicates the medial area of the brainstem. Scale bar (A–N) = 50 μm; (O–AB) = 10 μm. [Color figure can be viewed in the online issue, which is available at wileyonlinelibrary.com.]

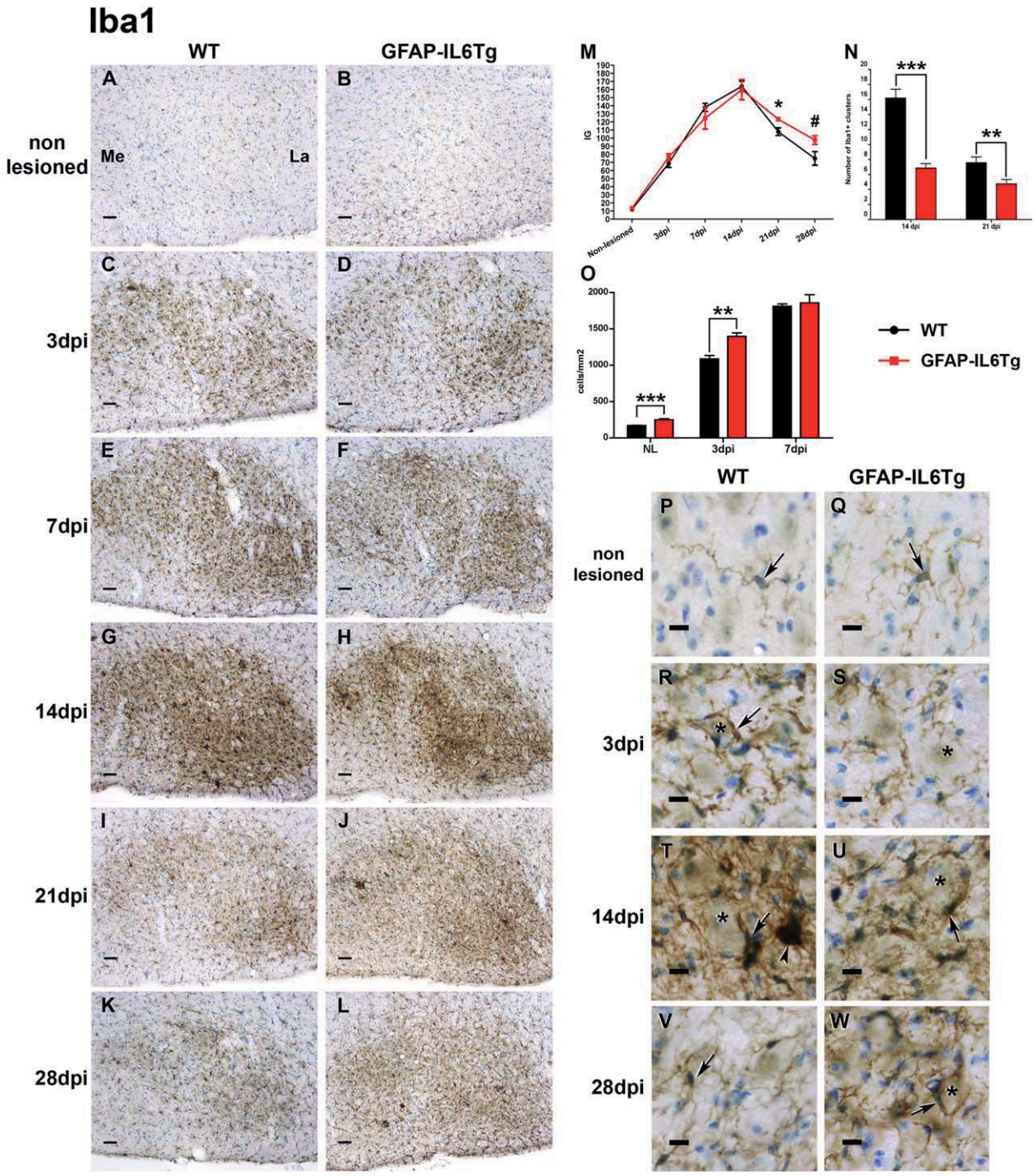

FIGURE 3: Iba1 expression. Representative images of Iba1 immunohistochemistry in the nonlesioned FN (**A** and **B**) and in the ipsilateral side of both WT (**C, E, G, I** and **K**) and GFAP-IL6Tg animals (**D, F, H, J** and **L**) at the different survival times after axotomy. In A, La indicates the lateral area, whereas Me indicates the medial area of the brainstem. (**M**) Histogram showing the quantification of the IG of Iba1 staining in WT and GFAP-IL6Tg animals along the evolution of facial nerve axotomy. Note that at 21 and 28 dpi the IG is significantly higher in GFAP-IL6Tg animals (*$P \leq 0.05$; #$P \leq 0.06$). (**N**) Histogram showing the quantification of Iba1$^+$ microglial clusters in both WT and GFAP-IL6Tg mice at 14 and 21 dpi. Note that at the two times analyzed the number of clusters is significantly lower in GFAP-IL6Tg animals (***$P \leq 0.0001$; **$P \leq 0.008$). (**O**) Histogram showing the quantification of the Iba1$^+$ cell density (cells/mm^2) in both WT and GFAP-IL6Tg mice in the nonlesioned (NL) FN and at 3 and 7 dpi. Note that in the nonlesioned FN and at 3 dpi the density of Iba1$^+$ cells is significantly higher in GFAP-IL6Tg animals (***$P \leq 0.0001$; **$P \leq 0.005$). Magnifications on **P** to **W** show the progressive changes in microglial morphology and their association with neuronal cell bodies (*) along the lesion progression. Arrows in P to W point to individual microglial cells and arrowhead in T to microglial clusters. Scale bar (A–L) = 50 μm; (N–U) = 10 μm. [Color figure can be viewed in the online issue, which is available at wileyonlinelibrary.com.]

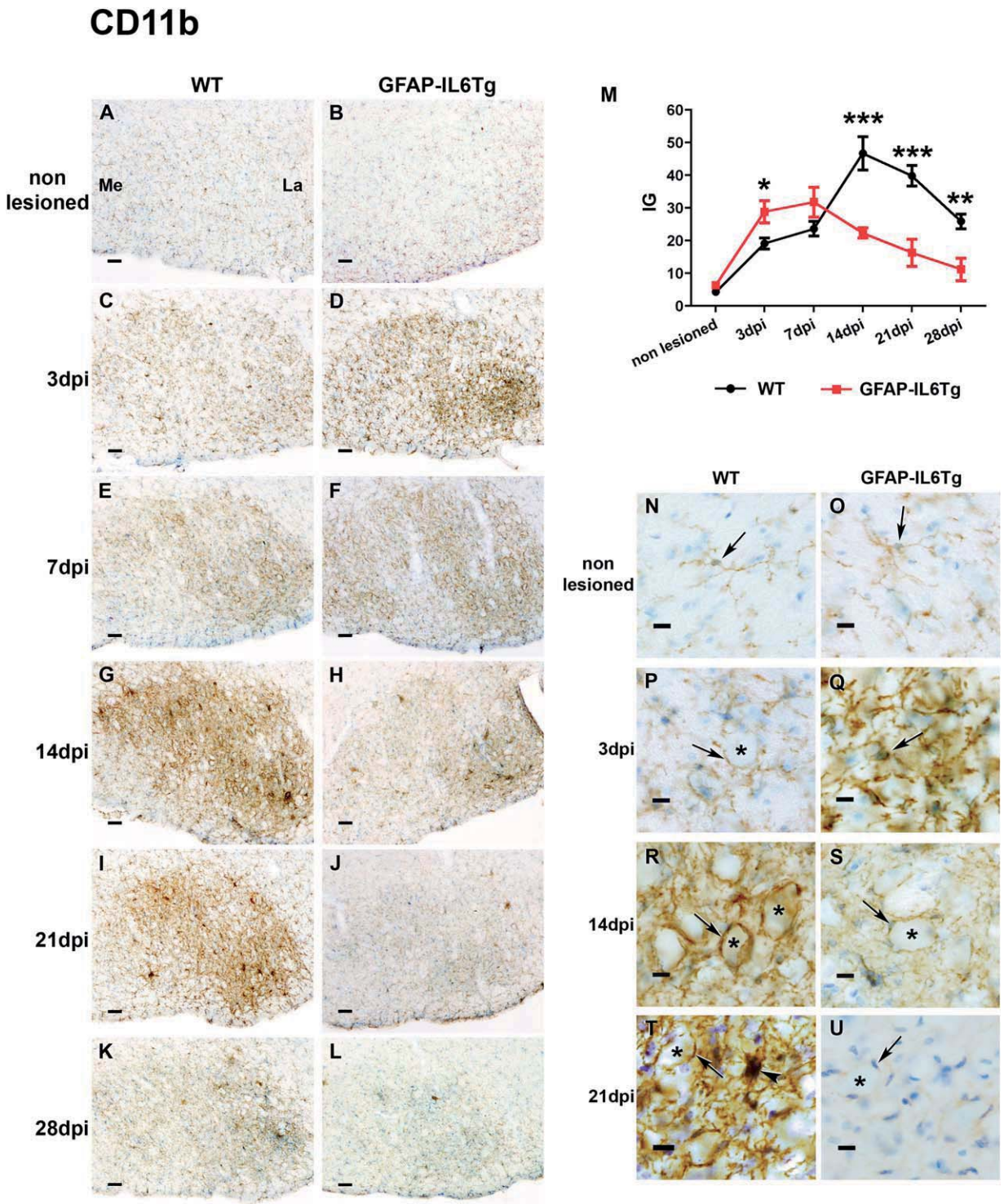

FIGURE 4: CD11b expression. Representative images showing the expression of CD11b in the nonlesioned FN (**A** and **B**) and in the ipsilateral side of both WT (**C, E, G, I** and **K**) and GFAP-IL6Tg animals (**D, F, H, J** and **L**) at the different survival times analyzed. In A, La indicates the lateral area, whereas Me indicates the medial area of the brainstem. (**M**) Histogram showing the IG quantification of CD11b staining in WT and GFAP-IL6Tg animals along the evolution of facial nerve axotomy. Note that at 3 dpi the IG is higher in GFAP-IL6Tg animals, whereas at later time-points (from 14 to 28 dpi) expression of CD11b is significantly lower in these transgenic mice (*$P \leq 0.05$; **$P \leq 0.005$; ***$P \leq 0.001$). High magnification images in nonlesioned (**N** and **O**) and the ipsilateral side of axotomized animals (**P–U**) showing the morphology and spatial location of CD11b$^+$ cells: ramified microglial-like cells in the nonlesioned FN (arrows in N and O) and activated cells surrounding motor neuron cell bodies (*) at 3 dpi (arrows in P and Q), 14 dpi (arrows in R and S) and 21 dpi (arrows in T and U). Arrowhead in T point to the characteristic CD11b$^+$ microglial clusters observed in WT animals at 21 dpi. Scale bar (A–L) = 50 μm; (O–V) = 10 μm. [Color figure can be viewed in the online issue, which is available at wileyonlinelibrary.com.]

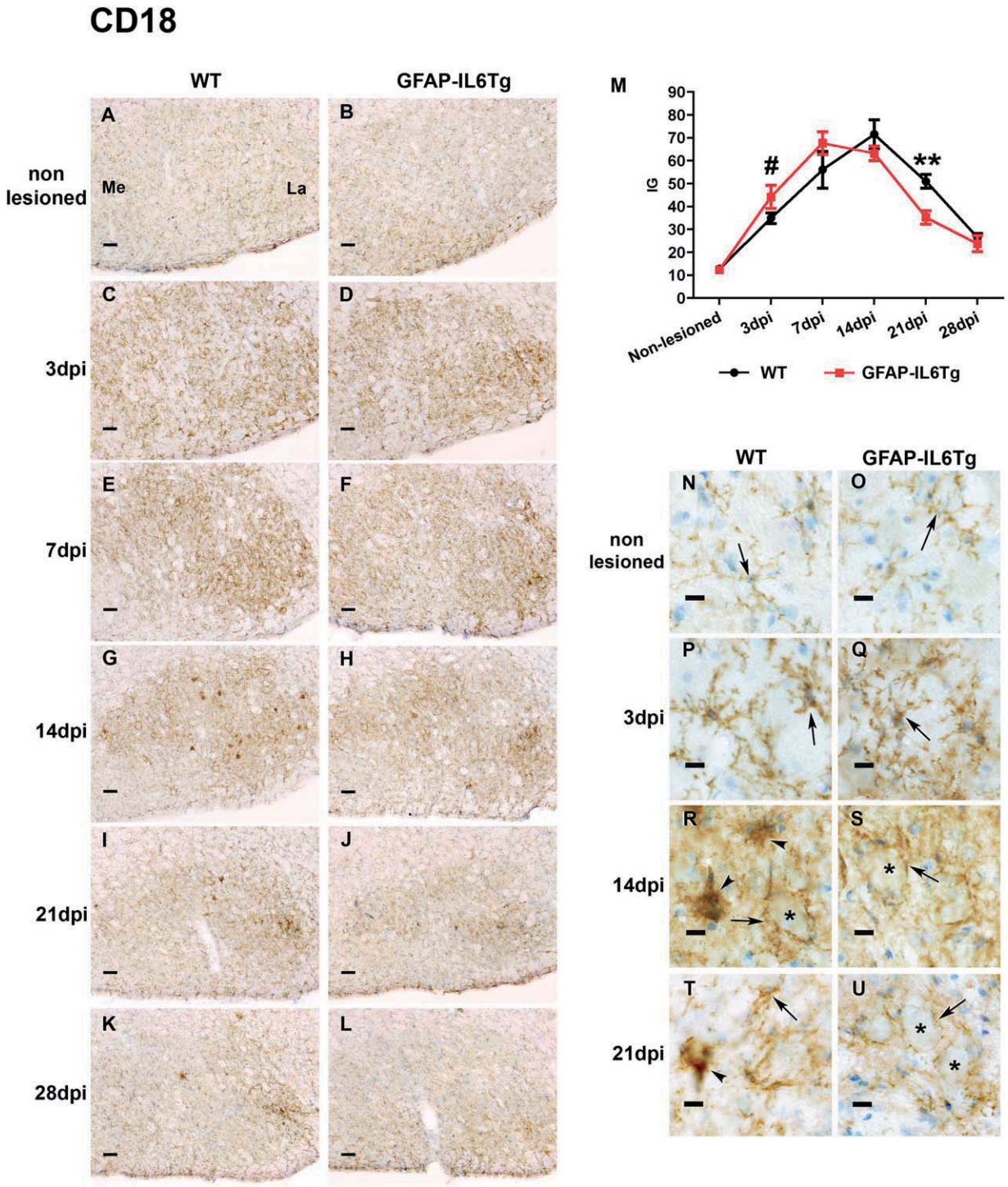

FIGURE 5: CD18 expression. Representative images showing the expression of CD18 in nonlesioned FN (**A** and **B**) and in the ipsilateral side of both WT (**C, E, G, I** and **K**) and GFAP-IL6Tg animals (**D, F, H, J** and **L**) at the different survival time-points after facial nerve axotomy. In A, La indicates the lateral area, whereas Me indicates the medial area of the brainstem. (**M**) Histogram showing the IG quantification of CD18 staining in WT and GFAP-IL6Tg animals along the evolution of facial nerve axotomy. Note that at 3 dpi the IG is slightly higher in GFAP-IL6Tg animals, whereas at 21 dpi the IG is significantly lower in transgenic mice (#$P \leq 0.1$; **$P \leq 0.005$). High magnification images in nonlesioned FN (**N** and **O**) and the ipsilateral side of axotomized FN (**P–U**) showing the morphology and distribution of $CD18^+$ cells: arrows point to ramified microglial-like cells in nonlesioned FN (N and O) and activated cells (P–U). Note the microglial wrapping of facial motor neuron cell bodies (*) at 14 dpi (R and S) and 21 dpi (T and U). Arrowheads in R and T point to characteristics $CD18^+$ microglial clusters. Scale bar (A–L) = 50 μm; (N–U) = 10 μm. [Color figure can be viewed in the online issue, which is available at wileyonlinelibrary.com.]

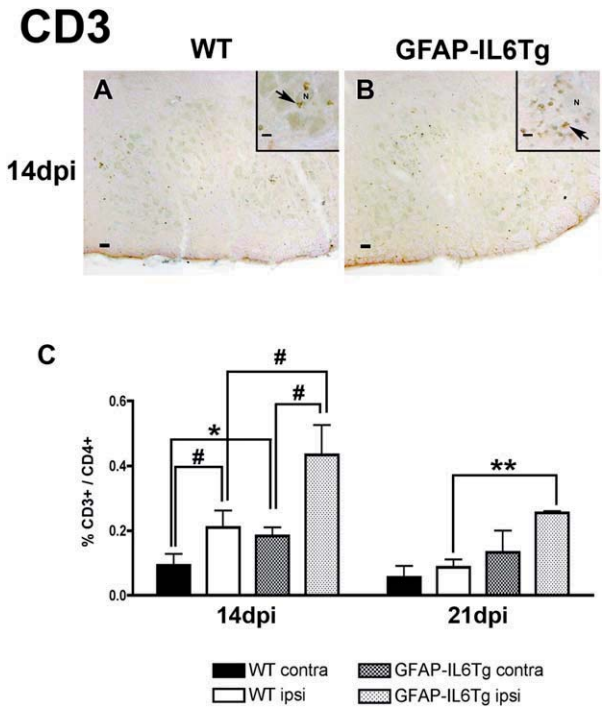

FIGURE 6: T-cell infiltration. Representative images showing the CD3$^+$ cells (arrows in inserts) found in the ipsilateral FN of both WT (A) and GFAP-IL6Tg animals (B) at 14 dpi. Scale bar = 50 μm. (C) Histogram showing the relative percentage of CD3$^+$/CD4$^+$ cells detected in WT and GFAP-IL6Tg animals at 14 and 21 dpi. Note that the percentage of this population of lymphocytes is always higher in the ipsilateral side (ipsi) of GFAP-IL6Tg than in WT animals (#$P \leq 0.2$; *$P \leq 0.05$; **$P \leq 0.01$). [Color figure can be viewed in the online issue, which is available at wileyonlinelibrary.com.]

NDPase$^+$ or Iba1$^+$ microglial cells. In comparison with 21 dpi, a reduction in both the number of motor neurons wrapped by microglial processes and the number of microglial clusters was found at this time-point in WT animals (Figs. 2AA and 3V), whereas, noticeably, in GFAP-IL6Tg mice, the number of neurons remaining covered by microglial processes (Figs. 2AB and 3W) was similar to that observed at 21 dpi. The IG of both CD11b (Fig. 4M) and CD18 (Fig. 5M) decreased at 28 dpi in WT and GFAP-IL6Tg animals. Remarkably, in the case of CD11b this downregulation was significantly more pronounced in GFAP-IL6Tg mice that in WT (Fig. 4M).

In addition to microglial reactivity, astrogliosis, characterized by a progressive increase in GFAP expression, was also observed from 3 to 28 dpi in the ipsilateral FN of both WT and GFAP-IL6Tg animals (Supp. Info. Fig. 1A–D). Although from 3 to 14 dpi, the increase in GFAP expression was similar in both WT and GFAP-IL6Tg mice, at 21 and 28 dpi, the astrogliosis was less intense in GFAP-IL6Tg mice than in WT (Supp. Info. Fig. 1E).

Overall, these findings showed that there were changes in the microglial response in GFAP-IL6Tg animals compared with WT, characterized principally by less attachment to motor neurons at the early time-points following nerve injury. Notably, at later time-points, 21 and 28 dpi, microglial cells in transgenic animals had higher neuronal attachment and lower CD11b and CD18 integrin staining, whereas astrogliosis monitored by GFAP immunostaining was less pronounced than in WT.

Lymphocyte Infiltration

In addition to microglial cell activation, facial nerve axotomy induces the infiltration of lymphocytes (Raivich et al., 1998) that has been commonly associated with a protective effect (Jones et al., 2005). To determine if the lymphocyte infiltration was altered in GFAP-IL6Tg animals, both immunohistochemistry and flow cytometry analysis was performed. As determined by immunohistochemical detection for CD3, the infiltration of T-lymphocytes was more pronounced in GFAP-IL6Tg animals when compared with their WT littermates (Fig. 6A,B). The quantification of T-cell infiltration in the FN at the different time-points after facial nerve axotomy was assessed by determining the proportion of CD3$^+$/CD4$^+$ cells by flow cytometry. As shown in Fig. 6C, a significant increase in the proportion of CD3$^+$/CD4$^+$ cells was detected in the ipsilateral FN of both WT and GFAP-IL6Tg animals. Although, in both groups of animals the temporal pattern of T-cell infiltration was similar, with the proportion of cells peaking at 14 dpi and decreasing thereafter at 21 dpi, the amount of CD3$^+$/CD4$^+$ cells detected in GFAP-IL6Tg animals was always significantly higher than observed in WT animals (Fig. 6C). Notably, a small and unchanging proportion of these CD3$^+$/CD4$^+$ cells was also found on the contralateral side of both WT and GFAP-IL6Tg animals at the two time-points studied, although this proportion was slightly higher in GFAP-IL6Tg than in WT mice.

In summary, IL-6 production in the CNS alters the amount of infiltrating T-cells in the FN parenchyma after axotomy inducing an increase in CD3$^+$ T-cells at 14 and 21 dpi.

OPN Expression

OPN is upregulated in numerous pathological situations and in response to injury (Carecchio and Comi, 2011). OPN promotes cell adhesion to facilitate cell migration or survival via interaction with integrins and CD44 (Kazanecki et al., 2007). The changes we observed in the pattern of microglial attachment to motor neurons in GFAP-IL6Tg animals suggested a possible alteration in the OPN expression and its receptors. The study of sections immunolabeled for OPN revealed that this protein was constitutively expressed in the neuronal cell bodies of motor neurons of the nonlesioned FN in both WT and GFAP-IL6Tg animals (Fig. 7A,B,N,O). No change in OPN staining was observed in the nonlesioned side of the FN at the different time-points studied (not shown).

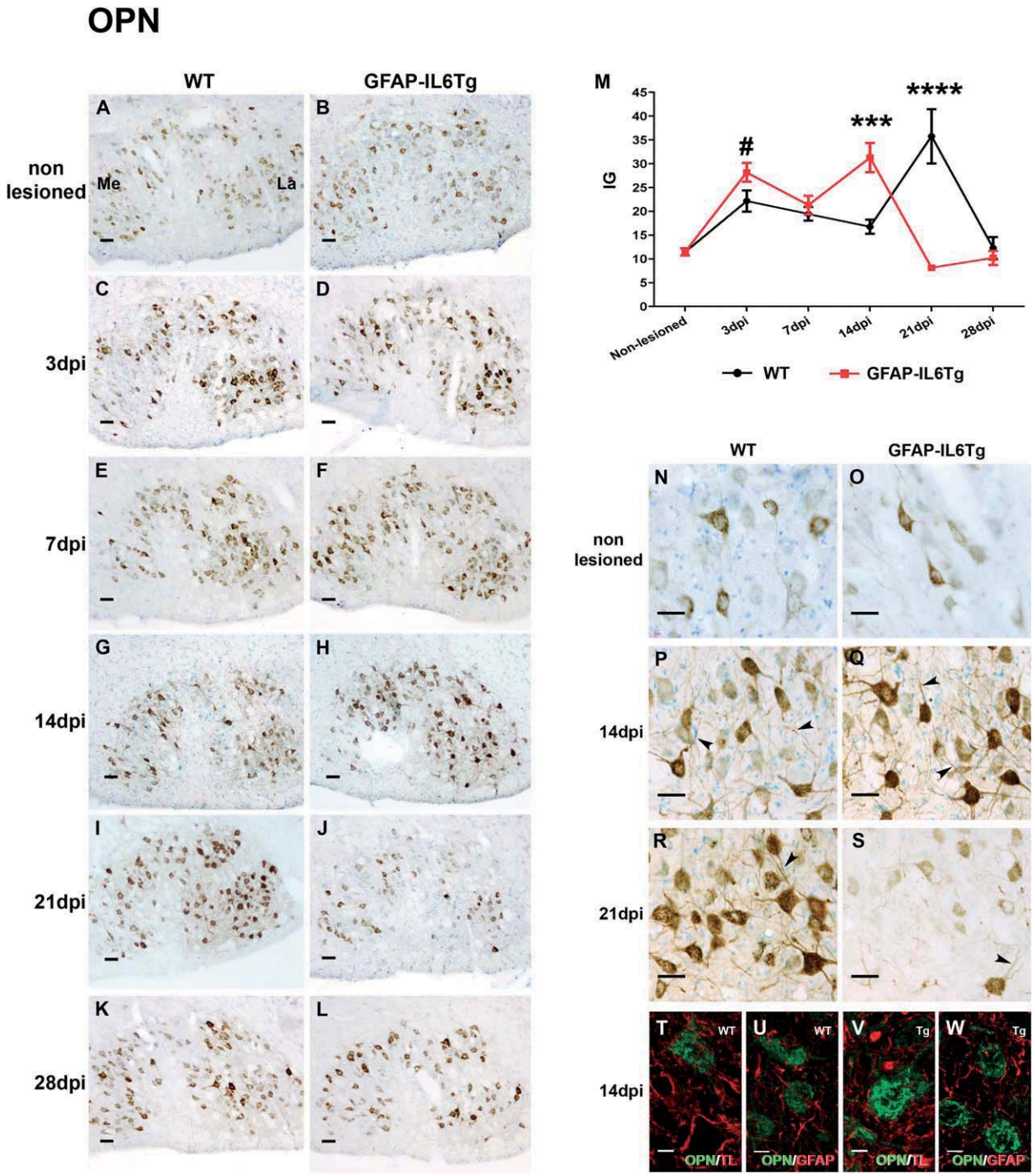

FIGURE 7: OPN expression. Representative microphotographs showing the expression of OPN in nonlesioned FN (**A** and **B**) and in the ipsilateral side of both WT (**C, E, G, I** and **K**) and GFAP-IL6Tg animals (**D, F, H, J** and **L**) at the different survival times after facial nerve axotomy. In A, La indicates the lateral area, whereas Me indicates the medial area of the brainstem. (**M**) Histogram showing the quantification of the IG of OPN staining in WT and GFAP-IL6Tg animals along the different time-points after facial nerve axotomy. Note that whereas at 14 dpi the IG is significantly higher in GFAP-IL6Tg animals, at 21 dpi the IG for OPN is significantly higher in WT mice (#$P \leq 0.06$; ***$P \leq 0.0005$; ****$P \leq 0.0001$). High magnification images show the morphology and distribution of OPN$^+$ cells in the nonlesioned FN (**N** and **O**) and in the ipsilateral side of axotomized animals at 14 dpi (**P** and **Q**) and 21 dpi (**R** and **S**). Note that, in nonlesioned animals, OPN is found exclusively in motor neurons of the FN in both WT and GFAP-IL6Tg animals. In addition to motor neuron cell bodies, OPN$^+$ neuronal prolongations are observed in the ipsilateral side of FN at 14 and 21 dpi (arrowheads in P to S). Double immunofluorescence does not show co-localization between OPN and either TL (**T** and **V**) or GFAP (**U** and **W**) in neither WT (T and U) nor GFAP-IL6Tg animals (V and W). Scale bar (A–L) = 50 μm; (N–Q) = 30 μm; (T–W) = 10 μm. [Color figure can be viewed in the online issue, which is available at wileyonlinelibrary.com.]

However, an increase in OPN was observed at 3 dpi in the axotomized FN side of both WT and GFAP-IL6Tg mice (Fig. 7C,D,M). The IG for OPN slightly decreased at 7 dpi in both groups of animals and from 14 dpi, marked differences in the OPN staining were found between WT and GFAP-IL6Tg animals (Fig. 7M). Expression of this protein in WT animals at 14 dpi showed similar levels to those found at 7 dpi and peaked thereafter at 21 dpi. In contrast, a significant increase in OPN was found in GFAP-IL6Tg mice at 14 dpi that decreased abruptly at 21 dpi. This rapid decrease in the transgenic mice was due not only to a reduction in the number of motor neurons but also noticeably to a large decrease in the intensity of OPN staining in comparison with WT (Fig. 7R,S). At 28 dpi, no difference in OPN IG of staining was observed between WT and GFAP-IL6Tg animals (Fig. 7K,L,M).

It is important to note that, in addition to expression in neuronal cell bodies, OPN was also observed in some neuronal projections along the ipsilateral FN side of both WT and GFAP-IL6Tg mice at the different time-points analyzed, especially at 14 and 21 dpi (Fig. 7P–S).

Double immunofluorescence which combined OPN with either tomato lectin (TL) for microglia or GFAP for astrocyte labeling, demonstrated no co-localization of this molecule with these two markers at any survival time in either WT or GFAP-IL6Tg animals (Fig. 7T–W).

In summary, GFAP-IL6Tg animals had an altered pattern of neuronal OPN expression characterized by higher levels at 14 dpi and lowers at 21 dpi.

OPN-Receptors Expression

Expression of two of the main OPN-receptors, CD44 and CD49e, was analyzed throughout the evolution of facial nerve injury. Our results demonstrated that there was no staining of these two OPN-receptors in the nonlesioned FN side of both WT and GFAP-IL6Tg at the different time-points studied (Figs. 8A,B and 9A,B). After facial nerve axotomy, *de novo* expression of both CD44 and CD49e receptors was detected in the ipsilateral FN side of both WT and GFAP-IL6Tg animals along the course of the lesion, and their expression was different between these two groups of mice, as specified below.

CD44 Expression. CD44 staining was detected initially at 3 dpi in the ipsilateral FN side of both WT and GFAP-IL6Tg animals, where a weak immunolabeling was observed mainly in the soma of motor neurons (Fig. 8C,D,N,O). In WT animals, the AI of CD44 staining increased progressively at 7 and 14 dpi, reaching maximum at 21 dpi (Fig. 8M). At these time-points, CD44 immunolabeling was found scattered in neuropil of the ipsilateral FN (Fig. 8P) and in some cells identified, by double immunolabeling, as T-lymphocytes ($CD3^+$), most of them in close relationship with the soma of motor neurons (Fig. 8R). At 28 dpi, an abrupt reduction in the CD44 AI was seen (Fig. 8M), and only a weak CD44 staining was observed in few small areas of the ipsilateral FN of WT animals (Fig. 8K). No co-localization of CD44 with TL was found at any survival time. Rather, CD44 staining was located in the periphery of OPN^+ motor neurons, just underneath TL^+ microglial processes (Fig. 8T).

Although in GFAP-IL6Tg animals CD44 followed a similar temporal pattern of staining, increasing at 7 and 14 dpi and peaking at 21 dpi, the AI index of labeling of this molecule, from 7 to 28 dpi, was significantly lower than that observed in WT animals (Fig. 8M). Similar to WT, in GFAP-IL6Tg animals, CD44 immunolabeling was observed scattered in the neuropil (Fig. 8Q), and, noticeably and in contrast to what was observed in WT animals, few $CD44^+$/$CD3^+$ T-lymphocytes were found (Fig. 8S). Again, CD44 staining detected in the neuropil did not co-localize with TL, but was located between OPN^+ motor neurons and TL^+ microglial processes (Fig. 8U).

CD49e Expression. Immunostaining for CD49e, which was absent in the nonlesioned FN (Fig. 9A,B), was first detected in the ipsilateral FN of both WT and GFAP-IL6Tg animals at 3 dpi (Fig. 9C,D). Although in both groups of animals this integrin markedly increased at 7 dpi (Fig. 9E,F), the AI index of staining was significantly lower in GFAP-IL6Tg than in WT animals (Fig. 9M). From 14 to 28 dpi, the CD49e AI index slightly decreased in both WT and transgenic animals (Fig. 9G–L,M). At 3 and 7 dpi, CD49e immunolabeling was found in processes wrapping the soma of FN motor neurons (Fig. 9N,O). From 14 dpi, in addition, characteristic clusters of cells with higher CD49e staining were found in both groups of animals (Fig. 9P,Q).

Double immunofluorescence demonstrated co-localization of CD49e and $Iba1^+$ microglial cells in all the time-points analyzed in both WT and GFAP-IL6Tg mice and especially in the clusters of microglial cells (Fig. 9R,S).

In summary, CD44 and CD49e immunolabeling were significantly lower in GFAP-IL6Tg animals than in WT from 7 to 28 dpi. Notably, T-cells and motor neurons but not microglia are the predominant $CD44^+$ cells, whereas CD49e was predominantly found in association with microglial clusters.

Discussion

In this study, we demonstrated that the astrocyte-targeted production of IL-6 within the CNS had a direct impact on the development of the nerve injury response to facial nerve axotomy. Axotomized GFAP-IL6Tg animals had higher neuronal death in the lesioned FN of the brainstem than WT and this

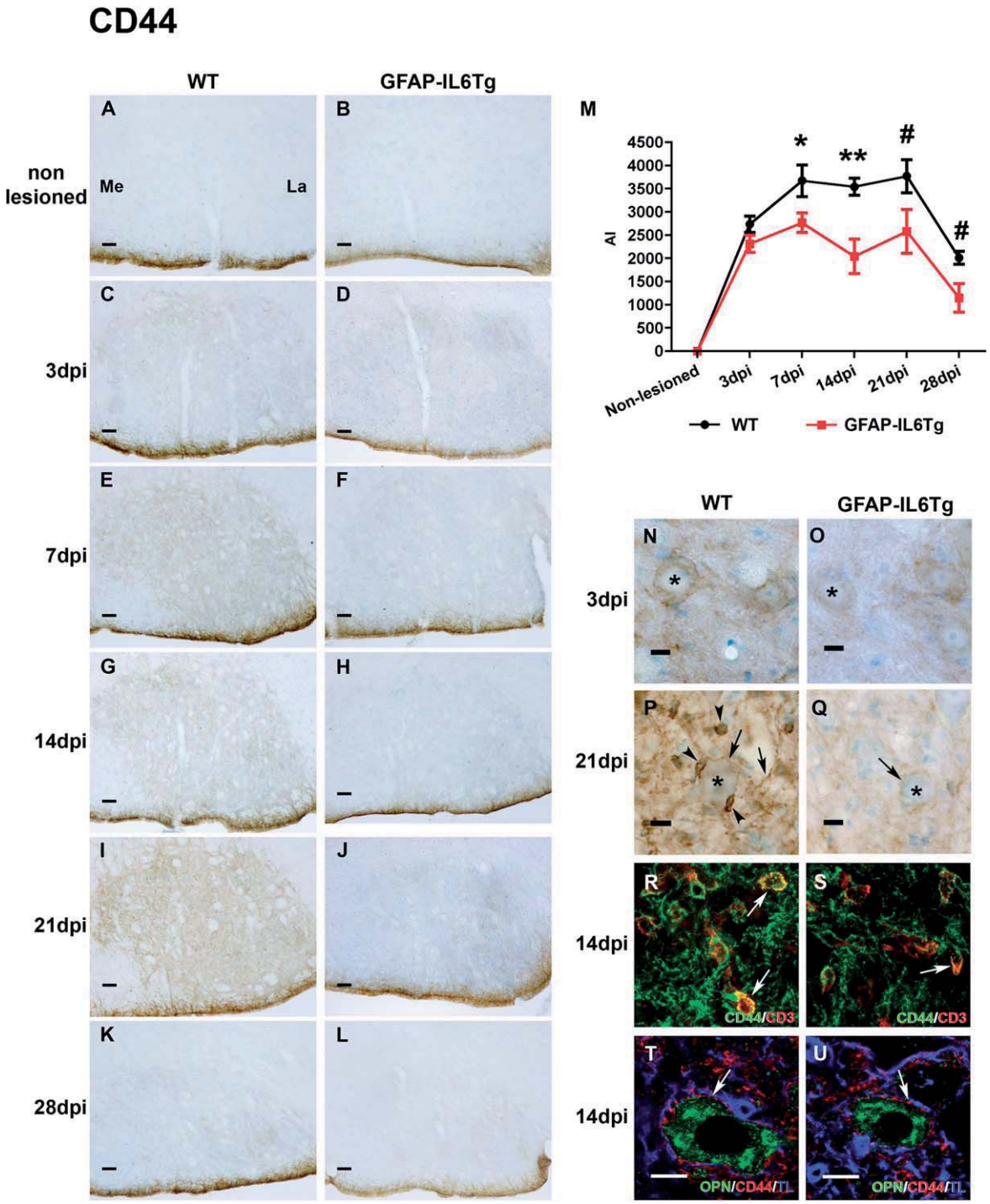

FIGURE 8: CD44 expression. Representative images showing CD44 expression in the nonlesioned FN (**A** and **B**) and in the ipsilateral side of both WT (**C, E, G, I** and **K**) and GFAP-IL6Tg animals (**D, F, H, J** and **L**) at the different survival times after facial nerve axotomy. In A, La indicates the lateral area, whereas Me indicates the medial area of the brainstem. (**M**) Histogram showing the quantification of AI index for CD44 in WT and GFAP-IL6Tg animals along the different time-points after facial nerve axotomy. Note that, although the dynamics of CD44 AI index is similar in both groups of animals, from 7 to 28 dpi the AI index is significantly lower in GFAP-IL6Tg animals than in WT (*$P \leq 0.05$; **$P \leq 0.005$; #$P \leq 0.08$). High magnification images show the morphology and spatial location of CD44$^+$ cells in the ipsilateral side of axotomized animals at 3 dpi (**N** and **O**) and 21 dpi (**P** and **Q**). Note that at early time-points CD44 is found within neuronal cell bodies (* in N and O), whereas at later survival times (21 dpi), CD44$^+$ prolongations (arrows) as well as little-round cells (arrowheads) around motor neurons (* in P and Q) are also detected. Double and triple immunofluorescence combining CD44 with CD3 (**R** and **S**) and with OPN and TL (**T** and **U**), demonstrate co-localization of CD44 with CD3 (arrows in R and S), but not with either OPN or TL (T and U) in both WT (R and T) and GFAP-IL6Tg animals (S and U). Note that, some CD44$^+$ processes are found surrounding neuronal OPN and covered by TL$^+$ ramifications in both WT and GFAP-IL6Tg animals (arrows in T and U). Scale bar (A–L) = 50 μm; (N–U) = 10 μm. [Color figure can be viewed in the online issue, which is available at wileyonlinelibrary.com.]

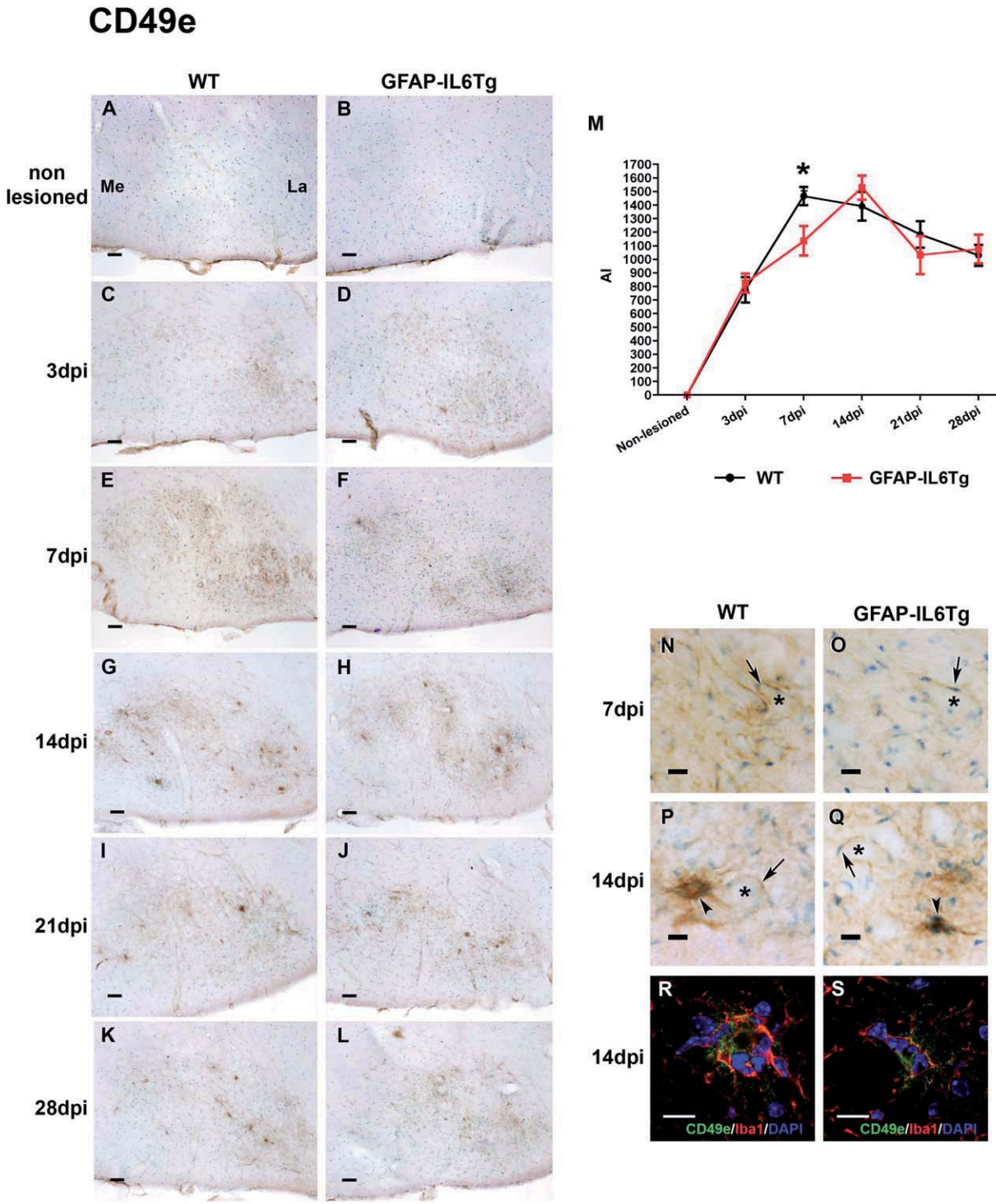

FIGURE 9: CD49e expression. Representative images showing the expression of CD49e in the nonlesioned FN (**A** and **B**) and in the ipsilateral side of both WT (**C, E, G, I** and **K**) and GFAP-IL6Tg animals (**D, F, H, J** and **L**) at the different survival times after facial nerve axotomy. In A, La indicates the lateral area, whereas Me indicates the medial area of the brainstem. (**M**) Histogram showing the quantification of the AI index for CD49e staining in WT and GFAP-IL6Tg animals along the evolution of facial nerve axotomy. Note that at 7 dpi the AI index is significantly lower in GFAP-IL6Tg than in WT animals (*$P \leq 0.05$). High magnification images show the morphology and disposition of CD49e$^+$ cells in the ipsilateral side at 7 dpi (**N** and **O**) and 14 dpi (**P** and **Q**). At 7 dpi, CD49e is found in ramified cells (arrows) surrounding neuronal cell bodies (*), whereas at 14 dpi, in addition, CD49e$^+$ microglial clusters (arrowheads in **P** and **Q**) are observed in both WT and GFAP-IL6Tg animals. Co-localization between CD49e and Iba1 is detected in both WT (**R**) and transgenic animals (**S**) especially in microglial clusters. Scale bar (A–L) = 50 μm; (N–S) = 10 μm. [Color figure can be viewed in the online issue, which is available at wileyonlinelibrary.com.]

difference was associated with significant changes in the temporal activation pattern of glial cells and lymphocyte infiltration. Moreover, we found variations in the pattern of OPN expression in neurons and its receptors CD44 and CD49e in lymphocytes and microglia, respectively, that, as we will discuss, can play a role in the process of neuronal wrapping and, therefore, exert an influence on the survival of axotomized motor neurons.

Increased Neuronal Death

Facial nerve axotomy is one of the most well-characterized models of peripheral nerve injury widely used for the study of retrograde neuronal degeneration (Moran and Graeber, 2004). After facial nerve axotomy in mice, a proportion of motor neurons located in the FN of the brainstem die over a period of several days, by a mechanism of apoptosis that is dependent on the type of axotomy (Ha et al., 2008), the mouse strain used (Ha et al., 2006) and the age of the animals (Dauer et al., 2011). In parallel with this neurodegeneration, a regenerative process of the axotomized axons is also induced in surviving neurons, leading to a partial functional recovery (Moran and Graeber, 2004). Although the exact mechanisms mediating neuronal survival remains unclear, both microglia and lymphocytes have been suggested to play a role in the maintenance of motor neuron viability (Byram et al., 2004; Jones et al., 2005; Serpe et al., 200). Our results revealed an increase in neuronal death in GFAP-IL6Tg animals suggesting that the proinflammatory environment created by IL-6 production may exert a negative influence in some of the key events involved in the processes of neurodegeneration, neuroregeneration, or in both.

IL-6 could have a direct neurotoxic effect on FN motor neurons as it has been shown that they express IL-6 receptor (IL-6R) (Klein et al., 1997) and the deficiency of IL-6 in KO animals has been associated with increased motor neuron survival (Galiano et al., 2001). However, our results clearly showed significant changes between WT and GFAP-IL6Tg animals in microglial reaction, lymphocyte infiltration, and the expression pattern of certain molecules that can be derived from higher neuronal death, although we cannot discard the possibility that these changes might be due to an effect of IL-6 through these cell types.

A point to take into account here is the fact that expression of IL-6 in the GFAP-IL6Tg mice is chronic and, therefore, we cannot evaluate the different effects if any, derived from early versus late IL-6 expression. In this way, further studies using conditional animals (Quintana et al., 2013) or animals lacking the intracellular signaling pathways of IL-6, such as mice with inducible gp130 deletion in myeloid cells (Sander et al., 2008) or in neurons (Stanke et al., 2006), may be useful to clarify the role of IL6 in this paradigm.

Altered Pattern of Glial Reactivity and Lymphocyte Infiltration

Following facial nerve axotomy, it has been reported that microglial cells become activated, proliferate, attach to axotomized motor neurons wrapping them, and participate in the so-called phenomenon known as "synaptic stripping" (Blinzinger and Kreutzberg, 1968; Kreutzberg, 1996). During synaptic stripping, microglial cells interpose between the healthy presynaptic and postsynaptic elements (Blinzinger and Kreutzberg, 1968; Kreutzberg, 1996) to disconnect excitatory inputs to motor neurons allowing axonal regeneration and functional recovery. Synaptic stripping has also been described in other circumstances such as inflammation in the cerebral cortex (Trapp et al., 2007) or after hypoglossal nerve injury (Svensson and Aldskogius, 1993). However, in these kinds of lesions, microglia appear to be involved in the active phagocytic removal of synaptic contacts rather than in disconnection of inputs. Our analysis of microglial reactivity in WT animals showed microglial processes wrapping motor neuron cell bodies from 3 to 21 dpi, decreasing thereafter at 28 dpi. Interestingly, in GFAP-IL6Tg animals, coinciding with a higher neuronal death at 21 dpi, the number of motor neurons wrapped by microglia was less during the previous time-points (3 to 14 dpi), supporting the idea that neuronal wrapping and synaptic stripping is a protective phenomenon in this paradigm (Kreutzberg, 1996). In agreement with this, some evidence suggests that defects in the microglia-neuron attachment after facial nerve axotomy, as occurs in microglial cathepsin deficient mice (Hao et al., 2007) and TGF-β1 deficient animals (Makwana et al., 2007) might lead to a higher neuronal death. Defects in motor neuron cell wrapping after facial nerve axotomy have also been described in other cytokine mutants, such as the IL-6 KO mice (Galiano et al., 2001) and the MCSF deficient mice (Kalla et al., 2001) suggesting that the cytokine microenvironment may regulate this phenomenon.

Our observations also showed that motor neuron wrapping in transgenic animals was higher than in WT at later time-points after facial nerve axotomy, being still evident at 28 dpi but almost absent in WT animals. Is unclear what, if any, consequences there might be of this delay. However, altogether, these results indicate that IL-6 production modifies the microglial response to nerve injury in the FN that impacts the wrapping of motor neurons that might be responsible for the increased neuronal death.

Microglial proliferation is another key event in the microglial activation pattern associated with a wide range of CNS injuries (Raivich et al., 1999) including facial nerve axotomy (Raivich et al., 1994). This proliferative capacity has been shown to be altered by different cytokines and other signaling molecules. Indeed, treatment of microglial-astroglial

co-cultures with IL-6 leads to a slight stimulatory effect on microglial proliferative capacity (Kloss et al., 1997), whereas a reduction of microglial proliferation was observed in IL-6 deficient mice after facial nerve axotomy (Klein et al., 1997). In agreement with these studies, our results revealed that in GFAP-IL6Tg animals, at 3 dpi, the number of microglial cells was higher than in WT, suggesting that IL-6 may play a role in the proliferative capacity of microglia.

In addition to changes in microglial cell number, morphology, and neuronal wrapping, our observations also showed, in agreement with other studies (Kloss et al., 1999; Raivich et al., 1999), a significant upregulation of CD11b and CD18 staining during lesion evolution, that is, indicative of microglial activation (Kettenmann et al., 2011). The upregulation of both markers was higher in GFAP-IL6Tg animals at 3 dpi suggesting a more rapid response of microglial cells to axotomy due to IL-6 production. In this sense, some studies have shown that IL-6 is able to induce microglial activation both *in vitro* (Krady et al., 2008) and after its acute administration *in vivo* (Tilgner et al., 2001). Moreover, strong microglial activation occurs in the brain of GFAP-IL6Tg animals, the extent of which overlaps with the level of transgene encoded IL-6 production (Campbell et al., 1993; Chiang et al., 1994; Heyser et al., 1997).

Strikingly, at later time-points, we found a marked reduction of CD18 IG, and especially of CD11b, in the GFAP-IL6Tg animals. Although the role played by these molecules in CNS pathology has not yet been well determined, particularly in the facial nerve axotomy model, expression of its principal counter-receptor ICAM-1 was demonstrated in lymphocytes (Werner et al., 1998). Consequently, the decrease in CD11b and CD18 expression observed in GFAP-IL6Tg animals, at later time-points, could be a signal of reduced microglial activation or even may involve a deficient attachment between microglia and lymphocytes. These observations in conjunction with the decrease in the neuronal wrapping described earlier in GFAP-IL6Tg animals, lead us to speculate that CD11b and perhaps also CD18, may be key molecules involved in the control of the mechanisms of neuronal wrapping and lymphocyte function in this paradigm.

It is important to point out here, the differences found in our study in terms of the microglial response depending on the microglial marker used for the analysis. This fact demonstrated the tremendous plasticity of microglia and the importance of studying the complex phenomenon of their activation using different markers.

Another interesting difference observed in GFAP-IL-6Tg animals in terms of microglial activation was the lower number of microglial clusters found. Despite not being extensively described in the literature, the few articles reporting the formation of microglial clusters following facial nerve axotomy suggest that this phenomenon is associated with neuronal death (Dauer et al., 2011; Petito et al., 2003; Raivich et al., 1998). In some of these studies, the amount of cluster formation was used as a measure of motor neuron cell death (Dauer et al., 2011; Petito et al., 2003). Notably, and in contrast to these previous studies, our observations indicated that in GFAP-IL6Tg mice, where there was a higher neuronal death, there were less microglial clusters. This decrease in the number of clusters in transgenic mice could be related with a faster or more effective microglial phagocytosis, although we cannot rule out the possibility that microglial clustering may play other, yet to be identified functions. In this sense, recent studies in multiple sclerosis showed the presence of microglial cell clusters in preactive lesions with high expression of IL-10, suggesting that they may play a role as regulators of inflammation (van Horssen et al., 2012). Further studies must be explored to better characterize, (1) the factors controlling their formation, (2) the molecules expressed within these microglial clusters, and (3) the interaction established, if any, with infiltrating lymphocytes.

Our findings showed that after facial nerve axotomy, the astroglial response monitored by GFAP staining was altered in GFAP-IL6Tg animals. As GFAP expression is regulated by IL-6 (reviewed in Pekny et al., 2014), we could expect a greater upregulation of GFAP in axotomized transgenic mice versus axotomized WT. In agreement with this hypothesis, some authors showed that after facial nerve axotomy, IL-6 deficient mice showed less GFAP than WT (Klein et al., 1997). However, our results revealed that, at later time-points after lesion, the transgenic animals displayed a less intense expression of GFAP than WT. We have not a single explanation to this phenomenon, although we cannot discard the possibility that chronic IL-6 expression produced an altered state of microglia and/or factors produced by T-cells that might downregulate GFAP expression.

Noticeably, the changes we have reported in glial activation correlates with an increase in the proportion of T-helper lymphocytes in the FN of transgenic animals at the two time-points analyzed, 14 and 21 dpi. It is well accepted that infiltration of lymphocytes in the FN after axotomy in the mouse occurs in two different waves, one as early as 3 dpi and a second at later time-points (14 dpi) (Raivich et al., 1998). Although not too much is known about the role played by these lymphocytes, it has been suggested that they may have a protective role because the lack of functional mature T and B cells, in either the SCID mutant mice or the RAG2-KO mice, have been correlated with a dramatic increase in neuronal death in this lesion paradigm (Serpe et al., 2000). Moreover, this higher neuronal death was prevented by reconstitution of these mice with functional T and B cells (Serpe et al., 1999). In our study, however, the higher

neuronal death correlated with an increase in lymphocyte infiltration. There are two plausible explanations for these contradictory results: the first may be that local production of IL-6 shifts the phenotype of T-cells infiltrating the FN parenchyma in GFAP-IL6Tg animals toward a proinflammatory Th17 phenotype, as it has been described in other neuroinflammatory conditions (Kimura and Kishimoto, 2010), instead of the protective Th2 described after facial nerve axotomy (Deboy et al., 2006), inducing a higher death of motor neurons. In this sense, it will be of considerable interest to identify, in a future study, the specific lymphocyte subpopulations entering the FN in GFAP-IL6Tg mice.

The second possibility is that production of IL-6 in transgenic animals can change the pattern of chemokine or adhesion molecules involved in lymphocyte recruitment in the FN after axotomy, inducing a higher infiltration of these cells. In support of this, increased lymphocyte infiltration has already been described in specific areas of the CNS of GFAP-IL6Tg mice concomitant with upregulation of VCAM-1 and ICAM-1 expression (Campbell et al., 1993; Milner and Campbell, 2006) as well as specific chemokines such as CCL5 and CCL12 (Quintana et al., 2009) important molecules involved in lymphocyte transmigration across blood brain barrier.

Changes in OPN Expression and its Receptors

Our study also demonstrated differences between WT and GFAP-IL6Tg animals, in the pattern of OPN expression in motor neurons and its receptors CD44 and CD49e in lymphocytes or microglia.

In contrast to previous studies reporting expression of this glycoprotein in microglia and astrocytes after different types of lesions such as spinal root avulsion (Fu et al., 2004), traumatic spinal cord injury (Hashimoto et al., 2003), ischemia (Choi et al., 2007), LPS (Iczkiewicz et al., 2005) and kainic acid injection (Kim et al., 2002), cuprizone-mediated demyelination (Selvaraju et al., 2004), scrapie infection (Jin et al., 2006), cryolesion (Shin et al., 2005) and Theiler's murine encephalitis (Shin and Koh, 2004), in our study, OPN expression was not found in either microglial cells or astrocytes. In agreement with previous studies in adult rat (Shin et al., 1999; Suzuki et al., 2012), we found OPN constitutively present in motor neurons of the nonlesioned FN of both WT and GFAP-IL6Tg animals. After facial nerve axotomy, we observed a similar increase in neuronal OPN at 3 dpi that drop at 7 dpi in both WT and transgenic animals. At 14 and 21 dpi, OPN staining in motor neurons drastically differed in these two groups of animals peaking at 21 dpi in WT and at 14 dpi in GFAP-IL6Tg animals. Increased OPN has been described in affected neurons in diverse types of CNS pathology such as spinal root avulsion (Fu et al., 2004), epilepsy (Borges et al., 2008), scrapie infection (Jin et al., 2006), cryolesion (Shin et al., 2005), oxygen-glucose-deprived hippocampal slices (Lee et al., 2010), Alzheimer's disease (Wung et al., 2007), multiple sclerosis (Sinclair et al., 2005), and different experimental autoimmune encephalomyelitis (EAE) models (Chabas et al., 2001). The exact role played by OPN in neurons is, however, still not completely known and both detrimental as well as neuroprotective roles (Carecchio and Comi, 2011) have been attributed to this glycoprotein in this cell type. We do not know what role is played by OPN in our paradigm because the increased neuronal death observed in GFAP-IL6Tg mice could be associated with either the increased OPN at 14 dpi or the lower expression at 21 dpi.

In addition to changes in OPN, differences in the level of the OPN receptors CD44 and CD49e were also observed in our study. Whereas, in agreement with other studies (Jones et al., 1997; Kloss et al., 1999), the IG of both CD44 and CD49e integrin in WT animals increased from 7 to 21 dpi, in GFAP-IL6Tg animals we found less CD44 at all these time-points and less CD49e specifically at 7 dpi. In WT animals, the simultaneous upregulation of OPN in motor neurons, CD44 in lymphocytes and CD49e in surrounding microglia could be an important factor for the adhesion of these lymphocytes and microglial cells to neurons during the synaptic stripping process and may regulate the survival or death of motor neurons. Indeed, it is well known that through binding with specific receptors, such as CD44, OPN favors the recruitment of innate cells by inducing migration and adhesion of dendritic cells, neutrophils, and macrophages (Giachelli et al., 1998; Weber et al., 1996). Our observation of CD44 expression in the periphery of motor neurons is in agreement with previous studies showing its presence in the plasma membrane of neurons (Jones et al., 1997). Although the function played by CD44 in motor neurons is not clear, some authors suggest that its presence in regenerative axons may indicate a putative role in regulation of axonal outgrowth (Makwana et al., 2010). The fact that GFAP-IL6Tg animals showed less expression of both CD44 and CD49e receptors at the time-points where the neuronal wrapping and synaptic stripping has been described, lead us to speculate that the increase in neuronal death observed in GFAP-IL6Tg animals could be due to a deficient attachment of microglia and/or lymphocytes to neurons. This deficiency may be due to an alteration in the expression of OPN, CD44 and CD49e, pointing to this molecular signaling mechanism as a key event in driving the cross talk among these three cell types and the subsequent further fate of axotomized motor neurons.

In conclusion, we have established that transgenic production of IL-6 in the CNS induces a major impact on the three main cellular components commonly related to the

neuro-degenerative and/or -regenerative processes after facial nerve axotomy: neurons, microglia, and lymphocytes. We demonstrated an increase in neuronal death in the FN of transgenic animals that was accompanied by changes in the association established between activated microglial cells and neurons and a decrease in the expression of microglial CD11b and CD18 integrins at the different time-points analyzed. Moreover, GFAP-IL6Tg animals showed an increase in the number of lymphocytes in the FN and a lower level of OPN in neurons, CD44 in lymphocytes and CD49e in microglial cells. Altogether, these results suggest that IL-6 mediates alterations in the pattern of microglial activation and the lymphocyte infiltration that impact negatively on the outcome of neuronal death after a lesion in the CNS.

Acknowledgment

Grant sponsor: Spanish Ministry of Science and Innovation; Grant numbers: BFU2011-27400 (to BC); Grant sponsor: SAF; Grant numbers: 2008-00435 and 2011-23272 (to JH); Grant sponsor: NHMRC project; Grant number: 632754 (to ILC).

The authors would like to thank Miguel A. Martil and Isabella Appiah for their outstanding technical help.

References

Abercrombie M. 1946. Estimation of nuclear population from microtome sections. Anat Rec 94:239–247.

Almolda B, Costa M, Montoya M, Gonzalez B, Castellano B. 2009. CD4 microglial expression correlates with spontaneous clinical improvement in the acute Lewis rat EAE model. J Neuroimmunol 209:65–80.

Almolda B, Costa M, Montoya M, Gonzalez B, Castellano B. 2011. Increase in Th17 and T-reg lymphocytes and decrease of IL22 correlate with the recovery phase of acute EAE in rat. PLoS One 6:e27473.

Almolda B, Gonzalez B, Castellano B. 2010. Activated microglial cells acquire an immature dendritic cell phenotype and may terminate the immune response in an acute model of EAE. J Neuroimmunol 223:39–54.

Almolda B, Gonzalez B, Castellano B. 2013. Microglia detection by enzymatic histochemistry. Methods Mol Biol 1041:243–259.

Benveniste EN. 1998. Cytokine actions in the central nervous system. Cytokine Growth Factor Rev 9:259–275.

Blinzinger K, Kreutzberg G. 1968. Displacement of synaptic terminals from regenerating motoneurons by microglial cells. Z Zellforsch Mikrosk Anat 85: 145–157.

Borges K, Gearing M, Rittling S, Sorensen ES, Kotloski R, Denhardt DT, Dingledine R. 2008. Characterization of osteopontin expression and function after status epilepticus. Epilepsia 49:1675–1685.

Brunello AG, Weissenberger J, Kappeler A, Vallan C, Peters M, Rose-John S, Weis J. 2000. Astrocytic alterations in interleukin-6/Soluble interleukin-6 receptor alpha double-transgenic mice. Am J Pathol 157:1485–1493.

Byram SC, Carson MJ, DeBoy CA, Serpe CJ, Sanders VM, Jones KJ. 2004. CD4-positive T cell-mediated neuroprotection requires dual compartment antigen presentation. J Neurosci 24:4333–4339.

Campbell IL. 1998. Transgenic mice and cytokine actions in the brain: Bridging the gap between structural and functional neuropathology. Brain Res Brain Res Rev 26:327–336.

Campbell IL, Abraham CR, Masliah E, Kemper P, Inglis JD, Oldstone MB, Mucke L. 1993. Neurologic disease induced in transgenic mice by cerebral overexpression of interleukin 6. Proc Natl Acad Sci USA 90:10061–10065.

Cao Z, Gao Y, Bryson JB, Hou J, Chaudhry N, Siddiq M, Martinez J, Spencer T, Carmel J, Hart RB, Filbin MT. 2006. The cytokine interleukin-6 is sufficient but not necessary to mimic the peripheral conditioning lesion effect on axonal growth. J Neurosci 26:5565–5573.

Carecchio M, Comi C. 2011. The role of osteopontin in neurodegenerative diseases. J Alzheimers Dis 25:179–185.

Castellano B, Gonzalez B, Dalmau I, Vela JM. 1991. Identification and distribution of microglial cells in the cerebral cortex of the lizard: A histochemical study. J Comp Neurol 311:434–444.

Chabas D, Baranzini SE, Mitchell D, Bernard CC, Rittling SR, Denhardt DT, Sobel RA, Lock C, Karpuj M, Pedotti R, Heller R, Oksenberg JR, Steinman L. 2001. The influence of the proinflammatory cytokine, osteopontin, on autoimmune demyelinating disease. Science 294:1731–1735.

Chiang CS, Stalder A, Samimi A, Campbell IL. 1994. Reactive gliosis as a consequence of interleukin-6 expression in the brain: Studies in transgenic mice. Dev Neurosci 16:212–221.

Choi JS, Kim HY, Cha JH, Choi JY, Lee MY. 2007. Transient microglial and prolonged astroglial upregulation of osteopontin following transient forebrain ischemia in rats. Brain Res 1151:195–202.

Conroy SM, Nguyen V, Quina LA, Blakely-Gonzales P, Ur C, Netzeband JG, Prieto AL, Gruol DL. 2004. Interleukin-6 produces neuronal loss in developing cerebellar granule neuron cultures. J Neuroimmunol 155:43–54.

Dauer DJ, Huang Z, Ha GK, Kim J, Khosrowzadeh D, Petitto JM. 2011. Age and facial nerve axotomy-induced T cell trafficking: Relation to microglial and motor neuron status. Brain Behav Immun 25:77–82.

Deboy CA, Xin J, Byram SC, Serpe CJ, Sanders VM, Jones KJ. 2006. Immune-mediated neuroprotection of axotomized mouse facial motoneurons is dependent on the IL-4/STAT6 signaling pathway in CD4(+) T cells. Exp Neurol 201:212–224.

Erta M, Quintana A, Hidalgo J. 2012. Interleukin-6, a major cytokine in the central nervous system. Int J Biol Sci 8:1254–1266.

Fisher J, Mizrahi T, Schori H, Yoles E, Levkovitch-Verbin H, Haggiag S, Revel M, Schwartz M. 2001. Increased post-traumatic survival of neurons in IL-6-knockout mice on a background of EAE susceptibility. J Neuroimmunol 119:1–9.

Fu Y, Hashimoto M, Ino H, Murakami M, Yamazaki M, Moriya H. 2004. Spinal root avulsion-induced upregulation of osteopontin expression in the adult rat spinal cord. Acta Neuropathol 107:8–16.

Gadient RA, Otten UH. 1997. Interleukin-6 (IL-6)—a molecule with both beneficial and destructive potentials. Prog Neurobiol 52:379–390.

Galiano M, Liu ZQ, Kalla R, Bohatschek M, Koppius A, Gschwendtner A, Xu S, Werner A, Kloss CU, Jones LL, Bluethmann H, Raivich G. 2001. Interleukin-6 (IL6) and cellular response to facial nerve injury: Effects on lymphocyte recruitment, early microglial activation and axonal outgrowth in IL6-deficient mice. Eur J Neurosci 14:327–341.

Giachelli CM, Lombardi D, Johnson RJ, Murry CE, Almeida M. 1998. Evidence for a role of osteopontin in macrophage infiltration in response to pathological stimuli in vivo. Am J Pathol 152:353–358.

Giralt M, Ramos R, Quintana A, Ferrer B, Erta M, Castro-Freire M, Comes G, Sanz E, Unzeta M, Pifarre P, Garcia A, Campbell IL, Hidalgo J. 2013. Induction of atypical EAE mediated by transgenic production of IL-6 in astrocytes in the absence of systemic IL-6. Glia 61:587–600.

Gruol DL, Nelson TE. 1997. Physiological and pathological roles of interleukin-6 in the central nervous system. Mol Neurobiol 15:307–339.

Ha GK, Huang Z, Streit WJ, Petitto JM. 2006. Endogenous T lymphocytes and microglial reactivity in the axotomized facial motor nucleus of mice: Effect of genetic background and the RAG2 gene. J Neuroimmunol 172:1–8.

Ha GK, Parikh S, Huang Z, Petitto JM. 2008. Influence of injury severity on the rate and magnitude of the T lymphocyte and neuronal response to facial nerve axotomy. J Neuroimmunol 199:18–23.

Hao HP, Doh-Ura K, Nakanishi H. 2007. Impairment of microglial responses to facial nerve axotomy in cathepsin S-deficient mice. J Neurosci Res 85: 2196–2206.

Hashimoto M, Koda M, Ino H, Murakami M, Yamazaki M, Moriya H. 2003. Upregulation of osteopontin expression in rat spinal cord microglia after traumatic injury. J Neurotrauma 20:287–296.

Heyser CJ, Masliah E, Samimi A, Campbell IL, Gold LH. 1997. Progressive decline in avoidance learning paralleled by inflammatory neurodegeneration in transgenic mice expressing interleukin 6 in the brain. Proc Natl Acad Sci USA 94:1500–1505.

Iczkiewicz J, Rose S, Jenner P. 2005. Increased osteopontin expression following intranigral lipopolysaccharide injection in the rat. Eur J Neurosci 21: 1911–1920.

Ikeda K, Iwasaki Y, Shiojima T, Kinoshita M. 1996. Neuroprotective effect of various cytokines on developing spinal motoneurons following axotomy. J Neurol Sci 135:109–113.

Jin JK, Na YJ, Moon C, Kim H, Ahn M, Kim YS, Shin T. 2006. Increased expression of osteopontin in the brain with scrapie infection. Brain Res 1072: 227–233.

Jones KJ, Serpe CJ, Byram SC, Deboy CA, Sanders VM. 2005. Role of the immune system in the maintenance of mouse facial motoneuron viability after nerve injury. Brain Behav Immun 19:12–9.

Jones LL, Kreutzberg GW, Raivich G. 1997. Regulation of CD44 in the regenerating mouse facial motor nucleus. Eur J Neurosci 9:1854–1863.

Kalla R, Liu Z, Xu S, Koppius A, Imai Y, Kloss CU, Kohsaka S, Gschwendtner A, Moller JC, Werner A, Raivich G. 2001. Microglia and the early phase of immune surveillance in the axotomized facial motor nucleus: Impaired microglial activation and lymphocyte recruitment but no effect on neuronal survival or axonal regeneration in macrophage-colony stimulating factor-deficient mice. J Comp Neurol 436:182–201.

Kazanecki CC, Uzwiak DJ, Denhardt DT. 2007. Control of osteopontin signaling and function by post-translational phosphorylation and protein folding. J Cell Biochem 102:912–924.

Kettenmann H, Hanisch UK, Noda M, Verkhratsky A. 2011. Physiology of microglia. Physiol Rev 91:461–553.

Kim SY, Choi YS, Choi JS, Cha JH, Kim ON, Lee SB, Chung JW, Chun MH, Lee MY. 2002. Osteopontin in kainic acid-induced microglial reactions in the rat brain. Mol Cells 13:429–435.

Kimura A, Kishimoto T. 2010. IL-6: Regulator of Treg/Th17 balance. Eur J Immunol 40:1830–1835.

Kishimoto T. 2006. Interleukin-6: Discovery of a pleiotropic cytokine. Arthritis Res Ther 8 (Suppl 2):S2.

Kishimoto T, Akira S, Narazaki M, Taga T. 1995. Interleukin-6 family of cytokines and gp130. Blood 86:1243–1254.

Klein MA, Moller JC, Jones LL, Bluethmann H, Kreutzberg GW, Raivich G. 1997. Impaired neuroglial activation in interleukin-6 deficient mice. Glia 19: 227–233.

Kloss CU, Kreutzberg GW, Raivich G. 1997. Proliferation of ramified microglia on an astrocyte monolayer: Characterization of stimulatory and inhibitory cytokines. J Neurosci Res 49:248–254.

Kloss CU, Werner A, Klein MA, Shen J, Menuz K, Probst JC, Kreutzberg GW, Raivich G. 1999. Integrin family of cell adhesion molecules in the injured brain: Regulation and cellular localization in the normal and regenerating mouse facial motor nucleus. J Comp Neurol 411:162–178.

Krady JK, Lin HW, Liberto CM, Basu A, Kremlev SG, Levison SW. 2008. Ciliary neurotrophic factor and interleukin-6 differentially activate microglia. J Neurosci Res 86:1538–1547.

Kreutzberg GW. 1996. Microglia: A sensor for pathological events in the CNS. Trends Neurosci 19:312–318.

Lacroix S, Chang L, Rose-John S, Tuszynski MH. 2002. Delivery of hyper-interleukin-6 to the injured spinal cord increases neutrophil and macrophage infiltration and inhibits axonal growth. J Comp Neurol 454:213–228.

Lee JY, Choi JS, Choi JY, Shin YJ, Yun H, Cha JH, Chun MH, Lee MY. 2010. Spatial and temporal changes of osteopontin in oxygen-glucose-deprived hippocampal slice cultures. Acta Neurobiol Exp (Wars) 70:1–12.

Loddick SA, Turnbull AV, Rothwell NJ. 1998. Cerebral interleukin-6 is neuroprotective during permanent focal cerebral ischemia in the rat. J Cereb Blood Flow Metab 18:176–179.

Makwana M, Jones LL, Cuthill D, Heuer H, Bohatschek M, Hristova M, Friedrichsen S, Ormsby I, Bueringer D, Koppius A, Bauer K, Doetschman T, Raivich G. 2007. Endogenous transforming growth factor beta 1 suppresses inflammation and promotes survival in adult CNS. J Neurosci 27:11201–11213.

Makwana M, Werner A, Acosta-Saltos A, Gonitel R, Pararajasingham A, Ruff C, Rumajogee P, Cuthill D, Galiano M, Bohatschek M, Wallace AS, Anderson PN, Mayer U, Behrens A, Raivich G. 2010. Peripheral facial nerve axotomy in mice causes sprouting of motor axons into perineuronal central white matter: Time course and molecular characterization. J Comp Neurol 518:699–721.

Milner R, Campbell IL. 2006. Increased expression of the beta4 and alpha5 integrin subunits in cerebral blood vessels of transgenic mice chronically producing the pro-inflammatory cytokines IL-6 or IFN-alpha in the central nervous system. Mol Cell Neurosci 33:429–440.

Moran LB, Graeber MB. 2004. The facial nerve axotomy model. Brain Res Brain Res Rev 44:154–178.

Mukaino M, Nakamura M, Yamada O, Okada S, Morikawa S, Renault-Mihara F, Iwanami A, Ikegami T, Ohsugi Y, Tsuji O, Katoh H, Matsuzaki Y, Toyama Y, Liu M, Okano H. 2010. Anti-IL-6-receptor antibody promotes repair of spinal cord injury by inducing microglia-dominant inflammation. Exp Neurol 224:403–414.

Murabe Y, Sano Y. 1981. Morphological studies on neuroglia. I. Electron microscopic identification of silver-impregnated glial cells. Cell Tissue Res 216:557–568.

Murphy PG, Borthwick LS, Johnston RS, Kuchel G, Richardson PM. 1999. Nature of the retrograde signal from injured nerves that induces interleukin-6 mRNA in neurons. J Neurosci 19:3791–3800.

Nakamura M, Okada S, Toyama Y, Okano H. 2005. Role of IL-6 in spinal cord injury in a mouse model. Clin Rev Allergy Immunol 28:197–204.

Okada S, Nakamura M, Mikami Y, Shimazaki T, Mihara M, Ohsugi Y, Iwamoto Y, Yoshizaki K, Kishimoto T, Toyama Y, Okano H. 2004. Blockade of interleukin-6 receptor suppresses reactive astrogliosis and ameliorates functional recovery in experimental spinal cord injury. J Neurosci Res 76:265–276.

Pekny M, Wilhelmsson U, Pekna M. 2014. The dual role of astrocyte activation and reactive gliosis. Neurosci Lett S0304–3940(14):00008–00001.

Petito CK, Adkins B, McCarthy M, Roberts B, Khamis I. 2003. CD4+ and CD8+ cells accumulate in the brains of acquired immunodeficiency syndrome patients with human immunodeficiency virus encephalitis. J Neurovirol 9:36–44.

Quintana A, Erta M, Ferrer B, Comes G, Giralt M, Hidalgo J. 2013. Astrocyte-specific deficiency of interleukin-6 and its receptor reveal specific roles in survival, body weight and behavior. Brain Behav Immun 27:162–173.

Quintana A, Muller M, Frausto RF, Ramos R, Getts DR, Sanz E, Hofer MJ, Krauthausen M, King NJ, Hidalgo J, Campbell IL. 2009. Site-specific production of IL-6 in the central nervous system retargets and enhances the inflammatory response in experimental autoimmune encephalomyelitis. J Immunol 183:2079–2088.

Raivich G, Bohatschek M, Kloss CU, Werner A, Jones LL, Kreutzberg GW. 1999. Neuroglial activation repertoire in the injured brain: Graded response, molecular mechanisms and cues to physiological function. Brain Res Brain Res Rev 30:77–105.

Raivich G, Jones LL, Kloss CU, Werner A, Neumann H, Kreutzberg GW. 1998. Immune surveillance in the injured nervous system: T-lymphocytes invade the axotomized mouse facial motor nucleus and aggregate around sites of neuronal degeneration. J Neurosci 18:5804–5816.

Raivich G, Moreno-Flores MT, Moller JC, Kreutzberg GW. 1994. Inhibition of posttraumatic microglial proliferation in a genetic model of macrophage colony-stimulating factor deficiency in the mouse. Eur J Neurosci 6:1615–1618.

Sander LE, Obermeier F, Dierssen U, Kroy DC, Singh AK, Seidler U, Streetz KL, Lutz HH, Muller W, Tacke F, Trautwein C. 2008. Gp130 signaling promotes development of acute experimental colitis by facilitating early neutrophil/macrophage recruitment and activation. J Immunol 181:3586–3594.

Selvaraju R, Bernasconi L, Losberger C, Graber P, Kadi L, Avellana-Adalid V, Picard-Riera N, Baron Van Evercooren A, Cirillo R, Kosco-Vilbois M, Feger G, Papoian R, Boschert U. 2004. Osteopontin is upregulated during in vivo demyelination and remyelination and enhances myelin formation in vitro. Mol Cell Neurosci 25:707–721.

Serpe CJ, Kohm AP, Huppenbauer CB, Sanders VM, Jones KJ. 1999. Exacerbation of facial motoneuron loss after facial nerve transection in severe combined immunodeficient (scid) mice. J Neurosci 19:RC7.

Serpe CJ, Sanders VM, Jones KJ. 2000. Kinetics of facial motoneuron loss following facial nerve transection in severe combined immunodeficient mice. J Neurosci Res 62:273–278.

Shin SL, Cha JH, Chun MH, Chung JW, Lee MY. 1999. Expression of osteopontin mRNA in the adult rat brain. Neurosci Lett 273:73–76.

Shin T, Ahn M, Kim H, Moon C, Kang TY, Lee JM, Sim KB, Hyun JW. 2005. Temporal expression of osteopontin and CD44 in rat brains with experimental cryolesions. Brain Res 1041:95–101.

Shin T, Koh CS. 2004. Immunohistochemical detection of osteopontin in the spinal cords of mice with Theiler's murine encephalomyelitis virus-induced demyelinating disease. Neurosci Lett 356:72–74.

Sinclair C, Mirakhur M, Kirk J, Farrell M, McQuaid S. 2005. Up-regulation of osteopontin and alphaBeta-crystallin in the normal-appearing white matter of multiple sclerosis: An immunohistochemical study utilizing tissue microarrays. Neuropathol Appl Neurobiol 31:292–303.

Spooren A, Kolmus K, Laureys G, Clinckers R, De Keyser J, Haegeman G, Gerlo S. 2011. Interleukin-6, a mental cytokine. Brain Res Rev 67:157–183.

Stanke M, Duong CV, Pape M, Geissen M, Burbach G, Deller T, Gascan H, Otto C, Parlato R, Schutz G, Rohrer H. 2006. Target-dependent specification of the neurotransmitter phenotype: Cholinergic differentiation of sympathetic neurons is mediated in vivo by gp 130 signaling. Development 133:141–150.

Suzuki S, Tanaka K, Suzuki N. 2009. Ambivalent aspects of interleukin-6 in cerebral ischemia: Inflammatory versus neurotrophic aspects. J Cereb Blood Flow Metab 29:464–479.

Suzuki T, Sato T, Ichikawa H. 2012. Osteocalcin- and osteopontin-containing neurons in the rat hind brain. Cell Mol Neurobiol 32:1265–1273.

Svensson M, Aldskogius H. 1993. Synaptic density of axotomized hypoglossal motorneurons following pharmacological blockade of the microglial cell proliferation. Exp Neurol 120:123–131.

Swartz KR, Liu F, Sewell D, Schochet T, Campbell I, Sandor M, Fabry Z. 2001. Interleukin-6 promotes post-traumatic healing in the central nervous system. Brain Res 896:86–95.

Taga T, Kishimoto T. 1997. Gp130 and the interleukin-6 family of cytokines. Annu Rev Immunol 15:797–819.

Tilgner J, Volk B, Kaltschmidt C. 2001. Continuous interleukin-6 application in vivo via macroencapsulation of interleukin-6-expressing COS-7 cells induces massive gliosis. Glia 35:234–245.

Trapp BD, Wujek JR, Criste GA, Jalabi W, Yin X, Kidd GJ, Stohlman S, Ransohoff R. 2007. Evidence for synaptic stripping by cortical microglia. Glia 55:360–368.

van Horssen J, Singh S, van der Pol S, Kipp M, Lim JL, Peferoen L, Gerritsen W, Kooi EJ, Witte ME, Geurts JJ, de Vries HE, Peferoen-Baert R, van den Elsen PJ, van der Valk P, Amor S. 2012. Clusters of activated microglia in normal-appearing white matter show signs of innate immune activation. J Neuroinflammation 9:156.

Van Wagoner NJ, Benveniste EN. 1999. Interleukin-6 expression and regulation in astrocytes. J Neuroimmunol 100:124–139.

Villacampa N, Almolda B, Gonzalez B, Castellano B. 2013. Tomato lectin histochemistry for microglial visualization. Methods Mol Biol 1041:261–279.

Weber GF, Ashkar S, Glimcher MJ, Cantor H. 1996. Receptor-ligand interaction between CD44 and osteopontin (Eta-1). Science 271:509–512.

Werner A, Kloss CU, Walter J, Kreutzberg GW, Raivich G. 1998. Intercellular adhesion molecule-1 (ICAM-1) in the mouse facial motor nucleus after axonal injury and during regeneration. J Neurocytol 27:219–232.

Wung JK, Perry G, Kowalski A, Harris PL, Bishop GM, Trivedi MA, Johnson SC, Smith MA, Denhardt DT, Atwood CS. 2007. Increased expression of the remodeling- and tumorigenic-associated factor osteopontin in pyramidal neurons of the Alzheimer's disease brain. Curr Alzheimer Res 4:67–72.

Zhong J, Dietzel ID, Wahle P, Kopf M, Heumann R. 1999. Sensory impairments and delayed regeneration of sensory axons in interleukin-6-deficient mice. J Neurosci 19:4305–4313.

RESEARCH ARTICLE

Astrocyte-Targeted Production of IL-10 Induces Changes in Microglial Reactivity and Reduces Motor Neuron Death After Facial Nerve Axotomy

Nàdia Villacampa,[1] Beatriz Almolda,[1] Antonietta Vilella,[2] Iain L. Campbell,[3] Berta González,[1] and Bernardo Castellano[1]

Interleukin-10 (IL-10) is a cytokine that plays a crucial role in regulating the inflammatory response and immune reactions. In the central nervous system (CNS), IL-10 is mainly produced by astrocytes and microglia and it is upregulated after various insults, such as experimental autoimmune encephalomyelitis, middle cerebral artery occlusion, excitotoxicity and traumatic brain injury. To better understand the effects of IL-10 in the normal and injured CNS, we generated transgenic mice (termed GFAP-IL-10Tg) that expressed the murine *IL-10* gene under the transcriptional control of the glial fibrillary acidic protein (GFAP) promoter. Previous studies demonstrated marked changes in the microglial phenotype in these mice under basal conditions. The objective of the present study was to investigate the effects of local astrocyte-targeted IL-10 production on glial activation, neuronal degeneration and leukocyte recruitment after axotomy. GFAP-IL-10Tg mice had marked changes in the phenotype of activated microglial cells, as well as in the number of microglial clusters and in microglial cell density. These microglial changes are accompanied by a twofold increase in lymphocyte infiltration in GFAP-IL-10Tg mice and around twofold decrease in neuronal cell death at 21 dpi. Altogether, our findings suggested that astrocyte-targeted production of IL-10 impacted the microglial response and lymphocyte recruitment and culminated in a beneficial effect on neuronal survival.

GLIA 2015;63:1166–1184

Key words: microglia, transgenic animal, neuronal survival, lymphocytes, nerve injury, neurodegeneration, cytokines, IL-10R, CD18, CD16/32, MHC-II, CD39, arginase-1, Ym-1, CD150

Introduction

Facial nerve axotomy (FNA) is a well-characterized model of peripheral nerve injury, extensively used for the study of retrograde neuronal degeneration and regeneration (Makwana and Raivich, 2005; Moran and Graeber, 2004). Facial motor neuron (FMN) degeneration is accompanied by a robust activation of microglial cells located in the facial nucleus (FN). In a first phase, from 2 to 14 dpi, activated microglial cells proliferate (Raivich et al., 1994), undergo changes in morphology and the expression of several activation markers (Galiano et al., 2001; Kloss et al., 1999; Raivich et al., 1998b; Werner et al., 1998), adhere to the neuronal cell body (Jones et al., 1997; Svensson et al., 1994), and then displace the neurite terminals in a process termed "synaptic stripping" (Blinzinger and Kreutzberg, 1968; Kreutzberg, 1996). Between 2 and 3 weeks after injury, activated microglia also form large clusters around dying motor neurons, phagocytose neuronal debris (Moller et al., 1996; Raivich et al., 1998b), and, by the expression of MHC-II and costimulatory factors (Bohatschek et al., 2004; Streit et al., 1999) interact with T-lymphocytes recruited to the axotomized FN (Byram et al., 2004; Raivich et al., 1998b). In addition to these neuronal and microglial changes, FNA leads to a biphasic induction of inflammation-associated cytokines: (1) a

View this article online at wileyonlinelibrary.com. DOI: 10.1002/glia.22807

Published online February 17, 2015 in Wiley Online Library (wileyonlinelibrary.com). Received July 29, 2014, Accepted for publication Jan 28, 2015.

Address correspondence to Nàdia Villacampa, Unitat d'Histologia, Torre M5., Facultat de Medicina, Universitat Autònoma de Barcelona, 08193 Bellaterra, Barcelona, Spain. E-mail: nadia.villacampa@uab.cat

From the [1]Department of Cell Biology, Physiology and Immunology, Institute of Neuroscience, Universitat Autònoma de Barcelona, Bellaterra, 08193, Barcelona, Spain; [2]Department of Biomedical, Metabolic and Neural Sciences, Università degli Studi di Modena e Reggio Emilia, 41125, Modena, Italy; [3]School of Molecular Bioscience, University of Sydney, Sydney, New South Wales, 2006, Australia

rapid upregulation of interleukin-6 (IL-6), TGF-beta, and MCSF receptor (Bohatschek et al., 2004; Jones et al., 2000; Raivich et al., 1998a) and (2) a second phase around 14 dpi, coinciding with the peak of neuronal cell death, with increased production of IL-1beta, TNF-alpha and IFN-gamma (Raivich et al., 1998b). These inflammation-associated cytokines impact on the fate of axotomized FMN (Galiano et al., 2001; Kalla et al., 2001; Raivich et al., 2003). To understand the effect of certain cytokines in the evolution of CNS lesions, we are currently working in transgenic mice with CNS-targeted production of specific cytokines. In recent work, we evaluated the effects of astrocyte-targeted production of IL-6 in the paradigm of FNA and showed that IL-6 induces an increase in FMN cell death associated with changes in microglial reactivity and increased T lymphocyte recruitment (Almolda et al., 2014b).

While IL-6 is considered a proinflammatory cytokine that acts as major modulator of inflammation in the CNS (Benveniste, 1998; Erta et al., 2012), interleukin-10 (IL-10) is an anti-inflammatory cytokine that has a pivotal role in controlling inflammation and modulates peripheral adaptive immune responses that cause tissue damage (Asadullah, 2003; Mosmann, 1991; Sabat, 2010; Trinchieri, 2007). In the CNS, astrocytes and microglia are potential sources of IL-10 production (Hulshof et al., 2002; Ledeboer et al., 2002; Park et al., 2007), whereas the expression of the IL-10 receptor (IL-10R) has been described on microglia (Mizuno et al., 1994; Strle et al., 2002), astrocytes (Pousset et al., 2001; Xin et al., 2011), oligodendrocytes (Molina-Holgado et al., 2001), and neurons (Xin et al., 2011; Zhou et al., 2009). IL-10 expression is upregulated under pathological conditions, mainly associated with the recovery phase (Kennedy et al., 1992; Samoilova et al., 1998) or later time-points after injury (Apelt and Schliebs, 2001; Gonzalez et al., 2009). Moreover, systemically administered IL-10 has beneficial effects after different CNS experimental injuries (Spera et al., 1998).

To study the specific effects of local IL-10 production within the CNS, we have generated a transgenic mouse model with astrocyte-targeted production of IL-10 (GFAP-IL-10Tg mice) (Almolda et al., 2014a). Characterization of these transgenic mice revealed altered microglial cell density and morphology as well as changes in the expression of several activation markers in different brain areas. In the present study, we investigated whether CNS-targeted IL-10 production exerts any effect on the microglial and astroglial response, lymphocyte recruitment and FMN cell death following FNA.

Materials and Methods

Animals

For this study, a total of 66 GFAP-IL-10Tg animals (3 months old) and a total of 61 wild-type (WT) littermates from both sexes were used. All mice were housed under a 12-h light/dark cycle, with food and water *ad libitum*. All experimental animal work was conducted according to Spanish regulations (Ley 32/2007, Real Decreto 1201/2005, Ley 9/2003, and Real Decreto 178/2004) in agreement with European Union directives (86/609/CEE, 91/628/CEE, and 92/65/CEE) and was approved by the Ethical Committee of the Autonomous University of Barcelona. Every effort was made to minimize the number of animals used to produce reliable scientific data, as well as animal suffering and pain.

Facial Nerve Axotomy and Experimental Groups

GFAP-IL-10Tg and WT mice were anesthetized with a solution of xylazine (20 mg/kg) and ketamine (80 mg/kg) injected intraperitoneally at dose of 0.01 mL/g. The skin behind the right ear was shaved and cleansed with 70% ethanol. A small incision was made and skin and muscle were gently separated to expose the right facial nerve. One millimeter of the facial nerve main branch was resected at the level of the stylomastoid foramen. Following the surgery, the skin was sutured with 5-0 nylon. Corneal dehydration was prevented by application of ***Lacri-lube***® eye ointment. After anesthesia recovery, the complete whisker paralysis was assessed to ensure correct facial nerve resection.

Nonlesioned and axotomized animals were distributed in different experimental groups and euthanized at 3, 7, 14, 21, and 28 days postinjury (dpi) for real-time polymerase chain reaction (RT-PCR) analysis and immunohistochemistry, whereas another set of animals were euthanized at 21 dpi and used for motor neuron survival quantification.

Sample Processing for RT-PCR

Nonlesioned and axotomized animals were used for RT-PCR analysis. Animals were deeply anesthetized with a solution of xylazine (20 mg/kg) and ketamine (80 mg/kg) injected intraperitoneally (0.015 mL/g) and intracardially perfused with a solution containing phosphate buffer solution (PBS) and 0.1% of diethyl pyrocarbonate water (DEPC, Sigma, 40718). Brains were quickly dissected out, frozen using dry ice and stored at −80°C until use. Two coronal 400-μm thick sections of the brainstem containing the facial nucleus region were obtained using a JUNG CM 3000 Leica cryostat and placed on glass slides under RNase-free conditions. The contralateral and the ipsilateral facial nucleus were separately collected, lysed by mechanical disruption in Trizol reagent (Qiagen) and homogenized following the procedure provided by the manufacturer. Isolated mRNA was reverse transcribed to cDNA using a first-strand synthesis kit and M-MLV Reverse Transcriptase (Promega Corporation, MA). Samples were heated at 70°C for 5 min to eliminate any secondary structures, then incubated at 23°C for 10 min, 1 h at 37°C, and 5 min at 95°C before being chilled at 4°C using a thermocycler T Gradient (Whatman, Biometra). The amount of cDNA was quantified with iTaq Universal SYBR® Green Supermix (Bio Rad) using a Bio Rad RT-PCR iCycler. Each PCR reaction was performed in triplicate with the following cycling parameters: 10 min at 95°C and 40 cycles of 1 min at 95°C, 1 min at 60°C and 1 min at 72°C, followed by a melting curve analysis. RT-PCR primers were designed in two different exons; primer length was comprised between 18 and

30 bp, GC content was between 40 and 60% and nonspecific primer annealing and mismatches were minimized. The presence of nonspecific products of amplification and primer-dimer presence were evaluated by melting curve analysis during RT-PCR primer validation. The following primers were used to amplify the transcripts of interest:

GADPH 5′: CATCAAGAAGGTGGTGAAGC
GADPH 3′: ACCACCCTGTTGCTGTAG
IL-10 5′: AAGGGTTACTTGGGTTGCCA
IL-10 3′: TTTCTGGGCCATGCTTCTCT

Fold differences of expression were calculated using the comparative method, also referred as ΔΔCt Method (Livak and Schmittgen, 2001). The sample of WT nonlesioned FN was used as the reference sample or calibrator.

Tissue Processing for Histological Analysis

Animals were deeply anesthetized as described above and perfused intracardially with 4% paraformaldehyde in 0.1 M phosphate buffer (pH 7.4). Brains were removed and postfixed in the same fixative for 4 h at 4°C and, after rinsing in phosphate buffer, cryopreserved for 48 h in a 30% sucrose solution and frozen with 2-methylbutane solution (Sigma-Aldrich). Coronal sections (30-µm-thick) of the brainstem containing the facial nucleus (FN) were obtained using a CM3050s Leica cryostat. For immunohistochemistry studies, series of parallel free-floating sections were stored at −20°C in Olmos antifreeze solution until their late use. For motor neuron survival quantification, consecutive FN sections were collected on gelatin-coated slides.

Motor Neuron Survival Quantification

Consecutive FN sections (30-µm-thick) mounted on gelatin-coated slides were stained with a solution containing 0.1% toluidine blue diluted in Wallpole buffer (0.05 M, pH 4.5). After staining, sections were dehydrated in a sequence of graded alcohols, N-butyl alcohol and xylene. Subsequently, sections were coverslipped with DPX, a nonaqueous mounting medium.

The contralateral and the ipsilateral side of every section through the entire FN were examined and photographed using a DXM1200 Nikon digital camera joined to a brightfield Nikon Eclipse E600 microscope. The photographs were analyzed with digital AnalySIS® software (Soft Imaging System). In addition to the total number of neurons, maximum and minimum diameters of neuronal profiles in the FN were recorded in order to obtain the mean diameter. To compensate for double counting neurons in adjacent sections, the Abercrombie's correction factor (Abercrombie, 1946) was applied as previously reported (Almolda et al., 2014b).

Single Immunohistochemistry

Free-floating cryostat sections were processed for the visualization of IL-10 receptor (IL-10R), Iba1, CD16/32, CD11b, CD18, Ym-1, CD150, Arginase-1, CD39, MHC-II, GFAP and CD3 markers as previously described (Almolda et al., 2011). Briefly, after 10 min of endogenous peroxidase blocking with 2% H_2O_2 in 70% methanol, sections were blocked for 1 h in 0.05 M Tris-buffered saline (TBS), pH 7.4, containing 10% foetal calf serum, 3% bovine serum albumin (BSA) and 1% Triton X-100. Subsequently, sections were incubated overnight at 4°C followed by 1 h at room temperature (RT) with rabbit anti-IL-10R (1:50; Sc-985; Santa Cruz), rabbit anti-Iba1 (1:3,000; 019-19741; Wako), rat anti-CD16/32 (1:1,000; 553142; BD Pharmingen), rat anti-CD18 (1:2,000; MCA1032G, AbD Serotec), rabbit anti-Ym-1 (1:400; 01404; Stem Cell Technology), rat anti-CD150 (1:125; MCA2274; AbD Serotec), goat anti-Arginase-1 (1:100; Sc-18354; Santa Cruz), sheep anti-CD39 (1:500; AF4398; R&D Systems), rat anti-MHC-II (1:25; TIB-120, Hybridoma supernatant ATCC), rabbit anti-GFAP (1:1,800; Z0334; Dakopatts), or hamster anti-CD3 (1:500; MCA2690; AbD Serotec) antibodies diluted in the same blocking solution. In the case of IL-10R, incubation was done for 48 h at 4°C followed by 1 h at room temperature (RT). In the case of Ym-1, all the washes were performed with TBS. Sections incubated in media lacking the primary antibody were used as negative control and spleen sections as positive control. After washes with TBS+1% Triton, sections were incubated at RT for 1 h with biotinylated anti-rabbit secondary antibody (1:500; BA-1000; Vector Laboratories; Burlingame, CA), biotinylated anti-rat secondary antibody (1:500; BA-4001; Vector Laboratories), biotinylated anti-goat secondary antibody (1:500; BA-9500; Vector Laboratories), biotinylated anti-sheep secondary antibody (1:500; BA-6000; Vector Laboratories), or biotinylated anti-hamster secondary antibody (1:500; BA-9100; Vector Laboratories) diluted in the blocking solution. After 1 h at RT in horseradish streptavidin-peroxidase (1:500; SA-5004; Vector Laboratories), the reaction was visualized by incubating the sections with a DAB kit (SK-4100; Vector Laboratories) following the manufacturer's instructions. Finally, sections were mounted on gelatin-coated slides, counterstained with toluidine blue, dehydrated in graded alcohols and, after xylene treatment, coverslipped with DPX. Sections were analyzed and photographed with a DXM 1200F Nikon digital camera joined to a Nikon Eclipse 80i microscope.

Double and Triple Immunohistochemistry

Double-immunolabelling was performed by firstly processing the free-floating sections for Iba1 as described above, but using Alexa Fluor® 488 conjugated anti-rabbit (1:1,000, A-21206; Molecular Probes) as secondary antibody. After several washes with TBS 1% Triton, sections were incubated overnight at 4°C followed by 1 h at RT with rat anti-MHC-II. Sections were then incubated for 1 h at RT in Alexa Fluor® 555 conjugated anti-rat secondary antibody (1:1,000; A31570; Molecular Probes). For the study of IL-10R colocalization, sections were processed for IL-10R staining as described above but using Alexa Fluor® 555 conjugated streptavidin instead of horseradish streptavidin-peroxidase (1:1,000; S-32355; Molecular Probes). Then, sections were incubated overnight at 4°C and 1 h at RT with mouse anti-GFAP (1:6,000; 63893, Sigma) followed by Alexa Fluor® 488-conjugated anti-mouse secondary antibody(1:1,000; A11029; Molecular Probes). Triple stain-immunolabelling combining CD3, MHC-II, and Iba1 was carried out by firstly incubating sections with CD3 as described above but using Alexa Fluor® 555 conjugated streptavidin at RT for 1 h (1:1,000; S-32355; Molecular Probes) instead of horseradish streptavidin-peroxidase. Then, sections were incubated overnight at

4°C and 1 h at RT with rat anti-MHC-II and rabbit anti-Iba1 followed by Alexa Fluor® 488-conjugated anti-rat (1:1,000; A11006; Molecular Probes) and Cy5-conjugated anti-rabbit (1:1,000; PA45004; Amersham Biosciences) secondary antibodies for 1 h at RT. Before being coverslipped with Fluoromount G™ (0100-01, SouthernBiotech), double and triple labeled sections were nuclei stained with 4′,6-diamidino-2-phenylindole (DAPI; 1:10,000; D9542; Sigma Aldrich). Colocalization was analyzed with a Zeiss LSM 700 confocal microscope.

Brightfield Microscopy Quantification

Quantitative analysis was performed on sections immunolabelled for Iba1, CD16/32, CD18 and MHC-II. At least three WT and three GFAP-IL-10Tg animals per time postaxotomy were analyzed. At least three representative sections from the brainstem containing the central part of the FN from both the contralateral and the ipsilateral sides from each animal were photographed at 10× magnification. The percentage of area covered by the immunolabelling and the intensity of the immunoreaction (Mean Gray Value) for each marker were analyzed using ImageJ® software (Wayne Rasband, National Institutes of Health). For each animal, the gray grade quotient (GGQ) was obtained by dividing the Mean Gray Value on the ipsilateral side by the Mean Gray Value on the contralateral side. The intensity grade (IG) was calculated by multiplying the percentage of the immunolabelled area by the GGQ. In the case of CD16/32 and MHC-II where staining of these molecules was absent or very low in the contralateral FN, the AI index (% Area immunolabelled multiplied by the Mean Gray Value) was used.

In order to quantify microglial cell density, sections stained for Iba1 from a minimum of five WT and five GFAP-IL-10Tg animals at 3, 7, and 28 dpi were analyzed. At least three representative sections from the brainstem containing the central part of the FN from both the contralateral and the ipsilateral FN were analyzed per animal. Three photographs of each section were taken at high magnification (40×). The total number of nucleated Iba1-positive cells were performed on each microphotograph (0.0037 mm^2 frame) using "Cell counter" plug-in from NIH Image J® software (Wayne Rasband, National Institutes of Health) and expressed as cells/mm^2.

Quantification of microglial clusters, i.e., groups of at least three or more nucleated microglial cells, was performed at 14 and 21 dpi on sections stained for Iba1, in a minimum of five WT and five GFAP-IL-10Tg animals. At least three representative sections from the brainstem containing the central part of the FN from each animal were captured at 10× magnification. The number of microglial clusters per section were obtained using "Cell counter" plug-in from NIH Image J® software (Wayne Rasband, National Institutes of Health) and expressed as Iba1 positive clusters/section.

To evaluate T lymphocyte infiltration in the FN, a minimum of five WT and five GFAP-IL-10Tg animals at 3, 7, 14, 21, and 28 dpi were used. At least three representative sections from the brainstem stained for CD3 containing the central part of the FN for each animal were captured at 10× magnification. All CD3 positive cells in each microphotograph were counted using the "Cell counter" plug-in from ImageJ® software (National Institutes of Health) and expressed as CD3 positive cells/section.

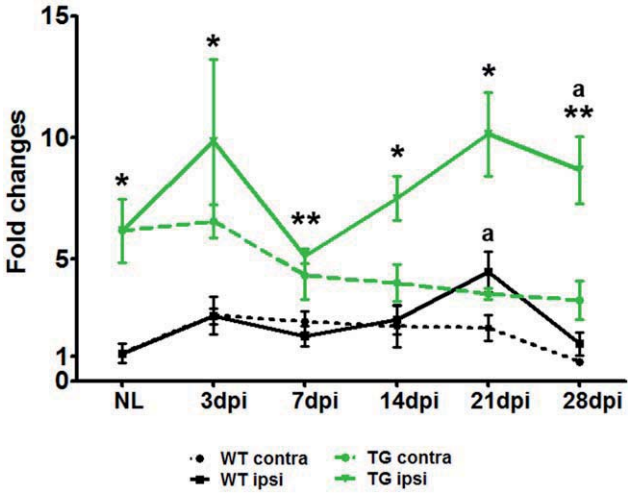

FIGURE 1: IL-10 mRNA expression levels. Graph shows IL-10 mRNA expression levels of both WT (black) and GFAP-IL-10Tg animals (green) in the nonlesioned FN (NL) as well as in the axotomized FN (continuous line) and its corresponding contralateral side (dotted line) at 3, 7, 14, 21, and 28 dpi after FNA. Levels are expressed as fold changes compared with the nonlesioned WT FN value. Note that, in the ipsilateral side of GFAP-IL-10Tg mice, IL-10 mRNA expression is always higher than the observed in WT (*$P<0.05$; **$P<0.01$). In both WT and GFAP-IL-10Tg, significant differences between the ipsilateral side and their corresponding contralateral side are indicated with letters (a: $P<0.05$). [Color figure can be viewed in the online issue, which is available at wileyonlinelibrary.com.]

Statistical Analysis

Statistics were performed using Graph Pad Prism® software and results were expressed as mean ± standard error of the mean (SEM). Statistical analysis for motor neuron survival was performed using a standard two-tailed, unpaired Student's *T* test. Two-way analysis of variance (ANOVA) was used for comparisons between groups across 3, 7, 14, 21, and 28 dpi and post hoc Bonferroni's multiple comparison test was applied to compare among groups.

Results

IL-10 mRNA Expression

Using RT-PCR quantification, we observed that although IL-10 mRNA is expressed constitutively in the nonlesioned FN of both WT and GFAP-IL-10Tg mice, expression was substantially higher in GFAP-IL-10Tg mice than in WT (Fig. 1). Similarly in lesioned animals, the amount of IL-10 mRNA was always higher in the contralateral side of GFAP-IL-10Tg animals than in the contralateral side of WT and remained unaltered along the different time-points studied. In the ipsilateral side of lesioned WT animals, IL-10 mRNA expression only increased at 21 dpi, in comparison with its corresponding contralateral; whereas in GFAP-IL-10Tg mice, the ipsilateral side (compared with its corresponding contralateral side) showed a marked increase at 28 dpi. Notably, in the ipsilateral side of GFAP-IL-10Tg mice, IL-10 mRNA

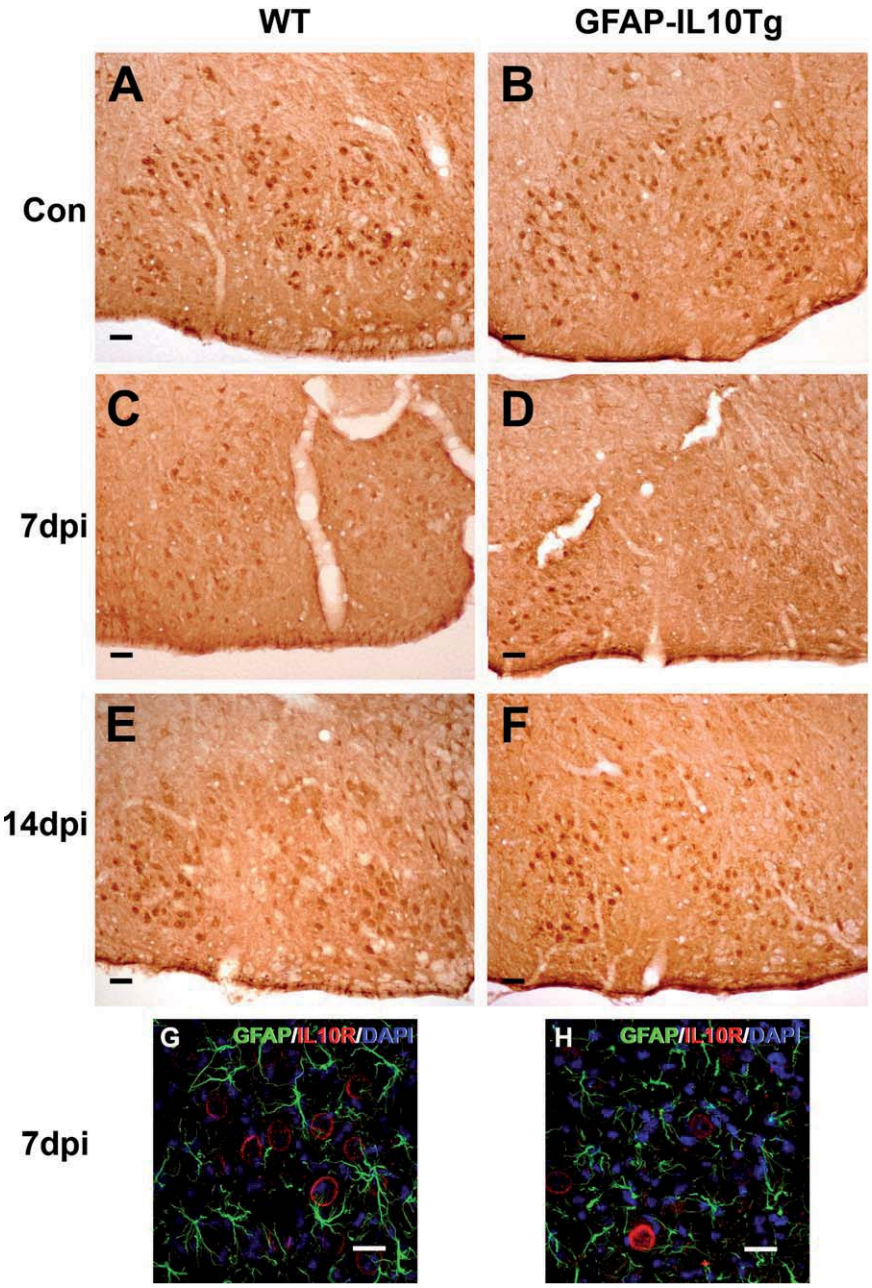

FIGURE 2: IL-10R immunhistochemistry. Representative microphotographs from WT and GFAP-IL-10Tg mice corresponding to the contralateral side at 3 dpi (Con; A and B) and the ipsilateral FN at 7 and 14 dpi (C–F). (G–H) Double immunohistochemistry combining IL-10R (red) with GFAP (green). Nuclei were stained with DAPI (blue). No colocalization of IL-10R and GFAP was observed. Scale bar (A–F) = 50 μm. Scale bar (G–H) = 20 μm. [Color figure can be viewed in the online issue, which is available at wileyonlinelibrary.com.]

expression was significantly higher than in the ipsilateral side of WT in all time-points analyzed after FNA.

IL-10R Staining

IL-10R staining was found in the FMN of the contralateral side of both WT and GFAP-IL-10Tg (Fig. 2A,B). After FNA, IL-10R staining intensity was considerably lower in the ipsilateral side of both WT and GFAP-IL-10Tg at 7 dpi (Fig. 2C,D). At 14 dpi, whereas IL-10R staining remained low in the ipsilateral side of WT, GFAP-IL-10Tg mice presented an increase in IL-10R (Fig. 2E,F). When observed at 28 dpi, GFAP-IL-10Tg showed higher IL-10R staining than WT in the ipsilateral, though, the intensity was still lower than the observed in the contralateral side. Along all time-points analyzed after FNA, IL-10R staining was restricted to the FMN and it was not detected in astrocytes, as assessed by double immunohistochemistry (Fig. 2G,H).

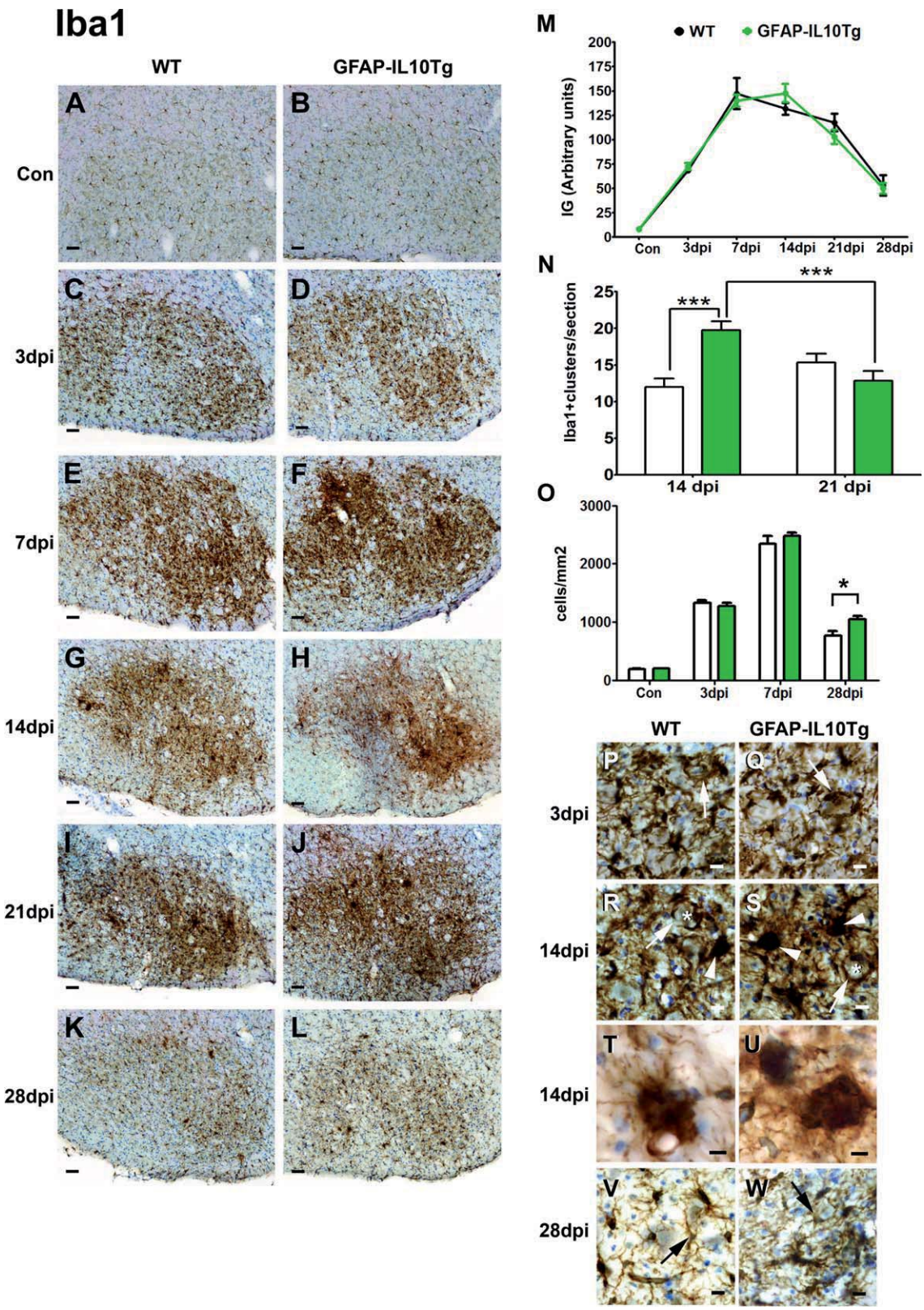

FIGURE 3: Iba1 immunohistochemistry. Representative microphotographs from WT and GFAP-IL-10Tg mice corresponding to the contralateral side at 3 dpi (Con; **A** and **B**) and the ipsilateral FN at 3, 7, 14, 21, and 28 dpi (**C–L**). (**M**) Graph showing the time course of Iba1 staining, expressed as IG (intensity grade), on the ipsilateral FN of WT and GFAP-IL-10Tg mice in comparison with their corresponding contralateral. (**N**) Graph showing the quantification of Iba1 positive microglial clusters at 14 and 21 dpi. Note that GFAP-IL-10Tg animals presented higher number of clusters/section than WT animals at 14 dpi (***$P < 0.0001$). (**O**) Graph showing the density of Iba1 positive cells in the axotomized FN. Note that at 28 dpi, Iba1 positive cell density was higher in GFAP-IL-10Tg mice (*$P < 0.05$). (**P–W**) High-magnification photographs showing the morphology of Iba1 positive microglial cells (arrows) at 3, 14, and 28 dpi. Note that at 14 dpi, microglial cells are surrounding motor neurons (*) as well as forming clusters (arrowheads in R and S, T and U). Scale bar (A–L) = 50 μm. Scale bar (P–S, V–W) = 10 μm. Scale bar (T–U) = 5 μm. [Color figure can be viewed in the online issue, which is available at wileyonlinelibrary.com.]

Microglial Activation

To assess the effects of astrocyte-targeted IL-10 production on the activation of microglial cells along the different time-points (3, 7, 14, 21, and 28 dpi) after FNA, we have analyzed the staining of Iba1, a commonly used microglial marker; CD16/32, the Fc gamma Receptor III and Fc gamma Receptor II expressed by phagocytosing microglia/macrophages; CD18, a subunit of the integrin MAC-1 expressed on the surface of some leukocytes including macrophages and related to cell adhesion; and CD150, Ym-1 and Arginase-1 as markers of alternatively activated microglia/macrophages. In addition, staining of the major histocompatibility complex II (MHC-II), involved in the process of antigen presentation; and CD39, an ectonucleotidase involved in the recruitment, activation and polarization of naive T cells (Dwyer et al., 2007) were analyzed. Due to the lack of differences between the nonlesioned FN and the contralateral side, in both WT and GFAP-IL-10Tg mice, all results relative to microglial activation analysis in the ipsilateral side along the different time-points after FNA are in reference to the corresponding contralateral side.

Iba1 *Staining.* In both WT and GFAP-IL-10Tg mice, staining of Iba1 in the contralateral side of the FN (Fig. 3A,B) at all studied time-points was observed in ramified microglial cells that were distributed homogenously throughout all the FN parenchyma without any special interaction with either facial motor neurons (FMN) or other glial cells. Moreover, the number of Iba1 positive cells in the contralateral sides was similar in WT and GFAP-IL-10Tg mice (Fig. 3O).

After FNA, noticeable changes in the morphology and density of microglial cells were observed in the ipsilateral FN of both WT and GFAP-IL-10Tg. At 3 dpi, in both WT and GFAP-IL-10Tg animals, microglial cells changed their morphology from a resting-ramified appearance to an activated appearance, i.e., enlarging their cell body, showing retraction of processes and starting to approach the FMN (Fig. 3C,D,P,Q). At this time-point, a similar increase in Iba1 staining was observed in both groups of animals (Fig. 3M). Also at this time-point, a 6 fold-increase in the number of Iba1 positive cells was observed in both WT and GFAP-IL-10Tg animals (Fig. 3O). At 7 dpi, microglial cells increased Iba1 staining (Fig. 3E,F,M) and adopted a satellite position surrounding the soma of FMN with their cell bodies and processes. At this time-point, quantitative analysis showed that the number of microglial cells increased 2 fold in both groups of animals (Fig. 3O). At 14 dpi, FMN were surrounded and completely wrapped by microglial cells but not appreciable differences were found when comparing both groups of animals (Fig. 3G-H,R-S). In addition, in both WT and GFAP-IL-10Tg, it was easy to distinguish the presence of microglial clusters which were highly stained for Iba1 (Fig. 3T,U). At this time-point, GFAP-IL-10Tg mice showed a higher number of microglial clusters compared with WT (Fig. 3N). At 21 dpi, Iba1 staining decreased in both WT and GFAP-IL-10Tg animals (Fig. 3I,J,M), however, when compared with the previous time-point, WT mice showed a slight increase in the number of microglial clusters whereas GFAP-IL-10Tg experienced a pronounced decrease (Fig. 3N). No significant changes in microglial distribution were observed in terms of FMN wrapping. At 28 dpi, a large decrease in the microglial Iba1 staining was found in both groups, but did not reach the basal levels observed in the contralateral FN (Fig. 3K,L,V,W). Also, a considerable reduction in the density of microglia was observed in both groups of animals when compared with 21 dpi, though, the number of Iba1 positive cell remained notably higher in GFAP-IL-10Tg animals (Fig. 3O).

CD18 *Staining.* In both WT and GFAP-IL-10Tg mice, CD18 stained microglial cells were observed in the contralateral side of the FN (Fig. 4A,B,N,O). In the ipsilateral side of both groups of animals, CD18 staining in microglial cells followed a similar pattern as described above for Iba1 staining (Fig. 4C–L,M) with strong CD18 staining in association with microglial clusters (Fig. 4T,U). GFAP-IL-10Tg mice showed slightly higher CD18 staining at 3 and 14 dpi when compared with WT (Fig. 4C,D,G,H,P,Q,T,U).

CD16/32 Staining. No CD16/32 staining was detected in the contralateral side of both groups of animals (Fig. 5A,B). However, after FNA, CD16/32 staining was observed in the ipsilateral FN side of both groups of animals as soon as 3 dpi (Fig. 5C,D,N,O). CD16/32 staining was always found in relation to microglial cells. A similar temporal staining pattern to that described for Iba1 immunostaining was observed in terms of CD16/32 positive cell distribution in the lesioned FN of both WT and GFAP-IL-10Tg mice (Fig. 5C–L). Moreover, in both groups, microglial clusters showed strong CD16/32 staining. In the ipsilateral FN of WT, CD16/32 staining increased from 3 dpi, peaked at 14 dpi, and progressively decreased at 21 and 28 dpi (Fig. 5M). In GFAP-IL-10Tg mice, CD16/32 staining was significantly higher than WT mice at 3 and 7 dpi (Fig. 5C–F,N–Q) and then drop at 21 dpi, showing lower levels than those observed in WT (Fig. 5I,J,R,S). Notably, in GFAP-IL-10Tg mice but not WT, an increase in CD16/32 staining was observed at 28 dpi (Fig. 5K,L,M,T,U).

Alternative *Activation Markers.* In both WT and GFAP-IL-10Tg mice, CD39 was found in ramified microglial cells as well as in blood vessels in the contralateral side. After FNA,

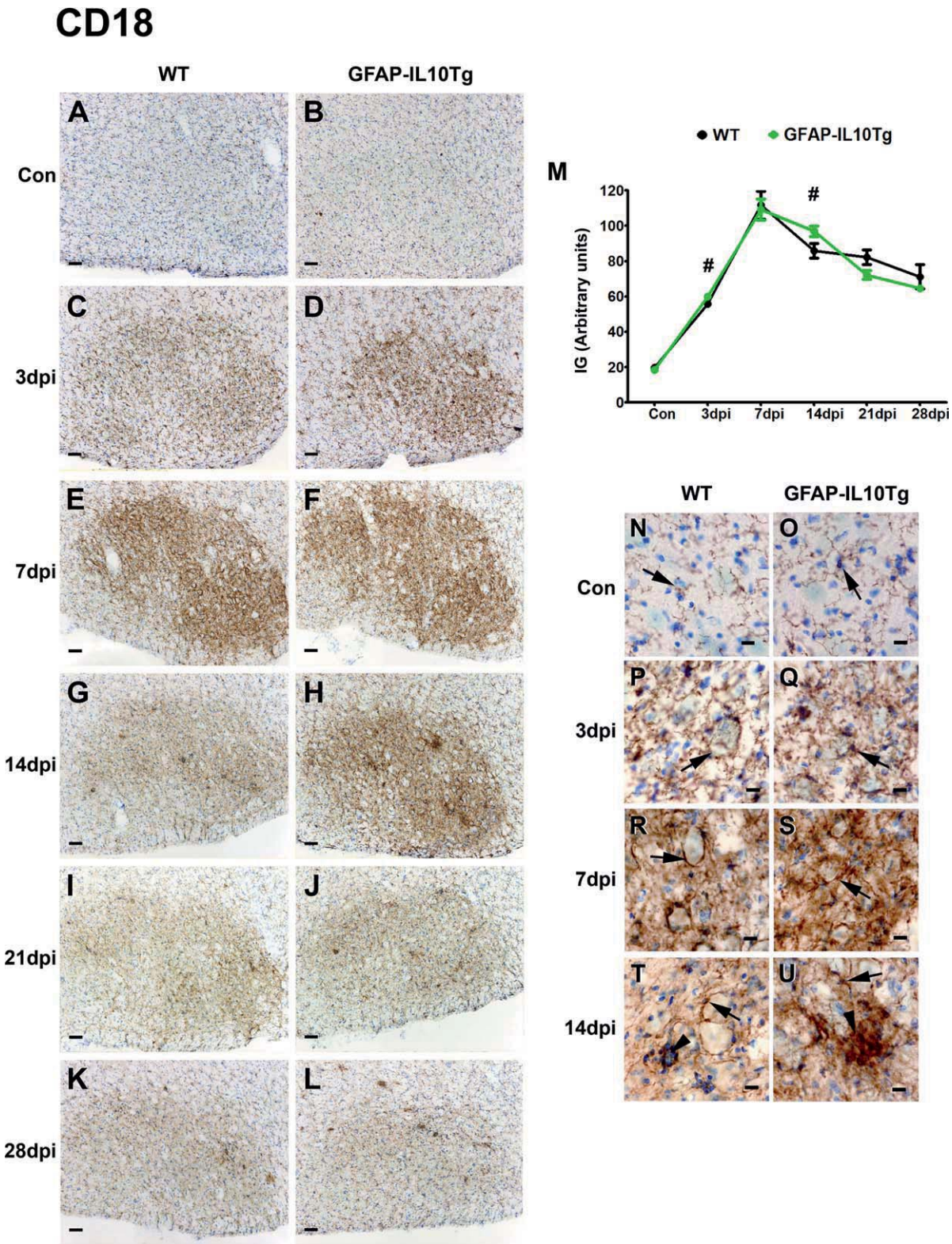

FIGURE 4: CD18 immunohistochemistry. Representative microphotographs corresponding to the contralateral side at 3 dpi (Con; A and B) and the ipsilateral FN at 3, 7, 14, 21, and 28 dpi (C–L) in WT and GFAP-IL-10Tg mice. (M) Graph showing the time course of CD18 intensity grade (IG) on the ipsilateral FN of WT and GFAP-IL-10Tg mice in comparison with their corresponding contralateral. Note that at 3 and 14 dpi, CD18 IG is higher in GFAP-IL-10Tg mice (#$P < 0.069$). (N–U) High-magnification photographs showing the morphology of CD18 positive microglial cells (arrows) in the 3 dpi contralateral (Con) and in the ipsilateral side at 3, 7, and 14 dpi. At 14 dpi, microglial clusters showed strong CD18 staining (arrowheads in T and U). Scale bar (A-L) = 50 μm. Scale bar (N-U) = 10 μm. [Color figure can be viewed in the online issue, which is available at wileyonlinelibrary.com.]

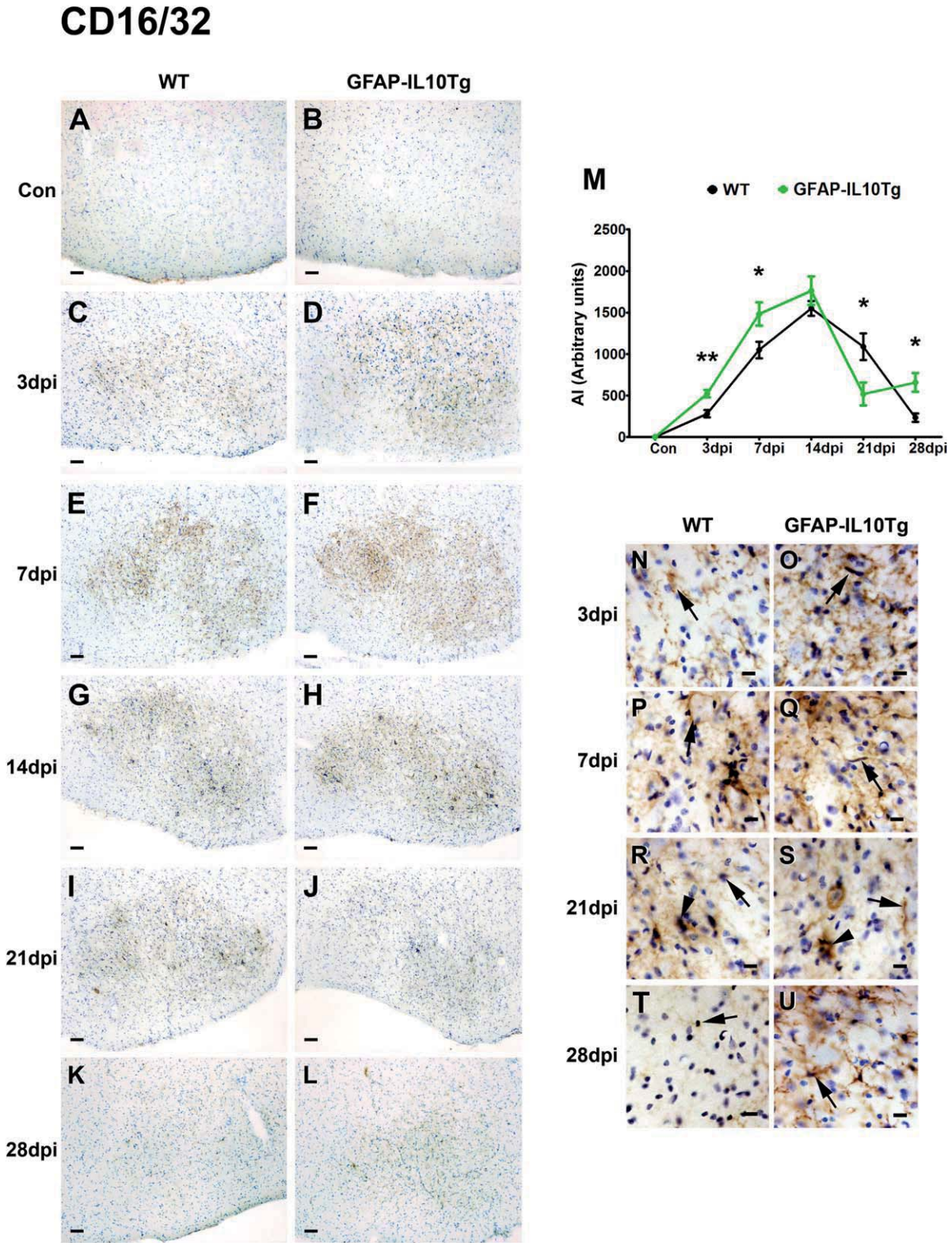

FIGURE 5: CD16/32 immunohistochemistry. Representative microphotographs corresponding to the contralateral side at 3 dpi (Con; **A** and **B**) and the ipsilateral FN at 3, 7, 14, 21, and 28 dpi (**C–L**) in WT and GFAP-IL-10Tg mice. (**M**) Graph showing the time course of CD16/32 staining on the ipsilateral FN of WT and GFAP-IL-10Tg mice in comparison with their corresponding contralateral (*$P < 0.05$; **$P < 0.01$). (**N–U**) High-magnification photographs showing the morphology of CD16/32 positive cells (arrows) in the ipsilateral FN at 3, 7 21, and 28 dpi. Note that at 21 dpi, high CD16/32 staining was found in microglial clusters (arrowheads in R and S). Scale bar (A–L) = 50 μm. Scale bar (N–U) = 10 μm. [Color figure can be viewed in the online issue, which is available at wileyonlinelibrary.com.]

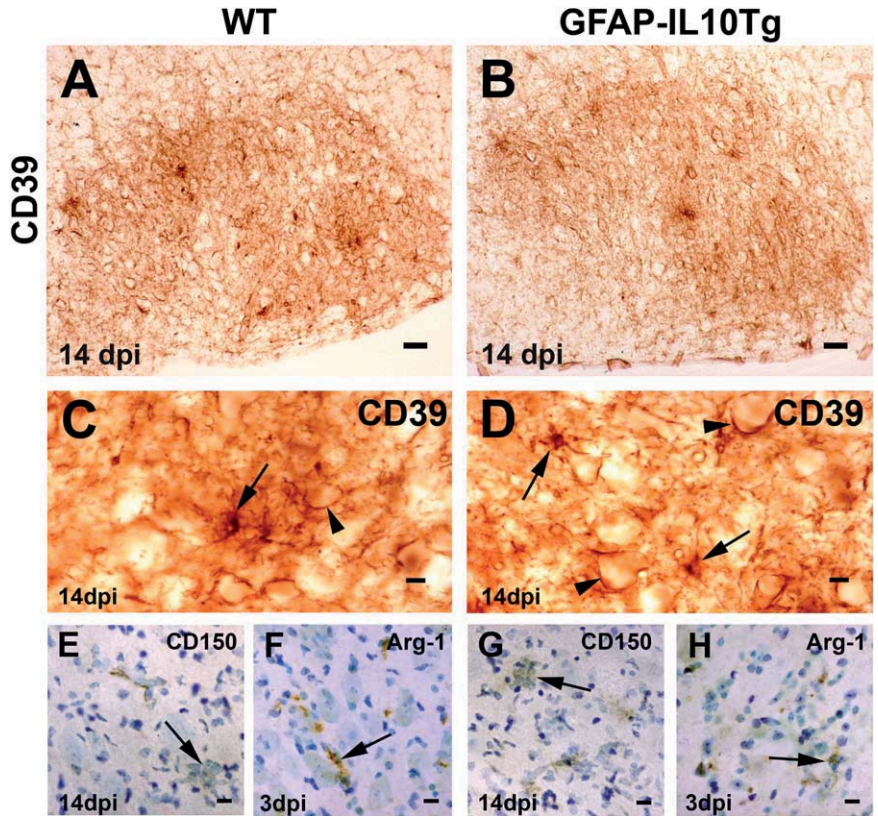

FIGURE 6: Alternative activation markers. (A and B) Representative microphotographs corresponding to the ipsilateral side of the FN stained with CD39 in WT and GFAP-IL-10Tg mice at 14 dpi. (C and D) High-magnification photographs showing CD39 staining in microglial clusters (arrows) and elongated microglial cells (arrowheads) wrapping FMN at 14 dpi. (E and G) High-magnification photographs showing faint CD150 staining associated with microglial clusters (arrows) at 14 dpi in both WT (E) and GFAP-IL-10Tg (G). (F and H) High-magnification photographs showing Arginase-1 (Arg-1) staining at 3 dpi in both WT (F) and GFAP-IL-10Tg (H). Scale bar (A and B) = 50 μm. Scale bar (C–H) = 10 μm. [Color figure can be viewed in the online issue, which is available at wileyonlinelibrary.com.]

CD39 staining resembles the pattern observed for Iba1, i.e., wrapping FMN at early time-points and forming clusters at 14 and 21 dpi (Fig. 6A–D). No marked differences were observed between the two groups of animals except that the number of clusters with CD39 positive staining was higher in the transgenic animals. Besides, CD39 staining in the blood vessels remained unaltered in both WT and GFAP-IL-10Tg along all time-points after FNA (Fig. 6A–D).

No staining of CD150, Ym-1 or Arginase-1 was found in the contralateral side of both WT and GFAP-IL-10Tg. After FNA, CD150 staining was occasionally found in both WT and GFAP-IL-10Tg in some ramified microglial-like cells along all time-points analyzed. At 14 dpi, CD150 expression was in close relationship to microglial clusters (Fig. 6E,G). No differences in CD150 distribution were observed between the two experimental groups. For Ym-1, neither WT nor GFAP-IL-10Tg mice showed staining in any of the time-points analyzed (data not shown). Arginase-1 staining was found in both WT and GFAP-IL-10Tg only at 3 dpi in some poorly ramified microglial-like cells and no differences between the two groups of animals were observed (Fig. 6F,H).

MHC-II Staining. No MHC-II staining was detected in the contralateral side of both groups of animals (data not shown). After FNA, MHC-II staining started to be detectable in the lesioned FN of both WT and GFAP-IL-10Tg animals at 7 dpi (Fig. 7A,B). Double immunohistochemistry demonstrated that MHC-II staining always colocalized with Iba1 (Fig. 7J–Q). At 7 dpi, based on their morphology, MHC-II positive cells appear to be perivascular macrophages (Fig. 7J–M) and did not associate with FMN. At 14 dpi, while MHC-II staining in WT remained similar to that observed at 7 dpi, in GFAP-IL-10Tg animals, a significant peak of MHC-II staining was observed at this time-point (Fig. 7C,D,I). At 14 dpi, in both WT and GFAP-IL-10Tg animals, in addition to perivascular macrophages, MHC-II staining was found in activated ramified microglial cells forming clusters (Fig. 7C,D,G,H,N,Q). At 21 dpi, although some ramified MHC-II positive cells were still observed in both groups (Fig. 7E,F), MHC-II staining started a progressive decrease until 28 dpi and no significant differences between WT and GFAP-IL-10Tg mice were found at these two time-points (Fig. 7I).

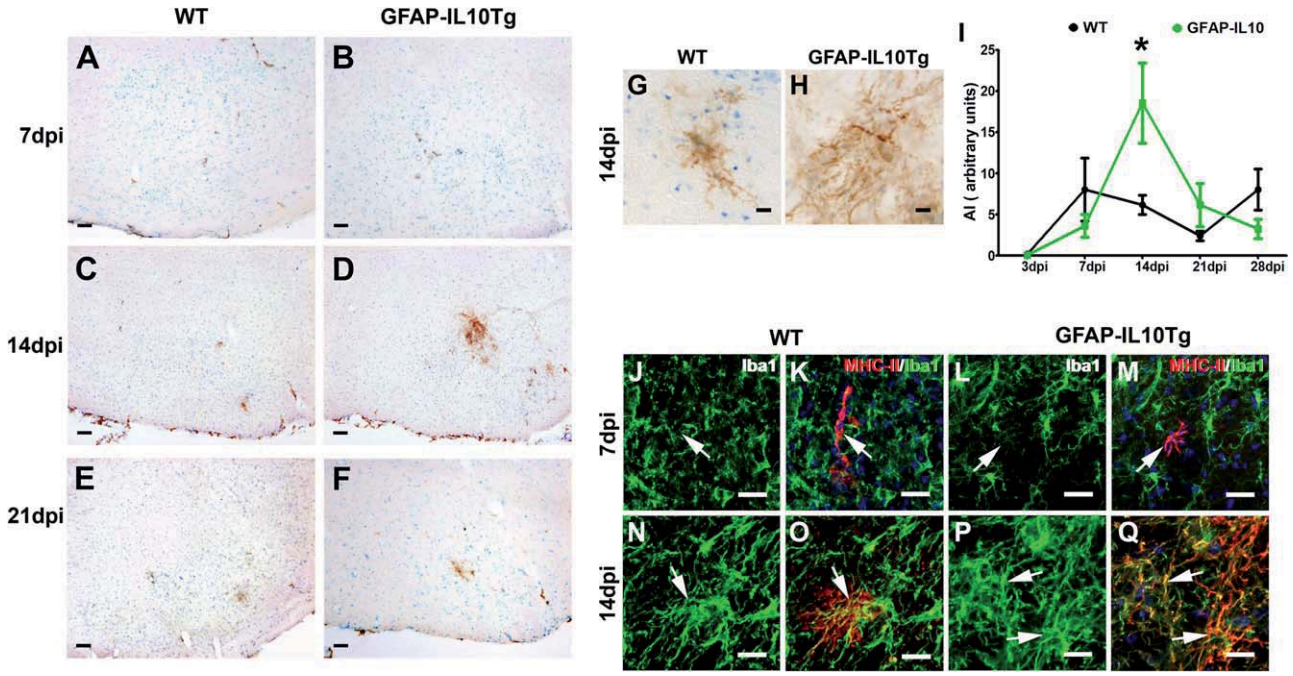

FIGURE 7: MHC-II immunohistochemistry. (A–F) Representative microphotographs corresponding to the ipsilateral side of the FN in WT and GFAP-IL-10Tg mice at 7, 14, and 21 dpi. (G–H) High-magnification photographs showing the characteristic ramified morphology of MHC-II positive cells found at 14 dpi in WT and GFAP-IL-10Tg mice. (I) Graph showing the quantification of the AI index for MHC-II in WT and GFAP-IL-10Tg animals along the different time-points after FNA. Note the higher staining of MHC-II found in GFAP-IL-10Tg mice at 14 dpi (*$P < 0.05$). (J–Q) Double immunohistochemistry combining MHC-II (red) with Iba1 (green). Yellow color indicates co-localization. Arrows point to the elongated perivascular MHC-II positive cells (J–M) or ramified MHC-II positive/Iba1 positive cells (N–Q) found in WT and GFAP-IL-10Tg animals at 7 and 14 dpi. Scale bar (A–F) = 50 μm. Scale bar (G–H, J–Q) = 10 μm. [Color figure can be viewed in the online issue, which is available at wileyonlinelibrary.com.]

Astrocyte Activation

GFAP staining was used to assess astrocyte activation. Both WT and GFAP-IL-10Tg mice presented considerably low levels of GFAP expression in the contralateral side of the FN (Fig. 8A,B). After FNA, in both groups, GFAP staining intensity started to increase at 3 dpi, reaching a maximum at 14 dpi and remaining elevated until 28 dpi (Fig. 8C–F,G). No significant differences in either distribution or intensity of GFAP between WT and GFAP-IL-10Tg mice in any of the different time-points analyzed were observed.

Lymphocyte Infiltration

To assess lymphocyte infiltration in the axotomized FN, sections immunolabelled for CD3 were analyzed. No CD3 positive cells were found in the nonlesioned FN in neither WT nor GFAP-IL-10Tg animals and in the contralateral side at any of the time-points studied (data not shown). In the ipsilateral FN of axotomized WT animals, CD3 positive cells started to be seen at 3 dpi and their number progressively increased until 21 dpi and remained similar at 28 dpi (Fig. 9A). In GFAP-IL-10Tg mice, CD3 positive cells were also detected at 3 dpi and increased reaching a peak at 21 dpi before abruptly falling in number at 28 dpi (Fig. 9A). When compared with the WT, a twofold increase in the total number of CD3 positive T-cells was found in GFAP-IL-10Tg mice at 14 and 21 dpi (Fig. 9A–C). As assessed by triple immunohistochemistry, in both WT and GFAP-IL-10Tg mice, CD3 positive cells were found in close relationship to MHC-II positive microglial clusters (Fig. 9D–I).

Neuronal Survival

To determine whether the altered phenotype of microglial cells and the increased infiltration of CD3 positive T-cells observed in GFAP-IL-10Tg animals had any effect on motor neuron survival after FNA, the total number of FMN in both the contralateral and the ipsilateral sides of the entire FN were counted on sections stained with Toluidine blue (Fig. 10). Whereas, no differences in neuronal cell number were found in the contralateral sides of both WT and GFAP-IL-10Tg mice, a significant decrease in the total number of FMN was detected in the ipsilateral sides of both groups of animals at 21 dpi (Fig. 10A–D). Notably, neuronal survival was higher in the ipsilateral FN of GFAP-IL-10Tg, where the percentage of surviving FMN was $81.49 \pm 3.12\%$, in front to the $65.41 \pm 3.16\%$ found in the ipsilateral side of WT (Fig. 10E).

Discussion

Our results showed that after FNA, GFAP-IL-10Tg mice showed significant changes in the staining of different molecules associated with the microglial activation pattern, such as

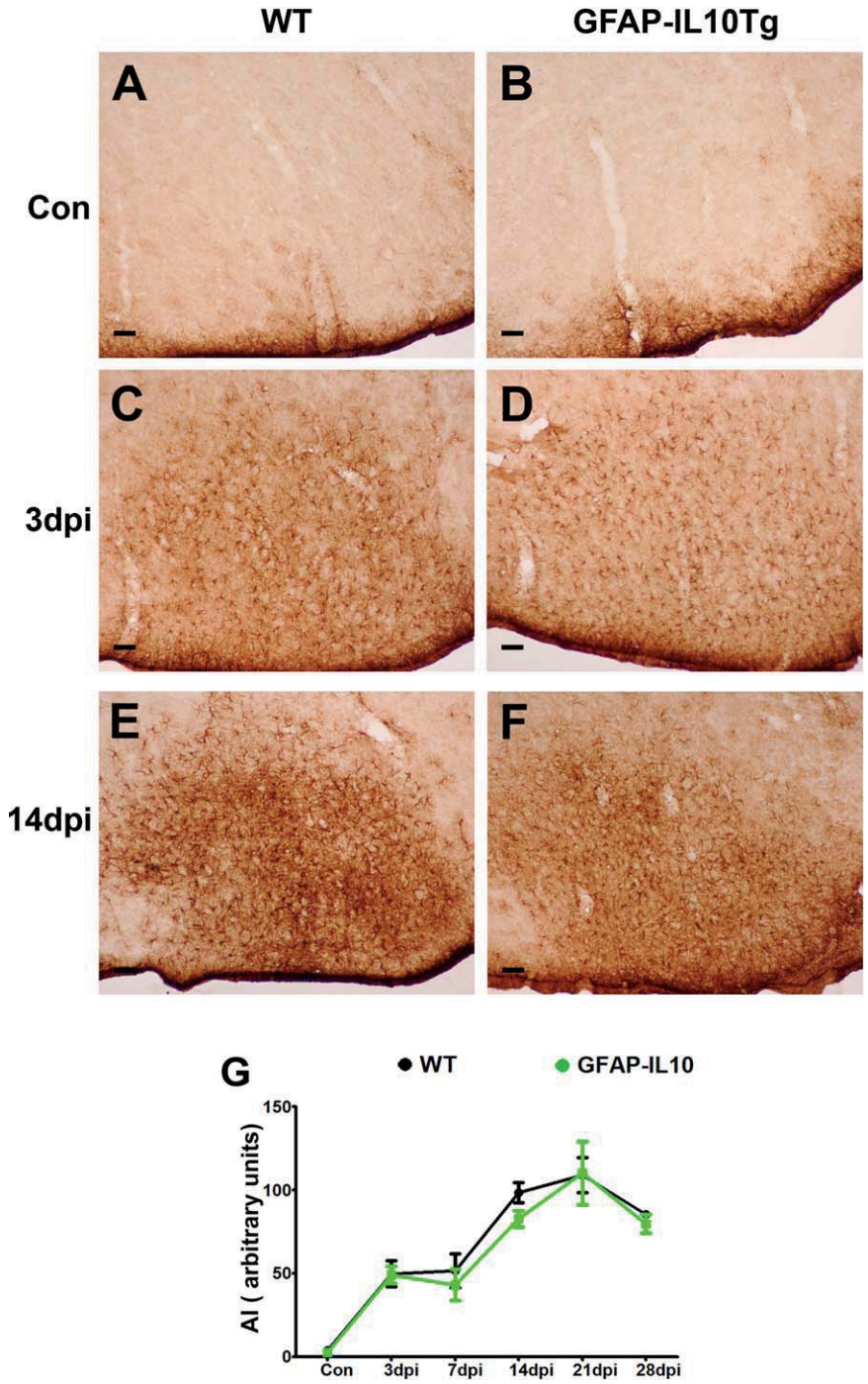

FIGURE 8: GFAP immunohistochemistry. Representative microphotographs corresponding to the contralateral side at 3 dpi (Con; A and B) and the ipsilateral FN at 3 and 14 dpi (C–F) in WT and GFAP-IL-10Tg mice. (G) Graph showing the time course of GFAP staining on the ipsilateral FN of WT and GFAP-IL-10Tg mice in comparison with their corresponding contralateral. [Color figure can be viewed in the online issue, which is available at wileyonlinelibrary.com.]

CD16/32, CD18 and MHC-II, as well as in the number of microglial clusters and in microglial cell density. Furthermore, a higher CD3 positive lymphocyte infiltration was observed on the axotomized FN of GFAP-IL-10Tg mice. These changes in microglial activation and lymphocyte recruitment correlated with a reduced motor neuron death at 21 dpi. Altogether, our findings suggest that astrocyte-targeted production of IL-10 in this paradigm exerts a beneficial effect on neuronal survival and has an impact over microglial and lymphocyte response after FNA.

Increased Neuronal Survival in GFAP-IL-10Tg Mice

Facial nerve axotomy is a well-established injury paradigm commonly used for the study of retrograde neuronal

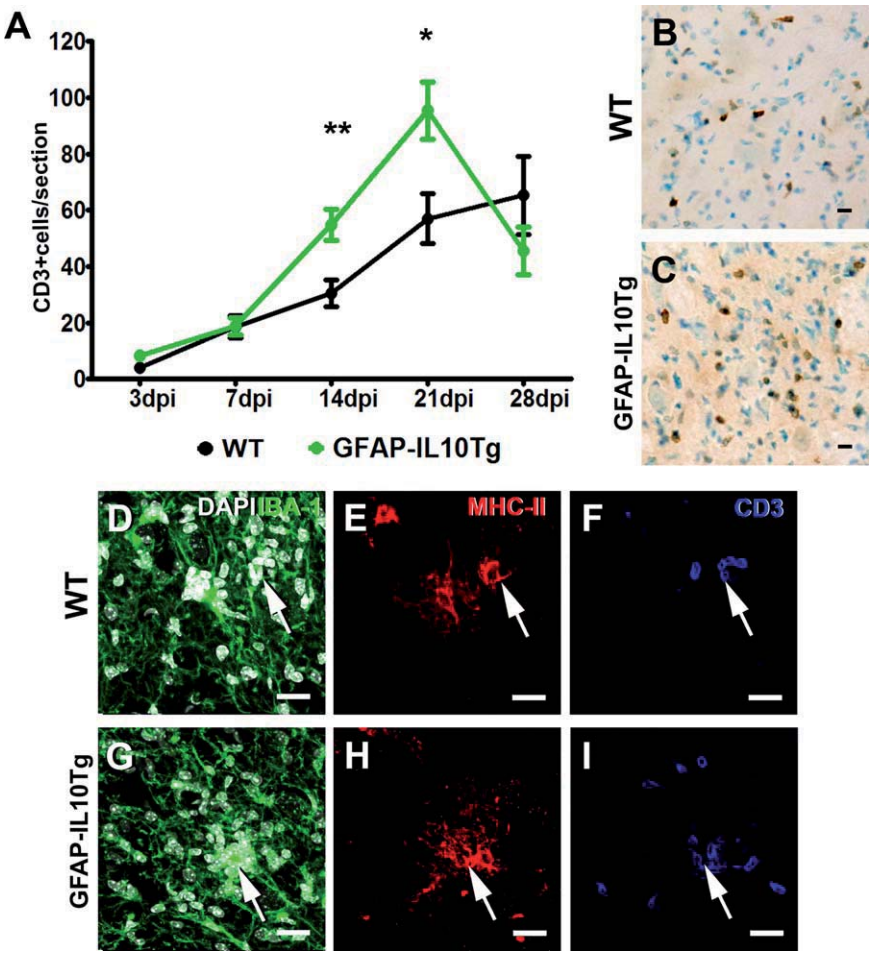

FIGURE 9: CD3 immunohistochemistry. (A) Graph showing the number of CD3 positive cells per section in the parenchyma of the axotomized FN at the different time-points after axotomy. Higher number of CD3 positive cells were observed at 14 and 21 dpi in GFAP-IL-10Tg mice ($P < 0.01$, *$P < 0.05$). (B and C) Representative microphotographs showing CD3 positive cells on both groups at 14 dpi. (D–I) Triple immunohistochemistry combining Iba1 (green), MHC-II (red), and CD3 (blue). Nuclei were stained with DAPI (white). Arrows indicate an Iba1 positive microglial cluster in WT (D–F) and GFAP-IL-10Tg mice (G–I) with numerous DAPI stained nuclei containing MHC-II positive cells (E and H). Note that CD3 positive cells are close to the microglial cluster (F and I). Scale bar (A and B) = 20 μm. Scale bar (D–I) = 25 μm. [Color figure can be viewed in the online issue, which is available at wileyonlinelibrary.com.]**

degeneration, neuronal survival and nerve regeneration (Moran and Graeber, 2004). After nerve transection in mice, most authors have reported around 20–40% of FMN loss (Ferri et al., 1998; Sendtner et al., 1996), peaking around 14 days postaxotomy (Moller et al., 1996), though, it has been reported that the total number of motor neurons can progressively decrease until 10 weeks after axotomy (Serpe et al., 2000). In our study, astrocyte-targeted IL-10 production showed a strong beneficial effect on neuronal survival. Consistent with our results, neuroprotective effects promoted by IL-10 administration have been described after focal stroke (Spera et al., 1998), excitotoxic (Brewer et al., 1999), or traumatic (Bethea et al., 1999) spinal cord injury and after peripheral sciatic nerve transection (Atkins et al., 2007). In agreement with other authors, (Xin et al., 2011), we found that FMN constitutively express IL-10R and after FNA, this expression is lower but maintained along all time-points of this study. Thus, neuroprotective actions of transgenic IL-10 could be explained by a direct effect on these motor neurons, either acting as a neurotrophic factor (Zhou et al., 2009) or preventing neuronal death (Sharma et al., 2011). In this regard, in our study IL-10 mRNA levels in GFAP-IL-10Tg mice were significantly higher in the ipsilateral side than in the corresponding contralateral side at later time-points. However, as GFAP-IL-10Tg mice presented important changes in microglial reactivity and lymphocyte infiltration, we cannot exclude that transgenic expression of IL-10 also exerts an indirect effect on both cell populations and hence it contributes to neuroprotective phenomenon we observe. Therefore, we will discuss these issues below.

Altered Microglial Reactivity in GFAP-IL-10Tg Mice After FNA

Microglial activation in the FNA paradigm has been extensively studied (Ha et al., 2006; Jinno and Yamada, 2011;

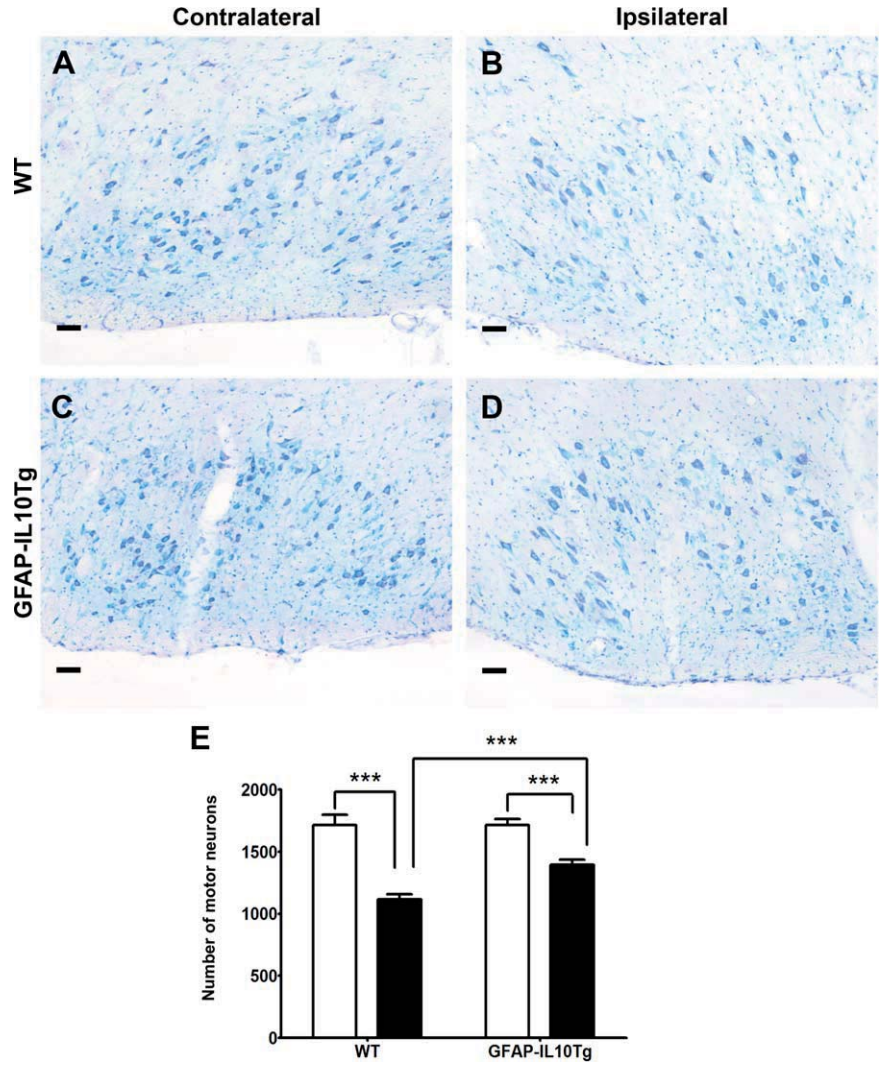

FIGURE 10: Neuronal survival. (A–D) Representative microphotographs of Toluidine blue staining showing the center of the contralateral (A and C) and the ipsilateral sides (B and D) of the FN of WT and GFAP-IL-10Tg mice at 21 dpi. (E) Graph showing the quantification of the total number of FMN in both animal groups at 21 dpi. Neuronal cell number after FNA was significantly lower in the ipsilateral side (black bars) of both WT and GFAP-IL-10Tg mice when compared with their corresponding contralateral side (white bars). Note that the number of FMN in the ipsilateral side of GFAP-IL-10Tg mice (1,394 ± 41.02) was considerably higher than WT (1115 ± 42.74) (*$P < 0.0001$). Scale bar = 50 μm. [Color figure can be viewed in the online issue, which is available at wileyonlinelibrary.com.]**

Kalla et al., 2001; Schoen et al., 1992). Within a few days after nerve transection, microglia become activated, proliferate and migrate, surrounding the axotomized FMN (Svensson et al., 1994). In these earlier stages, it has been described that perineuronal microglia or its processes are placed between the synaptic terminals and the surface of injured FMN, a phenomenon known as "synaptic stripping", in order to disconnect these neurons and allow further axonal regeneration (Graeber et al., 1993; Kreutzberg, 1996; Perry and O'Connor, 2010). At later stages after axotomy, those FMN that are not able to regenerate their axon undergo death, leading to further activation of microglia (Graeber et al., 1993). Around 28 dpi, when the functionality of regenerated FMN has been recovered, most microglial cells start to adopt a resting-ramified morphology (Almolda et al., 2014b).

These changes in morphology and distribution of microglial cells are accompanied by alterations in the level of a broad range of factors, including increased expression of cytokines, chemokines, cell adhesion molecules and markers of microglial activation, such as Iba1, CR3 complement receptors and MHC I and II (Moran and Graeber, 2004; Raivich et al., 1998b). In the present study, despite the absence of overt variation in the morphology of the cells or the amount of Iba1 staining on reactive microglial cells of GFAP-IL-10Tg animals when compared with WT, there were other changes in the phenotype of activated microglial cells in these

transgenic mice that may be closely related to the reduction in neuronal death.

A majority of these changes occurred during the early phase of microglial activation, from 3 to 14 dpi, when we observed an increase in the staining of CD16/32 and CD18 in activated microglial cells of GFAP-IL-10Tg animals, suggesting a more rapid or robust response of these cells probably due to the increased basal level of IL-10 observed in these animals. CD16/32 is a molecule extensively related to phagocytic activity (Indik et al., 1995; Jovanova-Nesic et al., 2012; Nimmerjahn and Ravetch, 2006), one of the important features displayed by microglial cells after FNA (Raivich et al., 1999; Rinaman et al., 1991). Due to the fact that in some circumstances, phagocytic activity of microglia has been linked with a beneficial role promoting the regenerative response (Neumann et al., 2009); together with the increased FMN survival detected in GFAP-IL-10Tg mice lead us to speculate that a higher microglial phagocytic activity at early time-points may support FMN survival.

In addition to changes in CD16/32, a higher staining of CD18 was found in activated microglia of GFAP-IL-10Tg mice at 3 and 14 dpi. CD18, an integrin that forms part of the complement receptor 3 (CR3), has been shown to be upregulated in microglial cells after FNA in both rats (Graeber et al., 1988; Moneta et al., 1993) and mice as early as 1 dpi (Galiano et al., 2001; Kloss et al., 1999) reaching a peak at 7 dpi, when microglial cells are wrapping the FMN. It is known that CD18 integrin is implicated in the adhesion of microglia to the axotomized FMN as well as to the infiltrated lymphocytes observed in the clusters (Kloss et al., 1999). It could be expected then, that in GFAP-IL-10Tg mice increased CD18 in microglial cells will lead to a stronger adhesion facilitating the phenomenon of "synaptic stripping" and therefore promoting a higher survival of FMN. In this regard, expression of this integrin by activated microglial cells has already been suggested to play a role in maintaining neuronal survival in this paradigm by some authors (Makwana et al., 2007). In contrast, it is also plausible that this increase in CD18 is involved and promotes the formation and preservation of microglial clusters in GFAP-IL-10Tg animals.

Moreover, our study showed that in either WT or GFAP-IL-10Tg animals activated microglia after FNA did not or barely expressed Ym-1, Arginase 1, and CD150, which are markers usually associated with the so-called alternative microglia/macrophage activation. However, in contrast, we observed high expression of CD39, an ectonucleotidase highly expressed in M2 macrophages. By regulating purine concentrations in the extracellular space, CD39 on alternative activated macrophages can reduce the ATP concentration in the extracellular environment which in turn can increase the anti-inflammatory and tissue remodeling activities of these cells (Csoka et al., 2012).

Altogether, our findings, in agreement with those of others (Aldskogius, 2011; Walter and Neumann, 2009), support the idea that microglial activation cannot be exclusively associated with harmful actions after peripheral nerve injury but rather it is a multi-faceted event that leads to neuroprotection under determined circumstances (Hao et al., 2007; Lalancette-Hebert et al., 2007).

Microglial proliferation is another important feature in the evolution of FNA (Svensson et al., 1994). At early stages after peripheral nerve injury, microglial cells undergo proliferation (Raivich et al., 1994) and, at later stages after lesion, activated microglia are gradually eliminated by programmed cell death (Jones et al., 1997), showing the maximum amount of death at 14 dpi (Conde and Streit, 2006), to achieve a steady state of microglial cell numbers. As expected, in our study the number of microglial cells significantly increased at 3 and 7 dpi on the lesioned FN. We did not find differences between WT and GFAP-IL-10Tg mice, suggesting that, in agreement with other studies (Kloss et al., 1997; Sawada et al., 1999), IL-10 production does not have a direct effect on microglial proliferation at least in this paradigm. Remarkably, at 28 dpi and coinciding with a higher IL-10 mRNA expression in GFAP-IL-10Tg mice, microglial cell density in the lesioned FN was notably higher in these animals than in WT, suggesting that overproduction of IL-10 could be protecting microglial cells in transgenic animals against programmed cell death. In this regard, it has been shown that, *in vitro*, IL-10 promotes microglial survival (Strle et al., 2002).

Increased Microglial Clustering and Lymphocyte Infiltration in GFAP-IL-10Tg Mice

One interesting difference found in our study in relation to the pattern of microglial activation in GFAP-IL-10Tg mice was the higher number of microglial clusters observed at 14 dpi. Microglial cluster formation has been commonly linked with phagocytosis of dead neurons (Raivich et al., 1998b), and some authors have used the number of microglial clusters as an indirect way to measure motor neuronal death (Petitto et al., 2003). However, we have shown that in GFAP-IL-6Tg animals a lower number of microglial clusters correlates with higher neuronal death (Almolda et al., 2014b). In the current study, we observed that GFAP-IL-10Tg mice exhibited an increased number of clusters correlating with less motor neuron cell death, indicating again that microglial cluster formation does not correlate with increased death of FMN. Changes in microglial cluster formation together with the higher CD16/32 and CD18 staining observed at earlier time-points in GFAP-IL-10Tg mice could be related to faster or more effective phagocytosis by microglial cells although,

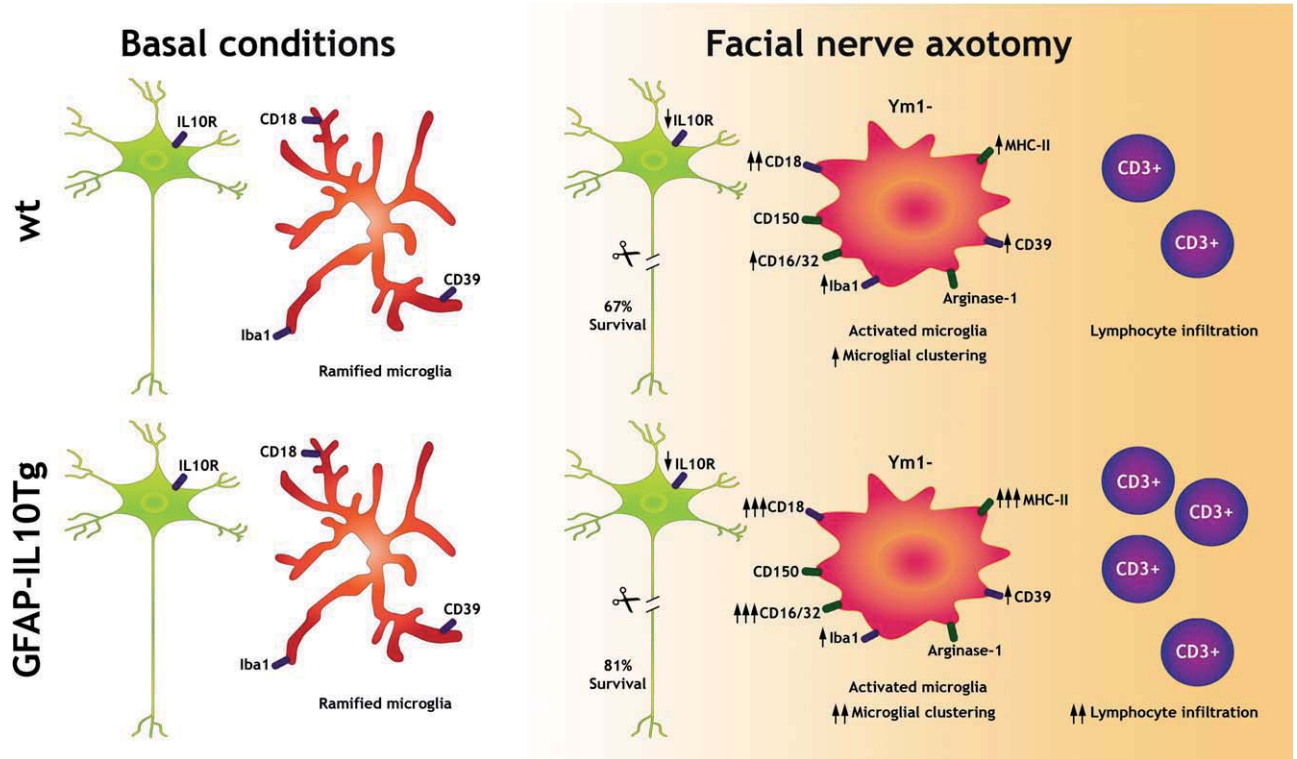

FIGURE 11: Schematic representation of the main changes after FNA in WT and GFAP-IL-10Tg mice. Basal conditions (left) in both WT (top) and GFAP-IL-10Tg mice (bottom) represented in the image showing constitutive expression of IL-10R in the FMN and CD18 and CD39 in ramified microglial cells. After FNA (right), changes in the expression of these molecules and "de novo" expression are depicted in their corresponding cells. Also, the differences in the amount of lymphocyte influx to the FN parenchyma are shown. [Color figure can be viewed in the online issue, which is available at wileyonlinelibrary.com.]

increased expression of CD39 in microglial clusters may also be related to an attenuated phagocytosis (Bulavina et al., 2013). In addition, it is also possible that microglial cluster formation may have another function rather than simple phagocytosis of degenerating neurons. Recent studies in multiple sclerosis showed the presence of microglial cell clusters in pre-active lesions with high expression of IL-10, suggesting that they may play a role as regulators of inflammation (van Horssen et al., 2012). Interestingly, MHC-II staining was found strictly in the microglial clusters of both groups of animals, with significantly higher staining in GFAP-IL-10Tg mice. The fact that GFAP-IL-10Tg animals had an increase in MHC-II staining was surprising as a down-regulatory effect of IL-10 on MHC-II expression has been described (Howard and O'Garra, 1992; Moore et al., 2001). The ability of activated microglial cells to express MHC-II after FNA has been widely described (Jones et al., 2005; Kiefer and Kreutzberg, 1991; Petitto et al., 2003) and linked to their capacity to interact with infiltrating lymphocytes (Byram et al., 2004; Olsson et al., 1992). Thus, the higher expression of this molecule in GFAP-IL-10Tg mice indicated possible changes in the microglial-lymphocyte cross-talk.

Besides microglial activation, a key event following FNA in mice is the ability of T-cells to infiltrate the FN parenchyma and aggregate around axotomized FMN (Raivich et al., 1998b). Signals involved in lymphocyte recruitment in this paradigm are poorly described. In this context, ectoenzymes and specifically ectonucleotidases are known to play an important role in leukocyte trafficking. CD39 is an ectonucleotidase associated with microglia, endothelial cells and Treg lymphocytes whose expression appears to regulate nucleotide and nucleoside-mediated signaling of lymphocyte migration and differentiation (Dwyer et al., 2007). The fact, that in our study we found expression of CD39 not only in parenchymal microglia but also in microglial cell clusters, points to this ectonucleotidase as a putative candidate to modulate lymphocyte infiltration after FNA. Numerous studies attributed a neuroprotective role to lymphocyte recruitment in this paradigm since lack of mature T and B cells leads to an increase in neuronal death after FNA (Serpe et al., 2000). Moreover, this neurodegeneration was reversed following reconstitution of mice with functional T and B cells (Serpe et al., 1999). In agreement with a putative protective role, our results showed higher T-lymphocyte infiltration in the FN parenchyma of GFAP-IL-10Tg animals at 14 and 21 dpi, correlating with an increase in neuronal survival. In both WT and GFAP-IL-10Tg animals, infiltrated CD3 positive T-cells were found in close relationship with microglial clusters

where enhanced expression of CD39 was found. As mentioned above, MHC-II staining was exclusively found in these clusters, reinforcing the idea that microglial cells might be acting as antigen presenting cells in these locations. Among the different subtypes of T-cells, specifically CD4+ Th2 cells are responsible for the neuroprotective effect in the axotomized FN (Serpe et al., 2003; Xin et al., 2008). IL-10 is known for its ability to induce the differentiation of CD4+ T-cells toward an immunoregulatory phenotype, the Tr1 cells (Groux et al., 1997). Whether CD4+ Th2 or another regulatory T-cell subtype are responsible for the neuroprotective effect in GFAP-IL-10Tg mice, as well as the activation state of these lymphocytes, need to be elucidated in further studies.

In conclusion, as summarized in Fig. 11, this study clearly demonstrated that astrocyte-targeted production of IL-10 induces an increase in neuronal survival that correlates with changes in the microglial phenotype, density and microglial clustering. This improvement in neuronal survival is also accompanied by a substantially higher T-cell recruitment to the axotomized FN. Taken together, our results suggest that IL-10 production within the CNS can lead to significant modifications in the pattern of microglial activation and T-cell infiltration and may exert a beneficial effect on the outcome of peripheral nerve injury.

Acknowledgment

Grant sponsor: Spanish Ministry of Science and Innovation; Grant number: BFU2011–27400 (to BCL); Grant sponsor: NHMRC; Grant number: 632754 (to ILC)

The authors would like to thank Miguel A. Martil and Isabella Appiah for their outstanding technical help and to Ignacio González for his help with graphic design.

References

Abercrombie M. 1946. Estimation of nuclear population from microtome sections. Anat Rec 94:239–247.

Aldskogius H. 2011. Mechanisms and consequences of microglial responses to peripheral axotomy. Front Biosci (Schol Ed) 3:857–868.

Almolda B, Costa M, Montoya M, Gonzalez B, Castellano B. 2011. Increase in Th17 and T-reg lymphocytes and decrease of IL22 correlate with the recovery phase of acute EAE in rat. PLoS One 6:e27473.

Almolda B, de Labra C, Barrera I, Gruart A, Delgado-Garcia JM, Villacampa N, Vilella A, Hofer MJ, Hidalgo J, Campbell IL, et al. 2014a. Alterations in microglial phenotype and hippocampal neuronal function in transgenic mice with astrocyte-targeted production of interleukin-10. Brain Behav Immun. pii: S0889-1591(14)00512-1. doi: 10.1016/j.bbi.2014.10.015. [Epub ahead of print]

Almolda B, Villacampa N, Manders P, Hidalgo J, Campbell IL, Gonzalez B, Castellano B. 2014b. Effects of astrocyte-targeted production of interleukin-6 in the mouse on the host response to nerve injury. Glia 62:1142–1161.

Apelt J, Schliebs R. 2001. Beta-amyloid-induced glial expression of both pro- and anti-inflammatory cytokines in cerebral cortex of aged transgenic Tg2576 mice with Alzheimer plaque pathology. Brain Res 894:21–30.

Asadullah K, Sterry W, Volk HD. 2003. Interleukin-10 therapy–review of a new approach. Pharmacol Rev 55:241–269.

Atkins S, Loescher AR, Boissonade FM, Smith KG, Occleston N, O'Kane S, Ferguson MW, Robinson PP. 2007. Interleukin-10 reduces scarring and enhances regeneration at a site of sciatic nerve repair. J Peripher Nerv Syst 12:269–276.

Benveniste EN. 1998. Cytokine actions in the central nervous system. Cytokine Growth Factor Rev 9:259–275.

Bethea JR, Nagashima H, Acosta MC, Briceno C, Gomez F, Marcillo AE, Loor K, Green J, Dietrich WD. 1999. Systemically administered interleukin-10 reduces tumor necrosis factor-alpha production and significantly improves functional recovery following traumatic spinal cord injury in rats. J Neurotrauma 16:851–863.

Blinzinger K, Kreutzberg G. 1968. Displacement of synaptic terminals from regenerating motoneurons by microglial cells. Z Zellforsch Mikrosk Anat 85: 145–157.

Bohatschek M, Kloss CU, Pfeffer K, Bluethmann H, Raivich G. 2004. B7.2 on activated and phagocytic microglia in the facial axotomy model: regulation by interleukin-1 receptor type 1, tumor necrosis factor receptors 1 and 2 and endotoxin. J Neuroimmunol 156:132–145.

Brewer KL, Bethea JR, Yezierski RP. 1999. Neuroprotective effects of interleukin-10 following excitotoxic spinal cord injury. Exp Neurol 159:484–493.

Bulavina L, Szulzewsky F, Rocha A, Krabbe G, Robson SC, Matyash V, Kettenmann H. 2013. NTPDase1 activity attenuates microglial phagocytosis. Purinergic Signal 9:199–205.

Byram SC, Carson MJ, DeBoy CA, Serpe CJ, Sanders VM, Jones KJ. 2004. CD4-positive T cell-mediated neuroprotection requires dual compartment antigen presentation. J Neurosci 24:4333–4339.

Conde JR, Streit WJ. 2006. Effect of aging on the microglial response to peripheral nerve injury. Neurobiol Aging 27:1451–1461.

Csoka B, Selmeczy Z, Koscso B, Nemeth ZH, Pacher P, Murray PJ, Kepka-Lenhart D, Morris SM, Jr., Gause WC, Leibovich SJ, Haskó G. et al. 2012. Adenosine promotes alternative macrophage activation via A2A and A2B receptors. FASEB J 26:376–386.

Dwyer KM, Deaglio S, Gao W, Friedman D, Strom TB, Robson SC. 2007. CD39 and control of cellular immune responses. Purinergic Signal 3:171–180.

Erta M, Quintana A, Hidalgo J. 2012. Interleukin-6, a major cytokine in the central nervous system. Int J Biol Sci 8:1254–1266.

Ferri CC, Moore FA, Bisby MA. 1998. Effects of facial nerve injury on mouse motoneurons lacking the p75 low-affinity neurotrophin receptor. J Neurobiol 34:1–9.

Galiano M, Liu ZQ, Kalla R, Bohatschek M, Koppius A, Gschwendtner A, Xu S, Werner A, Kloss CU, Jones LL, et al. 2001. Interleukin-6 (IL6) and cellular response to facial nerve injury: effects on lymphocyte recruitment, early microglial activation and axonal outgrowth in IL6-deficient mice. Eur J Neurosci 14:327–341.

Gonzalez P, Burgaya F, Acarin L, Peluffo H, Castellano B, Gonzalez B. 2009. Interleukin-10 and interleukin-10 receptor-I are upregulated in glial cells after an excitotoxic injury to the postnatal rat brain. J Neuropathol Exp Neurol 68: 391–403.

Graeber MB, Bise K, Mehraein P. 1993. Synaptic stripping in the human facial nucleus. Acta Neuropathol 86:179–181.

Graeber MB, Streit WJ, Kreutzberg GW. 1988. Axotomy of the rat facial nerve leads to increased CR3 complement receptor expression by activated microglial cells. J Neurosci Res 21:18–24.

Groux H, O'Garra A, Bigler M, Rouleau M, Antonenko S, de Vries JE, Roncarolo MG. 1997. A CD4+ T-cell subset inhibits antigen-specific T-cell responses and prevents colitis. Nature 389:737–742.

Ha GK, Huang Z, Streit WJ, Petitto JM. 2006. Endogenous T lymphocytes and microglial reactivity in the axotomized facial motor nucleus of mice: effect of genetic background and the RAG2 gene. J Neuroimmunol 172:1–8.

Hao HP, Doh-Ura K, Nakanishi H. 2007. Impairment of microglial responses to facial nerve axotomy in cathepsin S-deficient mice. J Neurosci Res 85: 2196–2206.

Howard M, O'Garra A. 1992. Biological properties of interleukin 10. Immunol Today 13:198–200.

Hulshof S, Montagne L, De Groot CJ, Van Der Valk P. 2002. Cellular localization and expression patterns of interleukin-10, interleukin-4, and their receptors in multiple sclerosis lesions. Glia 38:24–35.

Indik ZK, Park JG, Hunter S, Schreiber AD. 1995. The molecular dissection of Fc gamma receptor mediated phagocytosis. Blood 86:4389–4399.

Jinno S, Yamada J. 2011. Using comparative anatomy in the axotomy model to identify distinct roles for microglia and astrocytes in synaptic stripping. Neuron Glia Biol 7:55–66.

Jones KJ, Serpe CJ, Byram SC, Deboy CA, Sanders VM. 2005. Role of the immune system in the maintenance of mouse facial motoneuron viability after nerve injury. Brain Behav Immun 19:12–19.

Jones LL, Kreutzberg GW, Raivich G. 1997. Regulation of CD44 in the regenerating mouse facial motor nucleus. Eur J Neurosci 9:1854–1863.

Jones LL, Liu Z, Shen J, Werner A, Kreutzberg GW, Raivich G. 2000. Regulation of the cell adhesion molecule CD44 after nerve transection and direct trauma to the mouse brain. J Comp Neurol 426:468–492.

Jovanova-Nesic K, Shoenfeld Y, Spector NH. 2012. Aluminum excytotoxicity and neuroautotoimmunity: the role of the brain expression of CD32+ (FcgammaRIIa), ICAM-1+ and CD3xi in aging. Curr Aging Sci 5:209–217.

Kalla R, Liu Z, Xu S, Koppius A, Imai Y, Kloss CU, Kohsaka S, Gschwendtner A, Moller JC, Werner A, et al. 2001. Microglia and the early phase of immune surveillance in the axotomized facial motor nucleus: impaired microglial activation and lymphocyte recruitment but no effect on neuronal survival or axonal regeneration in macrophage-colony stimulating factor-deficient mice. J Comp Neurol 436:182–201.

Kennedy MK, Torrance DS, Picha KS, Mohler KM. 1992. Analysis of cytokine mRNA expression in the central nervous system of mice with experimental autoimmune encephalomyelitis reveals that IL-10 mRNA expression correlates with recovery. J Immunol 149:2496–2505.

Kiefer R, Kreutzberg GW. 1991. Effects of dexamethasone on microglial activation in vivo: selective downregulation of major histocompatibility complex class II expression in regenerating facial nucleus. J Neuroimmunol 34:99–108.

Kloss CU, Kreutzberg GW, Raivich G. 1997. Proliferation of ramified microglia on an astrocyte monolayer: characterization of stimulatory and inhibitory cytokines. J Neurosci Res 49:248–254.

Kloss CU, Werner A, Klein MA, Shen J, Menuz K, Probst JC, Kreutzberg GW, Raivich G. 1999. Integrin family of cell adhesion molecules in the injured brain: regulation and cellular localization in the normal and regenerating mouse facial motor nucleus. J Comp Neurol 411:162–178.

Kreutzberg GW. 1996. Microglia: a sensor for pathological events in the CNS. Trends Neurosci 19:312–318.

Lalancette-Hebert M, Gowing G, Simard A, Weng YC, Kriz J. 2007. Selective ablation of proliferating microglial cells exacerbates ischemic injury in the brain. J Neurosci 27:2596–2605.

Ledeboer A, Breve JJ, Wierinckx A, van der Jagt S, Bristow AF, Leysen JE, Tilders FJ, Van Dam AM. 2002. Expression and regulation of interleukin-10 and interleukin-10 receptor in rat astroglial and microglial cells. Eur J Neurosci 16:1175–1185.

Livak KJ, Schmittgen TD. 2001. Analysis of relative gene expression data using real-time quantitative PCR and the 2(−Delta Delta C(T)) Method. Methods 25:402–408.

Makwana M, Jones LL, Cuthill D, Heuer H, Bohatschek M, Hristova M, Friedrichsen S, Ormsby I, Bueringer D, Koppius A, et al. 2007. Endogenous transforming growth factor beta 1 suppresses inflammation and promotes survival in adult CNS. J Neurosci 27:11201–11213.

Makwana M, Raivich G. 2005. Molecular mechanisms in successful peripheral regeneration. FEBS J 272:2628–2638.

Mizuno T, Sawada M, Marunouchi T, Suzumura A. 1994. Production of interleukin-10 by mouse glial cells in culture. Biochem Biophys Res Commun 205:1907–1915.

Molina-Holgado F, Grencis R, Rothwell NJ. 2001. Actions of exogenous and endogenous IL-10 on glial responses to bacterial LPS/cytokines. Glia 33:97–106.

Moller JC, Klein MA, Haas S, Jones LL, Kreutzberg GW, Raivich G. 1996. Regulation of thrombospondin in the regenerating mouse facial motor nucleus. Glia 17:121–132.

Moneta ME, Gehrmann J, Topper R, Banati RB, Kreutzberg GW. 1993. Cell adhesion molecule expression in the regenerating rat facial nucleus. J Neuroimmunol 45:203–206.

Moore KW, de Waal Malefyt R, Coffman RL, O'Garra A. 2001. Interleukin-10 and the interleukin-10 receptor. Annu Rev Immunol 19:683–765.

Moran LB, Graeber MB. 2004. The facial nerve axotomy model. Brain Res Brain Res Rev 44:154–178.

Mosmann TR. 1991. Role of a new cytokine, interleukin-10, in the cross-regulation of T helper cells. Ann N Y Acad Sci 628:337–344.

Neumann H, Kotter MR, Franklin RJ. 2009. Debris clearance by microglia: an essential link between degeneration and regeneration. Brain 132:288–295.

Nimmerjahn F, Ravetch JV. 2006. Fcgamma receptors: old friends and new family members. Immunity 24:19–28.

Olsson T, Diener P, Ljungdahl A, Hojeberg B, van der Meide PH, Kristensson K. 1992. Facial nerve transection causes expansion of myelin autoreactive T cells in regional lymph nodes and T cell homing to the facial nucleus. Autoimmunity 13:117–126.

Park KW, Lee HG, Jin BK, Lee YB. 2007. Interleukin-10 endogenously expressed in microglia prevents lipopolysaccharide-induced neurodegeneration in the rat cerebral cortex in vivo. Exp Mol Med 39:812–819.

Perry VH, O'Connor V. 2010. The role of microglia in synaptic stripping and synaptic degeneration: a revised perspective. ASN Neuro 2:e00047.

Petitto JM, Huang Z, Lo J, Streit WJ. 2003. IL-2 gene knockout affects T lymphocyte trafficking and the microglial response to regenerating facial motor neurons. J Neuroimmunol 134:95–103.

Pousset F, Cremona S, Dantzer R, Kelley KW, Parnet P. 2001. IL-10 and IL-4 regulate type-I and type-II IL-1 receptors expression on IL-1 beta-activated mouse primary astrocytes. J Neurochem 79:726–736.

Raivich G, Bohatschek M, Kloss CU, Werner A, Jones LL, Kreutzberg GW. 1999. Neuroglial activation repertoire in the injured brain: graded response, molecular mechanisms and cues to physiological function. Brain Res Brain Res Rev 30:77–105.

Raivich G, Bohatschek M, Werner A, Jones LL, Galiano M, Kloss CU, Zhu XZ, Pfeffer K, Liu ZQ. 2003. Lymphocyte infiltration in the injured brain: role of proinflammatory cytokines. J Neurosci Res 72:726–733.

Raivich G, Haas S, Werner A, Klein MA, Kloss C, Kreutzberg GW. 1998a. Regulation of MCSF receptors on microglia in the normal and injured mouse central nervous system: a quantitative immunofluorescence study using confocal laser microscopy. J Comp Neurol 395:342–358.

Raivich G, Jones LL, Kloss CU, Werner A, Neumann H, Kreutzberg GW. 1998b. Immune surveillance in the injured nervous system: T-lymphocytes invade the axotomized mouse facial motor nucleus and aggregate around sites of neuronal degeneration. J Neurosci 18:5804–5816.

Raivich G, Moreno-Flores MT, Moller JC, Kreutzberg GW. 1994. Inhibition of posttraumatic microglial proliferation in a genetic model of macrophage colony-stimulating factor deficiency in the mouse. Eur J Neurosci 6:1615–1618.

Rinaman L, Milligan CE, Levitt P. 1991. Persistence of fluoro-gold following degeneration of labeled motoneurons is due to phagocytosis by microglia and macrophages. Neuroscience 44:765–776.

Sabat R. 2010. IL-10 family of cytokines. Cytokine Growth Factor Rev 21:315–324.

Samoilova EB, Horton JL, Chen Y. 1998. Acceleration of experimental autoimmune encephalomyelitis in interleukin-10-deficient mice: roles of interleukin-10 in disease progression and recovery. Cell Immunol 188:118–124.

Sawada M, Suzumura A, Hosoya H, Marunouchi T, Nagatsu T. 1999. Interleukin-10 inhibits both production of cytokines and expression of cytokine receptors in microglia. J Neurochem 72:1466–1471.

Schoen SW, Graeber MB, Kreutzberg GW. 1992. 5′-Nucleotidase immunoreactivity of perineuronal microglia responding to rat facial nerve axotomy. Glia 6:314–317.

Sendtner M, Gotz R, Holtmann B, Escary JL, Masu Y, Carroll P, Wolf E, Brem G, Brulet P, Thoenen H. 1996. Cryptic physiological trophic support of motoneurons by LIF revealed by double gene targeting of CNTF and LIF. Curr Biol 6:686–694.

Serpe CJ, Coers S, Sanders VM, Jones KJ. 2003. CD4+ T, but not CD8+ or B, lymphocytes mediate facial motoneuron survival after facial nerve transection. Brain Behav Immun 17:393–402.

Serpe CJ, Kohm AP, Huppenbauer CB, Sanders VM, Jones KJ. 1999. Exacerbation of facial motoneuron loss after facial nerve transection in severe combined immunodeficient (scid) mice. J Neurosci 19:RC7.

Serpe CJ, Sanders VM, Jones KJ. 2000. Kinetics of facial motoneuron loss following facial nerve transection in severe combined immunodeficient mice. J Neurosci Res 62:273–278.

Sharma S, Yang B, Xi X, Grotta JC, Aronowski J, Savitz SI. 2011. IL-10 directly protects cortical neurons by activating PI-3 kinase and STAT-3 pathways. Brain Res 1373:189–194.

Spera PA, Ellison JA, Feuerstein GZ, Barone FC. 1998. IL-10 reduces rat brain injury following focal stroke. Neurosci Lett 251:189–192.

Streit WJ, Walter SA, Pennell NA. 1999. Reactive microgliosis. Prog Neurobiol 57:563–581.

Strle K, Zhou JH, Broussard SR, Venters HD, Johnson RW, Freund GG, Dantzer R, Kelley KW. 2002. IL-10 promotes survival of microglia without activating Akt. J Neuroimmunol 122:9–19.

Svensson M, Eriksson P, Persson J, Liu L, Aldskogius H. 1994. Functional properties of microglia following peripheral nerve injury. Neuropathol Appl Neurobiol 20:185–187.

Trinchieri G 2007. Interleukin-10 production by effector T cells: Th1 cells show self control. J Exp Med 204:239–243.

van Horssen J, Singh S, van der Pol S, Kipp M, Lim JL, Peferoen L, Gerritsen W, Kooi EJ, Witte ME, Geurts JJ, et al. 2012. Clusters of activated microglia in normal-appearing white matter show signs of innate immune activation. J Neuroinflammation 9:156.

Walter L, Neumann H. 2009. Role of microglia in neuronal degeneration and regeneration. Semin Immunopathol 31:513–525.

Werner A, Kloss CU, Walter J, Kreutzberg GW, Raivich G. 1998. Intercellular adhesion molecule-1 (ICAM-1) in the mouse facial motor nucleus after axonal injury and during regeneration. J Neurocytol 27:219–232.

Xin J, Wainwright DA, Mesnard NA, Serpe CJ, Sanders VM, Jones KJ. 2011. IL-10 within the CNS is necessary for CD4+ T cells to mediate neuroprotection. Brain Behav Immun 25:820–829.

Xin J, Wainwright DA, Serpe CJ, Sanders VM, Jones KJ. 2008. Phenotype of CD4+ T cell subsets that develop following mouse facial nerve axotomy. Brain Behav Immun 22:528–537.

Zhou Z, Peng X, Insolera R, Fink DJ, Mata M. 2009. IL-10 promotes neuronal survival following spinal cord injury. Exp Neurol 220:183–190.

PURINE SIGNALING AND MICROGLIAL WRAPPING

Bernardo Castellano*, Mar Bosch-Queralt, Beatriz Almolda, Nàdia Villacampa, and Berta Gonzàlez

Unit of Histology, Torre M5. Dept. Cell Biology, Physiology and Immunology. Institute of Neurosciences. Universitat Autònoma de Barcelona.
08193 Bellaterra, Spain.

Abstract. Microglial cells are highly dynamic cells with processes continuously moving to survey the surrounding territory. Microglia possess a broad variety of surface receptors and subtle changes in their microenvironment cause microglial cell processes to extend, retract, and interact with neuronal synaptic contacts. When the nervous system is disturbed, microglia activate, proliferate and migrate to sites of injury in response to alert signals. Released nucleotides like ATP and UTP are among the wide range of molecules promoting microglial activation and guiding their migration and phagocytic function. The increased concentration of nucleotides in the extracellular space could be involved in the microglial wrapping found around injured neurons in various pathological conditions, especially after peripheral axotomy. Microglial wrappings isolate injured neurons from synaptic inputs and facilitate the molecular dialog between endangered or injured neurons and activated microglia. Astrocytes too may participate in neuronal ensheathment. Degradation of ATP by microglial ecto-nucleotidases and the expression of various purine receptors might be decisive in regulating the function of enwrapping glial cells and in determining the fate of damaged neurons, which may die or may regenerate their axons and survive.

Keywords: ATP, adenosine, CD39, eat-me signals, neuronal degeneration, nerve injury, microglial migration, phagocytosis, purine receptors, axotomy

* Corresponding author. e-mail: bernardo.castellano@uab.cat

Table 1. List of abbreviations

ADP	Adenosine diphosphate
AMP	Adenosine monophosphate
ATP	Adenosine triphosphate
CNS	Central nervous system
CREB	cAMP response element-binding protein
DAMPs	Damage associated molecular patterns
DAP12	DNAX activation protein of 12 kDa
EAE	Experimental autoimmune encephalomyelitis
ECM	Extracellular matrix
ENTPDase	Ecto-Nucleotide triphosphate diphosphohydrolase
GABA	Gamma-aminobutyric acid
IRF8	Interferon regulatory factor 8
KO	Knock-out
LPS	Lipopolysaccharide
NMDA	N-methyl-D-aspartate
PAMPs	Pathogen associated molecular patterns
PPT	Perforant path transection
SAMPs	Self-associated molecular patterns
TGF	Transforming growth factor
TLRs	Toll-like receptors
TREM2	Triggering Receptor Expressed on Myeloid cells 2
UDP	Uridine diphosphate
UTP	Uridine triphosphate

1 'Resting' microglia in the healthy CNS and their interaction with the microenvironment

The term quiescent or resting microglia, usually used to designate non-activated microglia in the normal adult central nervous system (CNS), might lead one to think that these cells are in a dormant state with no apparent movement and function. However, nothing could be further from the truth. The combined use of in vivo time-lapse transcranial two-photon microscopy and transgenic mice with green fluorescent protein in resident CNS microglia has made it possible to see microglia interacting with other cortical elements (Davalos et al. 2005; Nimmerjahn et al. 2005). Microglial cells are the most dynamic cells in the healthy CNS, as their morphological changes far exceed those of both neurons (Holtmaat et al. 2008; Knott and Holtmaat 2008) and astrocytes (Hirrlinger et al. 2004). Thus, in the healthy brain, microglial cells are continuously remodelling their shape by extending and retracting their processes, surveying the local microenvironment to scan the surface of the surrounding cells and the interstitial fluid (Davalos et al. 2005; Nimmerjahn et al. 2005). Under normal conditions, each microglial cell seems to be responsible for checking its own territory, and its highly dynamic processes do not overlap or enter in the territory of neighbouring microglial cells. While the microglial soma and main branches remain stable in the nervous parenchyma, with few signs of movement and without any clear relationship to other cells or blood vessels, its motile processes are continuously making direct contacts with nearby neuronal cell bodies, macroglia and blood vessels (Nimmerjahn et al. 2005; Wake et al. 2009; Tremblay et al. 2010). Although it might appear at first glance that motility of microglial processes is random (Nimmerjahn et al. 2005), a wide range of studies indicates that microglial cells express a broad variety of surface receptors that allows them to sense subtle changes in the microenvironment (Kierdorf and Prinz 2013). In particular, in the healthy adult brain, movement of microglial processes seems to be closely related to local concentration of some neurotransmitters, neuropeptides and neuromodulators (Pocock and Kettenmann 2007). Although not conclusive, the current data suggest that microglial motility is increased by global excitatory neurotransmission and decreased by global inhibitory neurotransmission (Eyo and Wu 2013; Nimmerjahn et al. 2005; Fontainhas et al. 2011).

Furthermore, electron microscopic studies demonstrate that, under normal conditions, microglial cell processes directly contact presynaptic and postsynaptic elements and have a special predilection for excitatory synapses (Fig.1) although the existence of microglial cell interactions with inhibitory synapses under normal physiological conditions remains yet unknown (Siskova and Tremblay 2013; Perry and O'Connor 2010). Microglial cell processes contact synapses about once per hour, remain in a close proximity to presynaptic boutons for 5 min, and then retract (Wake et al. 2009). The interactions between microglia and synapses depend on neuronal activity and, therefore, the frequency of contact declines with decreased synaptic transmission (Wake et al. 2009).

2 Signaling mechanisms involved in activation of microglia

Microglia are activated by various changes in their microenvironment caused by acute insults and chronic disease states (Kettenmann et al. 2011; Gonzalez et al. 2014; Chen et al. 2014). Transformation of the finely branched resting microglia into enlarged cells with short and stout processes is a hallmark of microglial cell activation (Kettenmann et al. 2011). In addition to morphological changes, microglial activation involves a stereotypical pattern of changes, including proliferation and migration to sites of injury, increased or de novo expression of cytokines and growth factors and, in some circumstances, the full transformation into phagocytes capable of clearing damaged cells and debris (Kettenmann et al. 2011). There is a wide range of molecules promoting microglial activation that can be classified as two main types: PAMPs (Pathogen associated molecular patterns) and DAMPs (damage associated molecular patterns). PAMPs warn of the presence of exogenous material, such as components of bacterial cell walls or repeats of bacterial or viral nucleic acids, whereas DAMPs

warn of internal damage to the cells of the own organism and include molecules released by injured cells or modified as a consequence of tissue damage, such as oxidized lipoproteins or fragments of extracellular matrix molecules (Bianchi 2007; Matzinger 2007). Microglial cells possess a wide range of surface molecules, such as toll-like receptors (TLRs) (Lehnardt 2010), scavenger receptors (Husemann et al. 2002) and numerous cytokine and chemokine receptors, whose interaction with DAMPs and PAMPs results in a rapid activation of resting microglia to become motile effector cells (Kierdorf and Prinz 2013).

However, it would be a mistake to think that activation of microglia is a simple event; on the contrary, it is complex and includes still unidentified signaling mechanisms. In the healthy CNS, microglia exhibit a deactivated phenotype due to the interaction of inhibitory receptors (Off receptors) in their plasma membrane, with the corresponding ligands (Self-associated molecular patterns or SAMPs) located on neurons and glial cells that keep microglia in a resting or non-activated stage (Biber et al. 2007; Eyo and Wu 2013; Kierdorf and Prinz 2013), (Fig. 1). Some of the proposed inhibitory receptors in microglia are CX3CR1 and CD200R, which interact with their respective ligands, CX3CL1 (fractalkine) and CD200 on the surface of healthy neurons (Chertoff et al. 2013; Eyo and Wu 2013). Another proposed microglial inhibitory system is CD45/CD22. Recognition of CD22 on the surface of neurons by CD45 on microglia dampens microglial activation (Mott et al. 2004). Moreover, in addition to displaying membrane bound Off-signals, neurons also release soluble Off-signals into the extracellular space, such as TGF-, neurotransmitters and neurotrophins including NGF, BDNF and NT-3 (Biber et al. 2007). If any of these Off-signals are lost, due to changes in the microenvironment, or are downregulated, as may occur in pathological conditions, microglial activation is triggered.

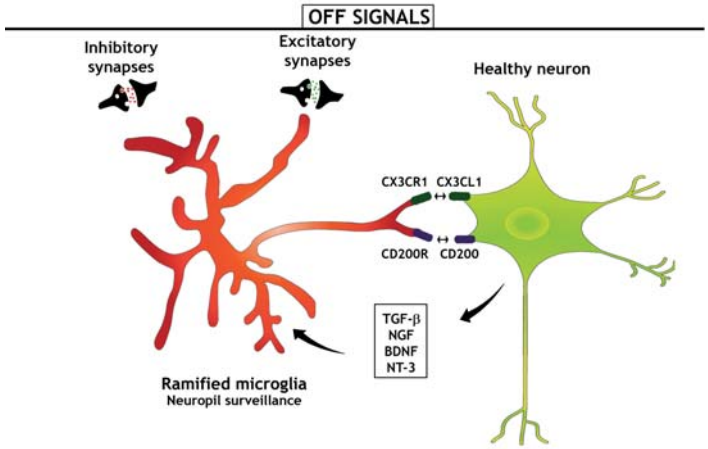

Fig. 1. In the healthy normal brain, ramified microglia is a very dynamic cell and their processes are continuously extending and retracting, monitoring the surface of neurons and having a special predilection for excitatory synapses. Interaction between inhibitory receptors in microglia with both specific ligands in the neuronal surface and neuronal released molecules keeps microglia in a non-activated state. These signals that are expressed constitutively are known as *Off-signals*.

In contrast to Off-signals, which are expressed constitutively in the healthy adult brain, On-signals are produced on demand to initiate either a pro- or anti-inflammatory microglial activation program (Kettenmann et al. 2013) (Fig. 2). Some of the On-signals are the so-called help-me/find-me molecules (Marin-Teva et al. 2011; Panatier and Robitaille 2012; Xing et al. 2014). When neurons are overactive, impaired or endangered, they release these "alert" signals (Noda et al. 2013) which include nucleotides such as ATP and UTP (Sperlagh and Illes 2007); chemokines such as CCL21 and CXCL10 (Rappert et al. 2004; de Jong et

al. 2005); cytokines like Interleukin 1 (Cartier et al. 2005); neuropeptides such as bradykinin (Ifuku et al. 2007), endothelin (Fleisher-Berkovich et al. 2010), galanin (Ifuku et al. 2011) and neurotensin (Martin et al. 2005); neurotransmitters such as glutamate, adrenaline and dopamine (Liu et al. 2009; Farber et al. 2005); and cannabinoids (Walter et al. 2003) and morphine (Takayama and Ueda 2005). In response to help-me/find-me signals, microglia approach to the source of these molecules and develop either a close surveillance or a phagocytic function, depending on the presence of additional signals in the damaged neuron. If the receptor SIRP-alpha (CD172a) in the membrane of microglia interacts with the ligand CD47 on neurons, a Do-not-eat-me signal is presented to microglia (Biber et al. 2007; Ravichandran 2010). However, if the microglial receptor TREM2 (Triggering Receptor Expressed on Myeloid cells 2) recognizes its still-unknown-ligand on the surface of the damaged neuron, this interaction is interpreted as an Eat-me signal and therefore the microglial cell is able to initiate an intracellular signaling cascade, through the adaptor protein DAP12, leading to phagocytosis (Linnartz and Neumann 2013). TREM2 expression has been suggested to regulate not only phagocytic but also the migratory capacity of microglia (Melchior et al. 2010).

3 Migration of microglia is guided by purinergic signaling

Release of danger signals that act as chemoattractants at the site of damage, initiates microglial activation and stimulates migration. Time-lapse two-photon imaging demonstrates that, for example, after a small laser ablation in the cerebral cortex, all microglial cells located in the surroundings respond within minutes by enlarging and extending their processes towards the damaged site, converging and forming a spherical shaped containment around it, but without migration of the somata (Davalos et al. 2005; Nimmerjahn et al. 2005). Quick extension of microglial processes to the site of injury without significant displacement of the cell body was previously described using histological sections (Jensen et al. 1994). In this work we showed that, a few hours after a perforant path transection (PPT), microglial cells located in the inner zone of the dentate molecular layer polarise and extend their processes towards and into the denervated PP zone, and it is not until 2-3 days after PPT when microglial cell bodies move to the denervated PP zone, where they accumulate and proliferate (Jensen et al. 1994). Therefore, migration of microglial cells is probably a complex process that involves two stages: a first phase of reconnaissance and damage assessment by microglial cells processes and, if damage persists and is important enough, a second phase where the entire cell body migrates. An intense cross-talk, involving the signaling mechanisms referred in the previous section, between extended microglial processes and damaged neurons and glial cells, will determine this microglial cell migration.

Purine nucleotides are among the most potent molecules involved in the migration of microglia. In fact, (Davalos et al. 2005) demonstrated that ATP or ADP microinjection in the brain parenchyma was able to mimic the rapid chemotactic response of microglial processes observed following laser ablation. Moreover, lowered ATP extracellular concentration results in reduced microglial cell process movements, whereas increased ATP gradients stimulate their motility (Haynes et al. 2006). In the healthy brain, release of ATP to the extracellular space is a common phenomenon, as this nucleotide and its derivatives act both as primary transmitter and as co-transmitter released with other neurotransmitters and peptides in many synapses. The mechanism by which intracellular ATP is released by neurons is a matter of intense debate (Cisneros-Mejorado et al. 2015), because in addition to being released by exocytosis, ATP leakage can also take place through large pores and transporters. Moreover, not only neurons but also glial cells, in particular astrocytes, can release ATP (Butt 2011; Cisneros-Mejorado et al. 2015). Under pathological conditions when neurons are overexcited, injured or stressed in acute or chronic neurological disorders, a massive release of ATP takes place into the extracellular space (Braun et al. 1998; Melani et al. 2005). As elevated concentrations of extracellular ATP can cause cell death (Matute et al. 2007; Ar-

beloa et al. 2012), ATP released from endangered or dying cells may aggravate the extent of the ongoing damage. In addition, increased extracellular levels of ATP may over activate the P2X7R in neurons and trigger signaling cascades leading to neurodegeneration (Le Feuvre et al. 2003). The concentrations of ATP, ADP, AMP and adenosine in the extracellular space are regulated by the activity of ecto-nucleotidases that are located in the plasma membrane of microglia and whose expression is dependent on the development and activation stage of these cells (Dalmau et al. 1998). One of these ecto-nucleotidases is CD39, also called Ecto-nucleoside triphosphate diphosphohydrolase 1 (E-NTPDase1), whose expression in the CNS is restricted to microglial cells and vascular endothelium (Braun et al. 2000). CD39 plays a main role hydrolysing extracellular nucleoside 5-triphosphates to nucleoside 5-diphosphates (NTPase enzymatic activity), as well as nucleoside 5-diphosphates to nucleoside 5-monophosphates (NDPase enzymatic activity). Nucleoside 5-monophosphates are further hydrolysed to adenosine by CD73, an ecto-5-nucleotidase also found, among other cells, in the membrane of microglia (Dalmau et al. 1998; Bulavina et al. 2013). Therefore, microglial cells could be considered as the cells responsible for the regulation of purinergic signaling in the CNS as they can control the rate, extent and timing of nucleotide degradation. On the other hand, we should consider that microglial cells have several types of purine receptors in on their surface (Ohsawa and Kohsaka 2011) whose interactions with changing concentrations of extracellular nucleotides and nucleosides (ATP/adenosine balance) may regulate microglial behaviour, including process extension and retraction, microglial migration and even phagocytosis.

Purine receptors are divided into P1 (adenosine receptors) and P2 (ATP receptors). Microglia express the four subtypes of P1 receptors (A1, A3, A2A and A2B) and only some of the different subtypes of P2 receptors cloned, which are divided into ionotropic (seven subtypes: P2X1-7) and metabotropic (eight subtypes: P2Y1, -2, -4, -6, -11, -12, -13, and -14) (Kettenmann et al. 2011). Simultaneous co-stimulation of P1 and P2 receptors seems to be required for microglial migration (Farber et al. 2008). In particular, microglial process extension is dependent upon ATP/ADP sensed through microglial P2Y12 receptors (Ohsawa and Kohsaka 2011), which are constitutively expressed on microglia in normal conditions (Sasaki et al. 2003) and upregulated when activated (Tozaki-Saitoh et al. 2008). P2Y12 receptors activate integrin-1, which accumulates in the tips of microglial processes, facilitating the adhesion of extended microglial processes with the extracellular matrix (ECM), which is a requisite for subsequent directional microglial migration (Haynes et al. 2006; Kurpius et al. 2007). Further activation of microglia, probably due to continuously elevated levels of ATP and ADP, or both (Kurpius et al. 2007), leads to upregulation of A2A and P2X4 receptors, whereas P2Y12 receptors are downregulated (Haynes et al. 2006; Orr et al. 2009). Signalling through P2X4 receptors enhances migration of microglia. As microglial activation involves increased expression of the ecto-enzymes CD39 and CD73 (causing ATP/ADP degradation), the abnormally increased levels of ATP generated by the pathological situation are gradually reduced, while the adenosine concentration increases and activates A2A receptors. Notably, adenosine causes retraction of microglial processes (Ohsawa and Kohsaka 2011). Therefore, gradually increased levels of adenosine may be the basis of microglial transformation from ramified cells into amoeboid migratory morphologies, usually found in various pathologies.

4 Microglial wrapping and synaptic stripping

It has been widely reported that activated microglia migrate and accumulate near injured neurons in various pathological conditions. In addition, in certain circumstances, the somata, proximal dendrites and axons of injured neurons become ensheathed by microglia. Microglial wrapping of neuronal cell bodies is one of the most prominent features after peripheral nerve axotomy (Fig. 3). Indeed, the phenomenon of microglial wrapping has been widely described in various CNS areas in several situations involving peripheral nerve axotomy, including the facial nucleus (Moran and Graeber 2004), the hypoglossal nucleus (Sumner

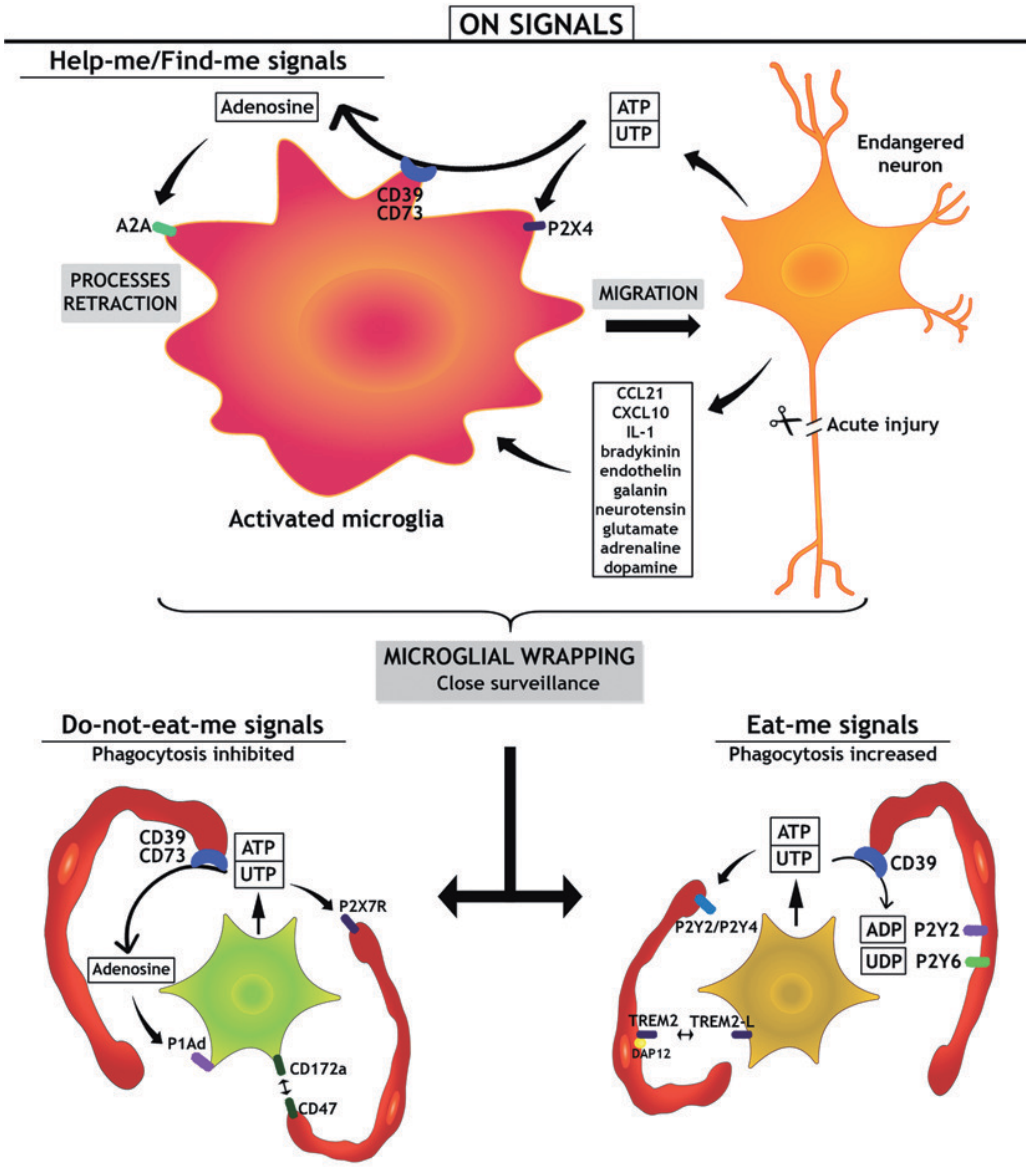

Fig. 2. On signals are produced when neurons are damaged and include *Help-me/Find-me*, *Do-not-eat-me*, and *Eat-me signals*. Endangered neurons may release a wide range of alert signals *(Help-me/Find-me)* including nucleotides that promote microglial activation, process retraction and migration towards neuronal somata. Microglial wrapping in one hand facilitates contact-dependent neuron-microglia interactions but also isolates damaged neurons leaking nucleotides. If *Do-not-eat-me* signaling predominates phagocytosis are inhibited and neurons are able to survive. If, on the contrary, *Eat-me* signaling prevails, an increase in the phagocytic ability of microglia takes place and damaged neurons are removed. Note the importance of the ecto-enzymes CD39 and CD73 regulating the levels of nucleotides and nucleosides in the extracellular space around injured neurons.

and Sutherland 1973; Yamada et al. 2011), the dorsal motor nucleus of the vagus nerve (Masui et al. 2002), and in the spinal cord after sciatic nerve axotomy (Gehrmann et al. 1991). Also, this phenomenon has been reported in experimental models where peripheral nerves are not affected such as hippocampal organotypic cultures after an ischemic insult (Neumann et al. 2006), in the cerebral cortex during either acute focal inflammation (Trapp et al. 2007) or following intraperitoneal LPS injection (Chen et al. 2012), and in the spinal cord after experimental autoimmune encephalomyelitis (EAE) induction (Almolda et al. 2009). Microglial wrapping occurs in parallel with a significant reduction of axosomatic synapses. It was (Blinzinger and Kreutzberg 1968) who first described, following facial nerve axotomy, the displacement of presynaptic terminals from the injured motor neuron surface by the interposing of microglial pseudopods and named this phenomenon as synaptic stripping. Although some authors claim that reactive microglia spread on the surface of motor neurons to physically disconnect synapses (Moran and Graeber 2004; Yamada et al. 2008), it is still not totally clear whether synaptic stripping is either the cause or the consequence of microglial wrapping. As microglial wrapping and synaptic stripping are associated with motor neuron regeneration, it has usually been considered to be a neuroprotective process (Kreutzberg 1996). As we will discuss below, recent studies support this neuroprotective view (Chen et al. 2014), whereas others suggest that microglial wrapping may reduce neuronal survival (Yamada et al. 2011).

Accumulating evidence indicate that synaptic striping of either inhibitory or excitatory synapses is beneficial to damaged neurons. Since microglia wrap neuronal cell bodies and the majority of synapses terminating on projection neuron somata in the cerebral cortex are GABAergic inhibitory synapses, it has been proposed that inhibitory axosomatic synapses are preferentially stripped after focal inflammation or peripheral immune challenge (Trapp et al. 2007; Chen et al. 2012). Evidence of microglia-mediated stripping of inhibitory GABAergic presynaptic terminals from cortical neurons in adult mice has been recently confirmed by 3D electron microscopy (Chen et al. 2014). Reduced axosomatic GABAergic innervation protects neurons against noxious insult (Hardingham et al. 2002) by increasing synchronization of neuronal firing (Woo and Lu 2006), which is critical for synaptic NMDAR-mediated neuronal survival through CREB activation and by increasing neuronal expression of anti-apoptotic and neuroprotective molecules (Hardingham and Bading 2003). However, it is nowadays clear that microglial wrapping is not always specifically directed to disconnect inhibitory synapses because in other locations, such as the facial nucleus in the rat after nerve axotomy (Raslan et al. 2014) and the spinal cord after either intramedullary axotomy in the cat (Linda et al. 2000) or sciatic nerve transection in the rat (Arbat-Plana et al. 2015), the outcome of microglia-mediated synaptic stripping is the preferential disconnection of excitatory glutamatergic synapses. Removal of the glutamatergic input to the axotomized motor neurons is considered relevant for neuronal survival, as glutamate may exert deleterious excitotoxic effects on nerve cells (Mehta et al. 2013). In support of this possibility, blocking of the NMDA-type glutamate receptor has been reported to increase motor neuron survival after neonatal axotomy in the rat (Mentis et al. 1993). Even assuming that any changes in the synaptic input, either inhibitory or excitatory, to the lesioned neurons may reduce their stress and be beneficial for survival and repair, the question of whether microglia actively participate in this process or if instead nerve terminals simply retract from the surface of neurons remains unsolved (Linda et al. 2000). It is generally accepted that synaptic stripping does not inevitably mean that the disconnected terminals have to be immediately engulfed by microglia, as they remain in the vicinity of ensheathed neurons and only after axotomized motor neurons regenerate their axons, synapses are restored (Navarro et al. 2007). However, some work indicates that, several weeks after nerve transection, restored synaptic inputs are not normal (Raslan et al. 2014). The usual prevalence of inhibitory over excitatory terminals seems to be shifted for surviving lesioned motor neurons in various locations (Borke et al. 1995; Linda et al. 2000; Raslan et al. 2014). Although microglia have been suggested to play a main role in regulating these synaptic rearrangements (Raslan et al. 2014), astrocytes

might also be involved (Tyzack et al. 2014). In the healthy brain, neurons, including their synapses, are generally ensheathed by fine processes of astrocytes that participate in the regulation of synapse formation, stability, and elimination. Coverage of synapses by astrocytic processes may change under various physiological conditions (Theodosis et al. 2008; Chung et al. 2013; Perez-Alvarez et al. 2014). Specifically, in the facial nerve of the mouse two weeks after axotomy, thin lamellar astrocyte processes begin to replace microglial wrapping around damaged motor neurons, and by 3 weeks they completely cover the neuron soma (Moran and Graeber 2004). Some authors have suggested that this delayed astrocyte behaviour might contribute to synaptic remodelling by engulfing some disconnected presynaptic terminals (Chung et al. 2013) and promoting the rearrangement of synaptic inputs on axotomized motor neurons (Tyzack et al. 2014).

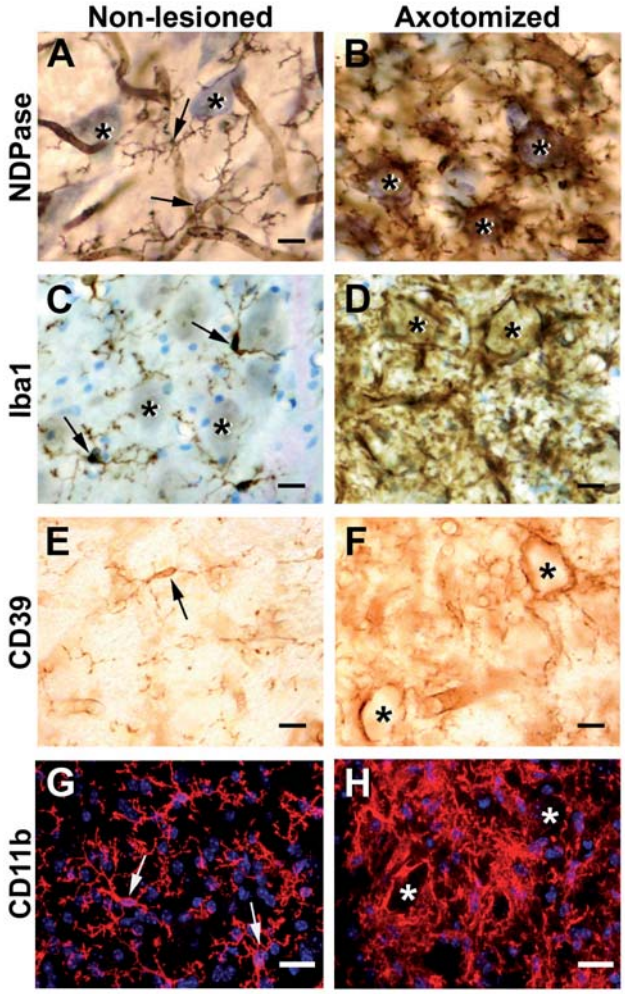

Fig. 3. Microglial wrapping in the facial nucleus of the mouse after facial nerve axotomy. In the normal, non-lesioned facial nucleus, microglia stained with different markers including NDPase histochemistry; an immunohistochemistry against Iba1, CD39 and CD11b **(A,C,E,G)**, appear as ramified cells (arrows) without any particular association with neuronal motor neuron somata (asterisks). After axotomy **(B, D, F, H)**, microglia enwrap motor neuron somata (asterisks). In A-D, sections are counterstained with toluidine blue. In G and H nuclei are stained in blue with DAPI. Scale bar=20μm.

5 Microglial wrapping: detrimental or beneficial

Glial wrapping, whether microglial, astroglial or both, may not only cause deafferentation, but might also facilitates contact-dependent neuronglia interactions that prevent neuron death and promote regeneration. After facial nerve axotomy in the mouse, for example, about 65 per cent of axotomized neurons regenerate axons and survive, whereas 35 per cent of neurons degenerate. Research in our laboratory performing facial nerve axotomy on transgenic mice with astrocyte-targeted expression of either IL6 or IL10 in order to investigate how the local expression of those cytokines may affect microglial activation, showed that in addition to changes in the microglial reactivity pattern, there is an altered survival/death ratio of motor neurons (Almolda et al. 2014; Villacampa et al. 2015). Interestingly, higher motor neuron survival in IL10 transgenic mice was not associated with significant changes in microglial wrapping (Villacampa et al . 2015) although increased motor neuronal death in IL6 transgenic mice coincides with reduced microglial wrapping (Almolda et al. 2014). Moreover, ongoing studies performed on IRF8 KO mice indicate that incomplete microglial wrapping of individual axotomized motor neurons correlates with increased motor neuron death (Xie et al. 2014). In agreement with this, some evidence suggests that defects in microglia-neuron attachment after facial nerve axotomy, as occurs in microglial cathepsin deficient mice (Hao et al. 2007) and TGF-b1 deficient animals (Makwana et al. 2007), might lead to more neuron death. These observations support the hypothesis that the intimate association between glial cells and neurons has a neurotrophic rather than neurotoxic function. The close physical proximity of microglia to injured neurons may facilitate the continuous supply of growth factors and other required molecules, thus supporting survival and regeneration (Trapp et al. 2007).

There is however an opposing view holding the possibility that prolonged contact of microglial cells with enwrapped neurons is detrimental (Yamada et al. 2011). Some studies have demonstrated that the survival ratio of injured motor neurons is markedly influenced by the species and the age of animals used (Kiryu-Seo et al. 2005; Moran and Graeber 2004). Interestingly, in this context, facial nerve axotomy in neonatal rats and mice kills damaged motor neurons within a week of lesion. Nevertheless, axotomized motor neurons in adult rats are able to survive, whereas in adult mice there is a slow and progressive motor neuron death after lesion (Kiryu-Seo et al. 2005). Some authors have suggested that these differences among adult rats and mice are due to differences in the ratio of microglial/astroglial wrapping (Yamada et al. 2011). If the astrocytic wrapping predominates, as found in the rat, some protective effects are exerted on axotomized motoneurons, whereas if the wrapping is mainly microglial, as observed in mouse, a slow apoptotic cell death of motor neurons might take place (Yamada et al. 2011).

Microglial wrapping may be the result of a continuous release or leakage of purine nucleotides that act as find-me signals, (Fig. 2). Neuron ensheathment by activated microglia expressing ecto-nucleotidases in their plasma membrane effectively isolates damaged neurons leaking purine nucleotides and contributes to their rapid degradation to adenosine around neurons. Increasing concentrations of extracellular adenosine may develop a potentially neuroprotective function on neurons through P1 adenosine receptors (Stone 2002). In addition, adenosine can impair the phagocytic function of peripheral macrophages by binding to the P1 adenosine receptors expressed on their membrane (Hasko et al. 2007). Also, microglial phagocytosis seems to be regulated by purinergic signaling (Bulavina et al. 2013). It has been shown that activation of P1 receptors by a non-hydrolysable analog of adenosine decreases microglial phagocytosis (Bulavina et al. 2013). In the opposite way, activation of P2Y12 receptor by ADP, activation of P2Y6 by UDP and activation of P2Y2/P2Y4 receptors by UTP markedly increase microglial phagocytosis both in vitro and in vivo (Koizumi et al. 2007; Fang et al. 2009). Therefore, the increasing concentration of these nucleotides around injured neurons may be an eat-me signal for wrapping microglia. In agreement with this, CD39-deficient animals presented higher microglial phagocytic activity (Bulavina et al. 2013), suggesting that an increased concentration of extracellular ATP/ADP and

UTP/UDP, due to the lack of CD39 enzymatic activity, leads to a chronic stimulation of the microglial phagocytic activity. However, other studies indicate that activation of P2X7 receptors by exposure to ATP induced inhibition of microglial phagocytic activity even if microglia are co-treated with UDP (Fang et al. 2009). Taken together, these observations suggest that a fine control of the levels of nucleosides and nucleotides in the extracellular space around injured neurons together with a fine regulation of purine receptors may be decisive to control phagocytosis and hence in determining the fate of damaged neurons wrapped by microglia.

6 Concluding remarks

The meaning of microglial wrapping around injured neurons is not completely understood. Microglial wrapping partially isolates endangered neurons from the adjacent neuropil, leading to an important deafferentation from synaptic inputs. Besides, the wide area of contact between microglia and neuronal surfaces enables an intense exchange of molecular signals between them. Injured neurons circumscribed by microglia may survive or die and their fate will depend on a plethora of signals. In this scenario, nucleosides and their phosphorylated nucleotides may play a key role, as they can be involved in regulation of apoptosis, in the synthesis and release of different trophic factors by astrocytes (Rathbone et al. 1999), in promotion of axonal growth (Heine et al. 2006), and in modulation of microglial phagocytosis (Inoue 2008). Although programmed neuronal cell death can result from axonal injury, cell regeneration and axonal outgrowth programs are also activated (Raivich and Makwana 2007; Kiryu-Seo and Kiyama 2011). The putative involvement of microglia and astroglia in the activation of these regenerative programs are still poorly understood and will be a challenge for researchers in the coming years.

Acknowledgments. This work was supported by the Spanish Ministry of Science and Innovation BFU2011-27400 and BFU2014-55459-P.

References

1. Almolda B, Costa M, Montoya M, Gonzalez B, Castellano B (2009) CD4 microglial expression correlates with spontaneous clinical improvement in the acute Lewis rat EAE model. J Neuroimmunol 209 (1-2):65-80. doi:S0165-5728(09)00031-9 [pii]10.1016/j.jneuroim.2009.01.026
2. Almolda B, Villacampa N, Manders P, Hidalgo J, Campbell IL, Gonzalez B, Castellano B (2014) Effects of astrocyte-targeted production of interleukin-6 in the mouse on the host response to nerve injury. Glia 62 (7):1142-1161. doi:10.1002/glia.22668
3. Almolda B, Villacampa N, Manders P, Hidalgo J, Campbell IL, Gonzalez B, Castellano B (2014) Effects of astrocyte-targeted production of interleukin-6 in the mouse on the host response to nerve injury. Glia 62 (7):1142-1161. doi:10.1002/glia.22668
4. Arbat-Plana A, Torres-Espin A, Navarro X, Udina E (2015) Activity dependent therapies modulate the spinal changes that motoneurons suffer after a peripheral nerve injury. Exp Neurol 263:293-305. doi:S0014-4886(14)00345-8 [pii] 10.1016/j.expneurol.2014.10.009
5. Arbeloa J, Perez-Samartin A, Gottlieb M, Matute C (2012) P2X7 receptor blockade prevents ATP excitotoxicity in neurons and reduces brain damage after ischemia. Neurobiol Dis 45 (3):954-961. doi:S0969-9961(11)00389-5 [pii] 10.1016/j.nbd.2011.12.014
6. Bianchi ME (2007) DAMPs, PAMPs and alarmins: all we need to know about danger. J Leukoc Biol 81 (1):1-5. doi:jlb.0306164 [pii] 10.1189/jlb.0306164
7. Biber K, Neumann H, Inoue K, Boddeke HW (2007) Neuronal 'On' and 'Off' signals control microglia. Trends Neurosci 30 (11):596-602. doi:S0166-2236(07)00248-2 [pii] 10.1016/j.tins.2007.08.007
8. Blinzinger K, Kreutzberg G (1968) Displacement of synaptic terminals from regenerating motoneurons by microglial cells. Z Zellforsch Mikrosk Anat 85 (2):145-157
9. Borke RC, Bridwell RS, Nau ME (1995) The progression of deafferentation as a retrograde reaction to hypoglossal nerve injury. J Neurocytol 24 (10):763-774

10. Braun N, Sevigny J, Robson SC, Enjyoji K, Guckelberger O, Hammer K, Di Virgilio F, Zimmermann H (2000) Assignment of ecto-nucleoside triphosphate diphosphohydrolase-1/cd39 expression to microglia and vasculature of the brain. Eur J Neurosci 12 (12):4357-4366. doi:ejn1342 [pii]
11. Braun N, Zhu Y, Krieglstein J, Culmsee C, Zimmermann H (1998) Upregulation of the enzyme chain hydrolyzing extracellular ATP after transient forebrain ischemia in the rat. J Neurosci 18 (13):4891-4900
12. Bulavina L, Szulzewsky F, Rocha A, Krabbe G, Robson SC, Matyash V, Kettenmann H (2013) NTPDase1 activity attenuates microglial phagocytosis. Purinergic Signal 9 (2):199-205. doi:10.1007/s11302-012-9339-y
13. Butt AM (2011) ATP: a ubiquitous gliotransmitter integrating neuron-glial networks. Semin Cell Dev Biol 22 (2):205-213. doi:S1084-9521(11)00036-X [pii]10.1016/j.semcdb.2011.02.023
14. Cartier L, Hartley O, Dubois-Dauphin M, Krause KH (2005) Chemokine receptors in the central nervous system: role in brain inflammation and neurodegenerative diseases. Brain Res Brain Res Rev 48 (1):16-42. doi:S0165-0173(04)00116-X [pii] 10.1016/j.brainresrev.2004.07.021
15. Cisneros-Mejorado A, Perez-Samartin A, Gottlieb M, Matute C (2015) ATP signaling in brain: release, excitotoxicity and potential therapeutic targets. Cell Mol Neurobiol 35 (1):1-6. doi:10.1007/s10571-014-0092-3
16. Chen JL, Villa KL, Cha JW, So PT, Kubota Y, Nedivi E (2012) Clustered dynamics of inhibitory synapses and dendritic spines in the adult neocortex. Neuron 74 (2):361-373. doi:S0896-6273(12)00267-X [pii]10.1016/j.neuron.2012.02.030
17. Chen Z, Jalabi W, Hu W, Park HJ, Gale JT, Kidd GJ, Bernatowicz R, Gossman ZC, Chen JT, Dutta R, Trapp BD (2014) Microglial displacement of inhibitory synapses provides neuroprotection in the adult brain. Nat Commun 5:4486. doi:ncomms5486 [pii] 10.1038/ncomms5486
18. Chertoff M, Shrivastava K, Gonzalez B, Acarin L, Gimenez-Llort L (2013) Differential modulation of TREM2 protein during postnatal brain development in mice. PLoS One 8 (8):e72083. doi:10.1371/journal.pone.0072083 PONE-D-13-15299 [pii
19. Chung WS, Clarke LE, Wang GX, Stafford BK, Sher A, Chakraborty C, Joung J, Foo LC, Thompson A, Chen C, Smith SJ, Barres BA (2013) Astrocytes mediate synapse elimination through MEGF10 and MERTK pathways. Nature 504 (7480):394-400. doi:nature12776 [pii]10.1038/nature12776
20. Dalmau I, Vela JM, Gonzalez B, Castellano B (1998) Expression of purine metabolism-related enzymes by microglial cells in the developing rat brain. J Comp Neurol 398 (3):333-346. doi:10.1002/(SICI)1096-9861(19980831)398:3¡333::AID-CNE3¿3.0.CO;2-0 [pii]
21. Davalos D, Grutzendler J, Yang G, Kim JV, Zuo Y, Jung S, Littman DR, Dustin ML, Gan WB (2005) ATP mediates rapid microglial response to local brain injury in vivo. Nat Neurosci 8 (6):752-758. doi:nn1472 [pii] 10.1038/nn1472
22. de Jong EK, Dijkstra IM, Hensens M, Brouwer N, van Amerongen M, Liem RS, Boddeke HW, Biber K (2005) Vesicle-mediated transport and release of CCL21 in endangered neurons: a possible explanation for microglia activation remote from a primary lesion. J Neurosci 25 (33):7548-7557. doi:25/33/7548 [pii]10.1523/JNEUROSCI.1019-05.2005
23. Eyo UB, Wu LJ (2013) Bidirectional microglia-neuron communication in the healthy brain. Neural Plast 2013:456857. doi:10.1155/2013/456857
24. Fang KM, Yang CS, Sun SH, Tzeng SF (2009) Microglial phagocytosis attenuated by short-term exposure to exogenous ATP through P2X receptor action. J Neurochem 111 (5):1225-1237. doi:JNC6409 [pii] 10.1111/j.1471-4159.2009.06409.x
25. Farber K, Markworth S, Pannasch U, Nolte C, Prinz V, Kronenberg G, Gertz K, Endres M, Bechmann I, Enjyoji K, Robson SC, Kettenmann H (2008) The ectonucleotidase cd39/ENTPDase1 modulates purinergic-mediated microglial migration. Glia 56 (3):331-341. doi:10.1002/glia.20606
26. Farber K, Pannasch U, Kettenmann H (2005) Dopamine and noradrenaline control distinct functions in rodent microglial cells. Mol Cell Neurosci 29 (1):128-138. doi:S1044-7431(05)00010-2 [pii] 10.1016/j.mcn.2005.01.003
27. Fleisher-Berkovich S, Filipovich-Rimon T, Ben-Shmuel S, Hulsmann C, Kummer MP, Heneka MT (2010) Distinct modulation of microglial amyloid beta phagocytosis and migration by neuropeptides (i). J Neuroinflammation 7:61. doi:1742-2094-7-61 [pii] 10.1186/1742-2094-7-61
28. Fontainhas AM, Wang M, Liang KJ, Chen S, Mettu P, Damani M, Fariss RN, Li W, Wong WT (2011) Microglial morphology and dynamic behavior is regulated by ionotropic glutamatergic and GABAergic neurotransmission. PLoS One 6 (1):e15973. doi:10.1371/journal.pone.0015973

29. Gehrmann J, Monaco S, Kreutzberg GW (1991) Spinal cord microglial cells and DRG satellite cells rapidly respond to transection of the rat sciatic nerve. Restor Neurol Neurosci 2 (4):181-198. doi:F2852H884540843H [pii] 10.3233/RNN-1991-245605
30. Gonzalez H, Elgueta D, Montoya A, Pacheco R (2014) Neuroimmune regulation of microglial activity involved in neuroinflammation and neurodegenerative diseases. J Neuroimmunol 274 (1-2):1-13. doi:S0165-5728(14)00227-6 [pii] 10.1016/j.jneuroim.2014.07.012
31. Hao HP, Doh-Ura K, Nakanishi H (2007) Impairment of microglial responses to facial nerve axotomy in cathepsin S-deficient mice. J Neurosci Res 85 (10):2196-2206. doi:10.1002/jnr.21357
32. Hardingham GE, Bading H (2003) The Yin and Yang of NMDA receptor signalling. Trends Neurosci 26 (2):81-89. doi:S0166-2236(02)00040-1 [pii] 10.1016/S0166-2236(02)00040-1
33. Hardingham GE, Fukunaga Y, Bading H (2002) Extrasynaptic NMDARs oppose synaptic NMDARs by triggering CREB shut-off and cell death pathways. Nat Neurosci 5 (5):405-414. doi:10.1038/nn835 nn835 [pii]
34. Hasko G, Pacher P, Deitch EA, Vizi ES (2007) Shaping of monocyte and macrophage function by adenosine receptors. Pharmacol Ther 113 (2):264-275. doi:S0163-7258(06)00150-1 [pii] 10.1016/j.pharmthera.2006.08.003
35. Haynes SE, Hollopeter G, Yang G, Kurpius D, Dailey ME, Gan WB, Julius D (2006) The P2Y12 receptor regulates microglial activation by extracellular nucleotides. Nat Neurosci 9 (12):1512-1519. doi:nn1805 [pii] 10.1038/nn1805
36. Heine C, Heimrich B, Vogt J, Wegner A, Illes P, Franke H (2006) P2 receptor-stimulation influences axonal outgrowth in the developing hippocampus in vitro. Neuroscience 138 (1):303-311. doi:S0306-4522(05)01295-9 [pii] 10.1016/j.neuroscience.2005.11.056
37. Hirrlinger J, Hulsmann S, Kirchhoff F (2004) Astroglial processes show spontaneous motility at active synaptic terminals in situ. Eur J Neurosci 20 (8):2235-2239. doi:10.1111/j.1460-9568.2004.03689.x EJN3689 [pii]
38. Holtmaat A, De Paola V, Wilbrecht L, Knott GW (2008) Imaging of experience-dependent structural plasticity in the mouse neocortex in vivo. Behav Brain Res 192 (1):20-25. doi:S0166-4328(08)00190-3 [pii] 10.1016/j.bbr.2008.04.005
39. Husemann J, Loike JD, Anankov R, Febbraio M, Silverstein SC (2002) Scavenger receptors in neurobiology and neuropathology: their role on microglia and other cells of the nervous system. Glia 40 (2):195-205. doi:10.1002/glia.10148
40. Ifuku M, Farber K, Okuno Y, Yamakawa Y, Miyamoto T, Nolte C, Merrino VF, Kita S, Iwamoto T, Komuro I, Wang B, Cheung G, Ishikawa E, Ooboshi H, Bader M, Wada K, Kettenmann H, Noda M (2007) Bradykinin-induced microglial migration mediated by B1-bradykinin receptors depends on Ca2+ influx via reverse-mode activity of the Na+/Ca2+ exchanger. J Neurosci 27 (48):13065-13073. doi:27/48/13065 [pii]10.1523/JNEUROSCI.3467-07.2007
41. Ifuku M, Okuno Y, Yamakawa Y, Izumi K, Seifert S, Kettenmann H, Noda M (2011) Functional importance of inositol-1,4,5-triphosphate-induced intracellular Ca2+ mobilization in galanin-induced microglial migration. J Neurochem 117 (1):61-70. doi:10.1111/j.1471-4159.2011.07176.x
42. Inoue K (2008) Purinergic systems in microglia. Cell Mol Life Sci 65 (19):3074-3080. doi:10.1007/s00018-008-8210-3
43. Jensen MB, Gonzalez B, Castellano B, Zimmer J (1994) Microglial and astroglial reactions to anterograde axonal degeneration: a histochemical and immunocytochemical study of the adult rat fascia dentata after entorhinal perforant path lesions. Exp Brain Res 98 (2):245-260
44. Kettenmann H, Hanisch UK, Noda M, Verkhratsky A (2011) Physiology of microglia. Physiol Rev 91 (2):461-553. doi:91/2/461 [pii] 10.1152/physrev.00011.2010
45. Kettenmann H, Kirchhoff F, Verkhratsky A (2013) Microglia: new roles for the synaptic stripper. Neuron 77 (1):10-18. doi:S0896-6273(12)01162-2 [pii] 10.1016/j.neuron.2012.12.023
46. Kierdorf K, Prinz M (2013) Factors regulating microglia activation. Front Cell Neurosci 7:44. doi:10.3389/fncel.2013.00044
47. Kiryu-Seo S, Hirayama T, Kato R, Kiyama H (2005) Noxa is a critical mediator of p53-dependent motor neuron death after nerve injury in adult mouse. J Neurosci 25 (6):1442-1447. doi:25/6/1442 [pii] 10.1523/JNEUROSCI.4041-04.2005
48. Kiryu-Seo S, Kiyama H (2011) The nuclear events guiding successful nerve regeneration. Front Mol Neurosci 4:53. doi:10.3389/fnmol.2011.00053
49. Knott G, Holtmaat A (2008) Dendritic spine plasticity–current understanding from in vivo studies. Brain Res Rev 58 (2):282-289. doi:S0165-0173(08)00004-0 [pii] 10.1016/j.brainresrev.2008.01.002

50. Koizumi S, Shigemoto-Mogami Y, Nasu-Tada K, Shinozaki Y, Ohsawa K, Tsuda M, Joshi BV, Jacobson KA, Kohsaka S, Inoue K (2007) UDP acting at P2Y6 receptors is a mediator of microglial phagocytosis. Nature 446 (7139):1091-1095. doi:nature05704 [pii] 10.1038/nature05704
51. Kreutzberg GW (1996) Microglia: a sensor for pathological events in the CNS. Trends Neurosci 19 (8):312-318. doi:0166-2236(96)10049-7 [pii]
52. Kurpius D, Nolley EP, Dailey ME (2007) Purines induce directed migration and rapid homing of microglia to injured pyramidal neurons in developing hippocampus. Glia 55 (8):873-884. doi:10.1002/glia.20509
53. Le Feuvre RA, Brough D, Touzani O, Rothwell NJ (2003) Role of P2X7 receptors in ischemic and excitotoxic brain injury in vivo. J Cereb Blood Flow Metab 23 (3):381-384
54. Lehnardt S (2010) Innate immunity and neuroinflammation in the CNS: the role of microglia in Toll-like receptor-mediated neuronal injury. Glia 58 (3):253-263. doi:10.1002/glia.20928
55. Linda H, Shupliakov O, Ornung G, Ottersen OP, Storm-Mathisen J, Risling M, Cullheim S (2000) Ultrastructural evidence for a preferential elimination of glutamate-immunoreactive synaptic terminals from spinal motoneurons after intramedullary axotomy. J Comp Neurol 425 (1):10-23. doi:10.1002/1096-9861(20000911)[pii]
56. Linnartz B, Neumann H (2013) Microglial activatory (immunoreceptor tyrosine-based activation motif)- and inhibitory (immunoreceptor tyrosine-based inhibition motif)-signaling receptors for recognition of the neuronal glycocalyx. Glia 61 (1):37-46. doi:10.1002/glia.22359
57. Liu GJ, Nagarajah R, Banati RB, Bennett MR (2009) Glutamate induces directed chemotaxis of microglia. Eur J Neurosci 29 (6):1108-1118. doi:EJN6659 [pii]10.1111/j.1460-9568.2009.06659.x
58. Makwana M, Jones LL, Cuthill D, Heuer H, Bohatschek M, Hristova M, Friedrichsen S, Ormsby I, Bueringer D, Koppius A, Bauer K, Doetschman T, Raivich G (2007) Endogenous transforming growth factor beta 1 suppresses inflammation and promotes survival in adult CNS. J Neurosci 27 (42):11201-11213. doi:27/42/11201 [pii] 10.1523/JNEUROSCI.2255-07.2007
59. Marin-Teva JL, Cuadros MA, Martin-Oliva D, Navascues J (2011) Microglia and neuronal cell death. Neuron Glia Biol 7 (1):25-40. doi:S1740925X12000014 [pii] 10.1017/S1740925X12000014
60. Martin S, Dicou E, Vincent JP, Mazella J (2005) Neurotensin and the neurotensin receptor-3 in microglial cells. J Neurosci Res 81 (3):322-326. doi:10.1002/jnr.20477
61. Masui K, Yamada E, Shimokawara T, Mishima K, Enomoto Y, Nakajima H, Yoshikawa T, Sakaki T, Ichijima K (2002) Expression of c-Jun N-terminal kinases after axotomy in the dorsal motor nucleus of the vagus nerve and the hypoglossal nucleus. Acta Neuropathol 104 (2):123-129. doi:10.1007/s00401-002-0519-7
62. Matute C, Torre I, Perez-Cerda F, Perez-Samartin A, Alberdi E, Etxebarria E, Arranz AM, Ravid R, Rodriguez-Antiguedad A, Sanchez-Gomez M, Domercq M (2007) P2X(7) receptor blockade prevents ATP excitotoxicity in oligodendrocytes and ameliorates experimental autoimmune encephalomyelitis. J Neurosci 27 (35):9525-9533. doi:27/35/9525 [pii] 10.1523/JNEUROSCI.0579-07.2007
63. Matzinger P (2007) Friendly and dangerous signals: is the tissue in control? Nat Immunol 8 (1):11-13. doi:ni0107-11 [pii] 10.1038/ni0107-11
64. Mehta A, Prabhakar M, Kumar P, Deshmukh R, Sharma PL (2013) Excitotoxicity: bridge to various triggers in neurodegenerative disorders. Eur J Pharmacol 698 (1-3):6-18. doi:S0014-2999(12)00900-4 [pii] 10.1016/j.ejphar.2012.10.032
65. Melani A, Turchi D, Vannucchi MG, Cipriani S, Gianfriddo M, Pedata F (2005) ATP extracellular concentrations are increased in the rat striatum during in vivo ischemia. Neurochem Int 47 (6):442-448. doi:S0197-0186(05)00143-9 [pii] 10.1016/j.neuint.2005.05.014
66. Melchior B, Garcia AE, Hsiung BK, Lo KM, Doose JM, Thrash JC, Stalder AK, Staufenbiel M, Neumann H, Carson MJ (2010) Dual induction of TREM2 and tolerance-related transcript, Tmem176b, in amyloid transgenic mice: implications for vaccine-based therapies for Alzheimer's disease. ASN Neuro 2 (3):e00037. doi:10.1042/AN20100010
67. Mentis GZ, Greensmith L, Vrbova G (1993) Motoneurons destined to die are rescued by blocking N-methyl-D-aspartate receptors by MK-801. Neuroscience 54 (2):283-285. doi:0306-4522(93)90253-C [pii]
68. Moran LB, Graeber MB (2004) The facial nerve axotomy model. Brain Res Brain Res Rev 44 (2-3):154-178. doi:10.1016/j.brainresrev.2003.11.004 S0165017303002595 [pii]
69. Mott RT, Ait-Ghezala G, Town T, Mori T, Vendrame M, Zeng J, Ehrhart J, Mullan M, Tan J (2004) Neuronal expression of CD22: novel mechanism for inhibiting microglial proinflammatory cytokine production. Glia 46 (4):369-379. doi:10.1002/glia.20009

70. Navarro X, Vivo M, Valero-Cabre A (2007) Neural plasticity after peripheral nerve injury and regeneration. Prog Neurobiol 82 (4):163-201. doi:S0301-0082(07)00109-8 [pii] 10.1016/j.pneurobio.2007.06.005
71. Neumann J, Gunzer M, Gutzeit HO, Ullrich O, Reymann KG, Dinkel K (2006) Microglia provide neuroprotection after ischemia. FASEB J 20 (6):714-716. doi:05-4882fje [pii] 10.1096/fj.05-4882fje
72. Nimmerjahn A, Kirchhoff F, Helmchen F (2005) Resting microglial cells are highly dynamic surveillants of brain parenchyma in vivo. Science 308 (5726):1314-1318. doi:1110647 [pii] 10.1126/science.1110647
73. Noda M, Ifuku M, Mori Y, Verkhratsky A (2013) Calcium influx through reversed NCX controls migration of microglia. Adv Exp Med Biol 961:289-294. doi:10.1007/978-1-4614-4756-6-24
74. Ohsawa K, Kohsaka S (2011) Dynamic motility of microglia: purinergic modulation of microglial movement in the normal and pathological brain. Glia 59 (12):1793-1799. doi:10.1002/glia.21238
75. Orr AG, Orr AL, Li XJ, Gross RE, Traynelis SF (2009) Adenosine A(2A) receptor mediates microglial process retraction. Nat Neurosci 12 (7):872-878. doi:nn.2341 [pii] 10.1038/nn.2341
76. Panatier A, Robitaille R (2012) The soothing touch: microglial contact influences neuronal excitability. Dev Cell 23 (6):1125-1126. doi:S1534-5807(12)00535-7 [pii] 10.1016/j.devcel.2012.11.015
77. Perez-Alvarez A, Navarrete M, Covelo A, Martin ED, Araque A (2014) Structural and functional plasticity of astrocyte processes and dendritic spine interactions. J Neurosci 34 (38):12738-12744. doi:34/38/12738 [pii] 10.1523/JNEUROSCI.2401-14.2014
78. Perry VH, O'Connor V (2010) The role of microglia in synaptic stripping and synaptic degeneration: a revised perspective. ASN Neuro 2 (5):e00047. doi:10.1042/AN20100024
79. Pocock JM, Kettenmann H (2007) Neurotransmitter receptors on microglia. Trends Neurosci 30 (10):527-535. doi:S0166-2236(07)00211-1 [pii] 10.1016/j.tins.2007.07.007
80. Raivich G, Makwana M (2007) The making of successful axonal regeneration: genes, molecules and signal transduction pathways. Brain Res Rev 53 (2):287-311. doi:S0165-0173(06)00110-X [pii] 10.1016/j.brainresrev.2006.09.005
81. Rappert A, Bechmann I, Pivneva T, Mahlo J, Biber K, Nolte C, Kovac AD, Gerard C, Boddeke HW, Nitsch R, Kettenmann H (2004) CXCR3-dependent microglial recruitment is essential for dendrite loss after brain lesion. J Neurosci 24 (39):8500-8509. doi:10.1523/JNEUROSCI.2451-04.2004 24/39/8500 [pii]
82. Raslan A, Ernst P, Werle M, Thieme H, Szameit K, Finkensieper M, Guntinas-Lichius O, Irintchev A (2014) Reduced cholinergic and glutamatergic synaptic input to regenerated motoneurons after facial nerve repair in rats: potential implications for recovery of motor function. Brain Struct Funct 219 (3):891-909. doi:10.1007/s00429-013-0542-6
83. Rathbone MP, Middlemiss PJ, Gysbers JW, Andrew C, Herman MA, Reed JK, Ciccarelli R, Di Iorio P, Caciagli F (1999) Trophic effects of purines in neurons and glial cells. Prog Neurobiol 59 (6):663-690. doi:S0301-0082(99)00017-9 [pii]
84. Ravichandran KS (2010) Find-me and eat-me signals in apoptotic cell clearance: progress and conundrums. J Exp Med 207 (9):1807-1817. doi:jem.20101157 [pii] 10.1084/jem.20101157
85. Sasaki Y, Hoshi M, Akazawa C, Nakamura Y, Tsuzuki H, Inoue K, Kohsaka S (2003) Selective expression of Gi/o-coupled ATP receptor P2Y12 in microglia in rat brain. Glia 44 (3):242-250. doi:10.1002/glia.10293
86. Siskova Z, Tremblay ME (2013) Microglia and synapse: interactions in health and neurodegeneration. Neural Plast 2013:425845. doi:10.1155/2013/425845
87. Sperlagh B, Illes P (2007) Purinergic modulation of microglial cell activation. Purinergic Signal 3 (1-2):117-127. doi:10.1007/s11302-006-9043-x
88. Stone TW (2002) Purines and neuroprotection. Adv Exp Med Biol 513:249-280
89. Sumner BE, Sutherland FI (1973) Quantitative electron microscopy on the injured hypoglossal nucleus in the rat. J Neurocytol 2 (3):315-328
90. Takayama N, Ueda H (2005) Morphine-induced chemotaxis and brain-derived neurotrophic factor expression in microglia. J Neurosci 25 (2):430-435. doi:25/2/430 [pii] 10.1523/JNEUROSCI.3170-04.2005
91. Theodosis DT, Poulain DA, Oliet SH (2008) Activity-dependent structural and functional plasticity of astrocyte-neuron interactions. Physiol Rev 88 (3):983-1008. doi:88/3/983 [pii] 10.1152/physrev.00036.2007
92. Tozaki-Saitoh H, Tsuda M, Miyata H, Ueda K, Kohsaka S, Inoue K (2008) P2Y12 receptors in spinal microglia are required for neuropathic pain after peripheral nerve injury. J Neurosci 28 (19):4949-4956. doi:28/19/4949 [pii] 10.1523/JNEUROSCI.0323-08.2008

93. Trapp BD, Wujek JR, Criste GA, Jalabi W, Yin X, Kidd GJ, Stohlman S, Ransohoff R (2007) Evidence for synaptic stripping by cortical microglia. Glia 55 (4):360-368. doi:10.1002/glia.20462
94. Tremblay ME, Lowery RL, Majewska AK (2010) Microglial interactions with synapses are modulated by visual experience. PLoS Biol 8 (11):e1000527. doi:10.1371/journal.pbio.1000527
95. Tyzack GE, Sitnikov S, Barson D, Adams-Carr KL, Lau NK, Kwok JC, Zhao C, Franklin RJ, Karadottir RT, Fawcett JW, Lakatos A (2014) Astrocyte response to motor neuron injury promotes structural synaptic plasticity via STAT3-regulated TSP-1 expression. Nat Commun 5:4294. doi:ncomms5294 [pii] 10.1038/ncomms5294
96. Villacampa N, Almolda B, Vilella A, Campbell IL, Gonzalez B, Castellano B (2015) Astrocyte-targeted production of IL-10 induces changes in microglial reactivity and reduces motor neuron death after facial nerve axotomy. Glia. doi:10.1002/glia.22807
97. Wake H, Moorhouse AJ, Jinno S, Kohsaka S, Nabekura J (2009) Resting microglia directly monitor the functional state of synapses in vivo and determine the fate of ischemic terminals. J Neurosci 29 (13):3974-3980. doi:29/13/3974 [pii]10.1523/JNEUROSCI.4363-08.2009
98. Walter L, Franklin A, Witting A, Wade C, Xie Y, Kunos G, Mackie K, Stella N (2003) Nonpsychotropic cannabinoid receptors regulate microglial cell migration. J Neurosci 23 (4):1398-1405. doi:23/4/1398 [pii]
99. Woo NH, Lu B (2006) Regulation of cortical interneurons by neurotrophins: from development to cognitive disorders. Neuroscientist 12 (1):43-56. doi:12/1/43 [pii] 10.1177/1073858405284360
100. Xie R, Villacampa N, Almolda B, Gonzlez B, Castellano B, Campbell IL (2014) Interferon regulator factor (IRF) 8 regulates the microglial response to neuronal injury. Cytokine 70 (1):77. doi:doi:10.1016/j.cyto.2014.07.209
101. Xing C, Wang X, Cheng C, Montaner J, Mandeville E, Leung W, van Leyen K, Lok J, Lo EH (2014) Neuronal production of lipocalin-2 as a help-me signal for glial activation. Stroke 45 (7):2085-2092. doi:STROKEAHA.114.005733 [pii] 10.1161/STROKEAHA.114.005733
102. Yamada J, Hayashi Y, Jinno S, Wu Z, Inoue K, Kohsaka S, Nakanishi H (2008) Reduced synaptic activity precedes synaptic stripping in vagal motoneurons after axotomy. Glia 56 (13):1448-1462. doi:10.1002/glia.20711
103. Yamada J, Nakanishi H, Jinno S (2011) Differential involvement of perineuronal astrocytes and microglia in synaptic stripping after hypoglossal axotomy. Neuroscience 182:1-10. doi:S0306-4522(11)00288-0 [pii] 10.1016/j.neuroscience.2011.03.030

ASTROCYTE-TARGETED IL-6 OR IL-10 PRODUCTION ALTERS EXPRESSION OF TREM AFTER PERIPHERAL NERVE INJURY

Nàdia Villacampa et al.*

Unit of Histology, Torre M5. Dept. Cell Biology, Physiology and Immunology. Institute of Neurosciences. Universitat Autònoma de Barcelona.
08193 Bellaterra, Spain.

Abstract. After an injury to central nervous System (CNS), microglia become activated and, among other functions, are engaged in phagocytosis of neuronal debris in order to initiate repair of tissue damage. Recent evidence points to triggering receptor expressed on myeloid cells-2 (TREM2) as an important microglial receptor involved in the phagocytic process. Although the induction of TREM2 in activated microglia has been demonstrated in many pathological conditions, studies addressing TREM2 expression after peripheral nerve injury are not available. In previous studies, we showed that astrocyte-targeted production of either IL-6 or IL-10 induced changes in neuronal death after facial nerve axotomy (FNA), linked to important differences in microglial activation. The objective of the present work is to determine whether activated microglia express TREM2 after FNA and whether the phagocytic phenotype of microglial cells is modified by the local expression of IL-6 and IL-10. We reported an induction of TREM2 expression in microglia throughout the evolution of FNA and we demonstrated that transgenic production of IL-6 and IL-10 altered the expression of TREM2, CD16/32 and CD68 in activated microglial cells. In the case of IL-6, the expression of the three phagocytic markers is induced earlier but remained higher than WT at later time-points, whereas IL-10, in contrast, induced a delay in the expression of the three molecules. Our results indicate that local cytokine microenvironment modifies the phagocytic phenotype of microglial cells after FNA and point to TREM2 as a key regulator of microglial activation, which play different roles in addition to phagocytosis.

Keywords: cytokines, neuronal survival, microglia, phagocytosis, neuroinflammation, DAP12, CD68, facial nerve axotomy, CD16/32

Highlights

- TREM2 is expressed in microglia after FNA, not restricted to phagocytic events
- Both IL-6 and IL-10 production induce changes in TREM2 expression
- The phagocytic phenotype of microglia is modified by IL-6 and IL-10

* Manuscript in preparation

Table 1. List of abbreviations

BBB	Blood brain barrier
BSA	Bovine serum albumin
CNS	Central nervous system
CNS	Central nervous system
DAP12	DNAX activation protein of 12 kDa
FMN	Facial motor neurons
FN	Facial nucleus
FNA	Facial nerve axotomy
GGQ	Grey grade quotient
IG	Intensity grade
IgG	Immunoglobulin
ITAM	Immunoreceptor tyrosine-based activation motif
ITIM	Immunoreceptor tyrosine-based inhibition motif
RT	Room temperature
TREM2	Triggering Receptor Expressed on Myeloid cells 2
WT	Wild-type

1 Introduction

Microglia are the resident macrophages of the central nervous system (CNS). In the normal brain, microglia are far from being considered resting cells, but sentinels with very motile branches that constantly survey their microenvironment (Davalos et al. 2005; Nimmerjahn et al. 2005; Wake et al. 2009), playing an important role in CNS homeostasis (Tremblay 2011; Tremblay and Majewska 2011; Kierdorf and Prinz 2013; Linnartz and Neumann 2013). Under conditions of altered homeostasis, microglia become activated and, as a first line of defense, display a wide range of functions including cytokine production, antigen presentation and phagocytosis (Aloisi 2001; Kettenmann et al. 2011; Kettenmann et al. 2013; Napoli and Neumann 2009).

Phagocytosis and the efficient removal of apoptotic cells along with clearance of tissue debris at the lesion site are thought to be critical in the reorganization of the neuronal networking and in the lesion resolution, generating an appropriate microenvironment for regeneration and repair (Polazzi and Monti 2010; Suzumura 2013; Neumann et al. 2009; Napoli and Neumann 2009; Nakajima and Kohsaka 2004; Kim and de Vellis 2005). Increasing evidence indicate the important role played by the signaling through the immunoreceptor tyrosine-based activation motifs (ITAMs) in the phagocytic process carried out by microglial cells (Linnartz and Neumann 2013). Among the different receptors associated with this signaling, the triggering receptor expressed on myeloid cells-2 (TREM2) is one of the most studied in the last years (Neumann and Takahashi 2007). TREM2 consist of an extracellular domain, a transmembrane region and a short cytoplasmic tail with no intracellular signaling motifs and is, therefore, completely dependent on the adaptor protein DNAX-activating protein of 12kDa (DAP12) to deliver activation signals within the cell (Bouchon et al. 2001; Lanier and Bakker 2000; Colonna 2003a; Kiialainen et al. 2005).

In the healthy CNS, several studies demonstrated that TREM2 is expressed by microglial cells in vitro (Schmid et al. 2002; Sessa et al. 2004; Kiialainen et al. 2005) and also by specific microglial subsets in vivo, during both postnatal brain development (Chertoff et al. 2013; Thrash et al. 2009) and in the adult (Schmid et al. 2002; Bisht et al. 2016). The role of TREM2 in modulating microglial activation has been addressed in many CNS diseases and challenges such as Nasu-Hakola disease (Bianchin et al. 2004; Paloneva et al. 2001), Alzheimers disease (Jiang et al. 2013; Rohn 2013), frontotemporal dementia (Thelen et al. 2014; Kleinberger et al. 2014), prion disease (Zhu et al. 2015), stroke (Kawabori et al. 2015; Kawabori et al. 2013; Sieber et al. 2013), cuprizone-induced demyelination (Poliani et al. 2015; Cantoni et al. 2015), amyotrophic lateral sclerosis (Cady et al. 2014), multiple sclerosis (Piccio et al. 2008) and its animal model experimental autoimmune encephalomyelitis (Piccio et al. 2007; Takahashi et al. 2007). In some of these pathological situations, TREM2 has been thought to play a role in the activation of microglia mediating not only their phagocytic activity but also their migration and survival (Ulland et al. 2016; Zhu et al. 2015; Cantoni et al. 2015; Kawabori et al. 2015; Poliani et al. 2015; Wang et al. 2015). However, studies addressing TREM2 expression and its role after peripheral nerve injury are not available.

Mechanical transection of the facial nerve leads to retrograde neuronal degeneration and a dramatic activation of microglia (Moran and Graeber 2004; Aldskogius 2011), which accumulates around axotomized facial motor neurons (FMN) and phagocytose neuronal debris (Moller et al. 1996; Raivich et al. 1998). In previous studies using the facial nerve axotomy model (FNA), we have demonstrated that astrocyte-targeted production of either IL-6 or IL-10 promotes opposite effects on the neuronal death/survival ratio: the pro-inflammatory cytokine IL-6 leads to an increased neuronal death (Almolda et al. 2014b); whereas, IL-10 production increases neuronal survival (Villacampa et al. 2015). In addition, transgenic expression of the mentioned cytokines resulted in remarkable alterations of the microglial activation pattern, suggesting that the interaction between activated microglia and endangered FMN may determine the outcome of FNA.

In this context, and since the putative roles of cytokines in the regulation of microglial-neuron interaction are still not well defined, the principal objectives of the present work is to

determine whether TREM2 is induced in activated microglial cells in response to FNA and whether the local-cytokine microenvironment influences the phagocytosis-related phenotype of microglial cells and specifically their pattern of TREM2 expression.

2 Material and Methods

2.1 Animals

For this study, a total of 22 GFAP-IL6Tg animals (Campbell et al. 1993), 22 GFAP-IL10Tg animals (Almolda et al. 2014a) and 44 C57BL/6 wild-type (WT) littermates of 3 months-old from both sexes were used. All mice were housed under a 12h light/dark cycle, with food and water ad libitum. All experimental animal work was conducted according to Spanish regulations (Ley 32/2007, Real Decreto 1201/2005, Ley 9/2003 and Real Decreto 178/2004) in agreement with European Union directives (86/609/CEE, 91/628/CEE and 92/65/CEE) and was approved by the Ethical Committee of the Autonomous University of Barcelona. Every effort was made to minimize the number of animals used to produce reliable scientific data, as well as animal suffering and pain.

2.2 Facial nerve axotomy and experimental groups

GFAP-IL6Tg, GFAP-IL10Tg and WT mice were anesthetized with a solution of xylazine (20mg/kg) and ketamine (80mg/kg) injected intraperitoneally at dose of 0.01ml/g. The skin behind the right ear was shaved and cleansed with 70% ethanol. A small incision was made and skin and muscle were gently separated to expose the right facial nerve. One millimeter of the facial nerve main branch was resected at the level of the stylomastoid foramen. Following the surgery, the skin was sutured with 5-0 nylon. Corneal dehydration was prevented by application of Lacri-lube eye ointment. After anesthesia recovery, the complete whisker paralysis was assessed to ensure correct facial nerve resection.Non-lesioned and axotomized animals were distributed in different experimental groups and euthanized at 3, 7, 14, 21 and 28 days post-injury (dpi) for immunohistochemistry.

2.3 Tissue processing for histological analysis

Animals were deeply anaesthetized as described above at dose of 0.015ml/g and perfused intracardially with 4% paraformaldehyde in 0.1 M phosphate buffer (pH 7.4). Brains were removed and post-fixed in the same fixative for 4h at 4C and, after rinsing in phosphate buffer, cryopreserved for 48h in a 30% sucrose solution and subsequently frozen with 2-methylbutane solution (Sigma-Aldrich). Parallel free-floating coronal sections (30-m-thick) of the brainstem containing the facial nucleus (FN) were obtained using a CM3050s Leica cryostat and were stored at -20C in Olmos antifreeze solution until their late use.

2.4 Single immunohistochemistry

Free-floating cryostat sections were processed for the visualization of TREM2, CD16/32, CD68 and Iba1. Briefly, after 10 min of endogenous peroxidase blocking with 2% H2O2 in 70% methanol, sections were blocked for 1h in blocking solution containing either 0.2% gelatine (powder food grade, 1.04078, Merck) in Tris-buffered saline (TBS, pH 7.4) with 0.3% Triton X-100 in the case of TREM2 or 10% foetal calf serum and 3% bovine serum albumin (BSA) in TBS with 1% Triton X-100 in the case of CD16/32, CD68 and Iba1. Subsequently, sections were incubated overnight at 4C and 1h at room temperature (RT) -in the case of CD16/32, CD68 and Iba1- or overnight at RT in the case of TREM2- with rat anti-CD16/32 (1:1000; 553142; BD Pharmingen), rat anti-CD68 (1:1000; MCA1957; AbD Serotec), rabbit anti-Iba1 (1:3000; 019-19741; Wako) or sheep anti-TREM2 (1:300; AF1729; R&D Systems).

Sections incubated in media lacking the primary antibody were used as negative control and spleen sections as positive control. After washes with either 0.5% TBS Triton X-100 or 1% TBS Triton X-100, sections were incubated at RT for 1h with either biotinylated anti-rat secondary antibody (1:500; BA-4001; Vector Laboratories, Inc; Burlingame, CA), biotinylated anti-rabbit secondary antibody (1:500; BA-1000; Vector Laboratories, Inc; Burlingame, CA) or biotinylated anti-sheep secondary antibody (1:500; BA-6000; Vector Laboratories, Inc; Burlingame, CA) diluted in the corresponding blocking solution. For the study of the blood brain barrier (BBB) integrity, after endogenous peroxidase inhibition and incubation in blocking solution, sections were incubated for 1h in biotinylated anti-mouse IgG (1:500, BA-2001; Vector Laboratories, Inc; Burlingame, CA) diluted in the same blocking solution. After 1h at RT in horseradish streptavidin-peroxidase (1:500; SA-5004; Vector Laboratories, Inc; Burlingame, CA), the reaction was visualized by incubating the sections with a DAB kit (SK-4100; Vector Laboratories, Inc; Burlingame, CA) following the manufacturers instructions. Finally, sections were mounted on gelatin-coated slides, counterstained with toluidine blue, dehydrated in graded alcohols and, after xylene treatment, coverslipped with DPX. Sections were analyzed and photographed with a DXM 1200F Nikon digital camera joined to a Nikon Eclipse 80i microscope.

2.5 Triple immunohistochemistry

For the characterization of cells expressing TREM2, triple-immunolabelings combining: 1) TREM2, CD16/32 and Iba1; 2) TREM2, CD68 and Iba1 and 3) TREM2, DAP12 and CD11b were performed. Briefly, free-floating sections were washed with 0.5% TBS Triton X-100 and incubated in the appropriate blocking solution at RT for 1h followed by 48h incubation at 4C and 1h at 37C with the specific primary antibody combinations: sheep anti-TREM2 (1:300; AF1729; R&D Systems), rat anti-CD68 (1:1000; MCA1957; AbD Serotec), rabbit anti-Iba1 (1:3000; 019-19741; Wako), rat anti-CD16/32 (1:1000; 553142; BD Pharmingen), rabbit anti-DAP12 (1:100; AB4070; Millipore) or rat anti-CD11b (1:1000; MCA74GA; AbD Serotec). After several washes with 0.5% TBS Triton X-100, sections in each combination were incubated for 1h at RT with the corresponding secondary antibodies: Alexa Fluor 488 conjugated anti-sheep (1:1000, A-11015; Molecular Probes), Alexa Fluor 555 conjugated anti-rat (1:1000; A31570; Molecular Probes), Cy5-conjugated anti-rabbit (1:1000; PA45004; Amersham Biosciences), Alexa Fluor 568 conjugated anti-rabbit (1:1000; A10042; Molecular Probes) or Alexa Fluor 647 conjugated anti-rat (1:1000; A21247; Molecular Probes). Before being coverslipped with Fluorescence Mounting Medium (S-3023; Dako), triple labeled sections were nuclei stained with 4,6-diamidino-2-phenylindole (DAPI; 1:10000; D9542; Sigma Aldrich). Colocalization was analyzed with a Zeiss LSM 700 confocal microscope.

2.6 Brightfield microscopy quantification

Quantitative analysis was performed on sections immunolabeled for CD16/32, CD68 and TREM2. At least three WT, three GFAP-IL6Tg and three GFAP-IL10Tg animals per time post-axotomy were analyzed. At least three representative sections from the brainstem containing the central part of the FN from both the contralateral and the ipsilateral sides from each animal were photographed at 10X magnification. The percentage of area covered by the immunolabeling and the intensity of the immunoreaction (Mean Grey Value) for each marker were analyzed using ImageJ software (Wayne Rasband, National Institutes of Health, USA). For each animal, the grey grade quotient (GGQ) was obtained by dividing the Mean Grey Value on the ipsilateral side by the Mean Grey Value on the contralateral side. The intensity grade (IG) was calculated by multiplying the percentage of the immunolabeled area by the GGQ. In the case of TREM2 and CD68, the IG was expressed as fold of increased compared to the corresponding WT of each group of transgenic mice to facilitate comprehension. In order to quantify microglial cell density, sections stained for Iba1 from a minimum of 4 WT and 4 GFAP-IL6Tg animals at 28 dpi were analyzed. At least 3 representative sections from

the brainstem containing the central part of the FN from both the contralateral and the ipsilateral FN were analyzed per animal. Three photographs of each section were taken at high magnification (40X). The total number of nucleated Iba1-positive cells were performed on each microphotograph (0.0037mm^2 frame) using Cell counter plug-in from NIH Image J software (Wayne Rasband, National Institutes of Health, USA) and expressed as cells/mm^2.

2.7 Statistical analysis

Statistics were performed using Graph Pad Prism software (Graph Pad Software Inc.) and results were expressed as mean standard error of the mean (SEM). Standard two-tailed unpaired Students T-test was used for comparison between each group of transgenic mice and their corresponding WT. Two-way analysis of variance (ANOVA) was used for comparisons between groups across 3, 7, 14, 21, and 28 dpi and post-hoc Bonferronis Multiple Comparison Test was applied to compare among groups.

3 Results

3.1 Local production of both IL-6 and IL-10 induces changes in TREM2 expression

As in previous studies we found important differences in microglial activation in both GFAP-IL6Tg and GFAP-IL10Tg mice that correlated with opposing outcomes of neuronal death/survival after FNA (Almolda et al. 2014b; Villacampa et al. 2015), we wanted to assess whether the expression and distribution of TREM2 is also altered in these two transgenic mice after FNA. In the contralateral side, TREM2 staining was detected around the nucleus of some microglial cells in WT, GFAP-IL6Tg and GFAP-IL10Tg mice (Fig. 1N-P), whereas after FNA, TREM2 staining started to be detected in the processes of all ramified microglial cells as soon as 3 dpi in the three groups of animals (Fig. 1A-C, Q-S) but levels were lower in GFAP-IL10Tg mice when compared with WT. At 7 dpi, an increase in TREM2 staining was observed in all experimental groups of animals when compared with the previous time-point (Fig. 1D-F, M). At this time-point, while no differences between WT and GFAP-IL6Tg mice were observed, GFAP-IL10Tg mice showed lower levels of TREM2 (Fig. 1M). At this time point, TREM2+ microglial cells were observed surrounding the cytoplasm of FMN in all groups. At 14 dpi, when compared to the previous time-point, both WT and GFAP-IL10Tg mice experienced an increase in TREM2, whereas in GFAP-IL6Tg mice levels remained similar. However, no differences in TREM2 staining were found when comparing the three experimental groups at this time point (Fig. 1M). In addition to ramified parenchymal TREM2+ cells wrapping the FMN, some TREM2+ cells were forming microglial clusters in all groups. At 21 dpi, no differences between WT and GFAP-IL6Tg or GFAP-IL10Tg mice were observed, (Fig. 1G-I, M) and, as in the previous time-point, both ramified parenchymal and clustering microglial cells presented strong TREM2 staining (Fig. 1T-V). At the last time-point analyzed, 28 dpi, both WT and GFAP-IL10Tg showed a marked decreased in TREM2 staining, which was pronounced in GFAP-IL10Tg; while in GFAP-IL6Tg mice levels remained similar to those found at 21 dpi and significantly higher than the observed in their corresponding WT (Fig. 1J-L, M). At this time-point, most TREM2+ microglial cells adopted a ramified morphology and sparsely formed clusters.

3.2 Increased microglial density in GFAP-IL6Tg mice

As a role in promoting microglial survival has been recently attributed to TREM2 (Wang et al. 2015), we wanted to assess if the substantial increase in TREM2 expression observed in the GFAP-IL6Tg mice at 28 dpi correlated with higher number of microglial cells at this time-point. Our results demonstrated that in the contralateral side of the FN, GFAP-IL6Tg mice presented a higher microglial density than WT (Figure 2, A-B, E), in agreement

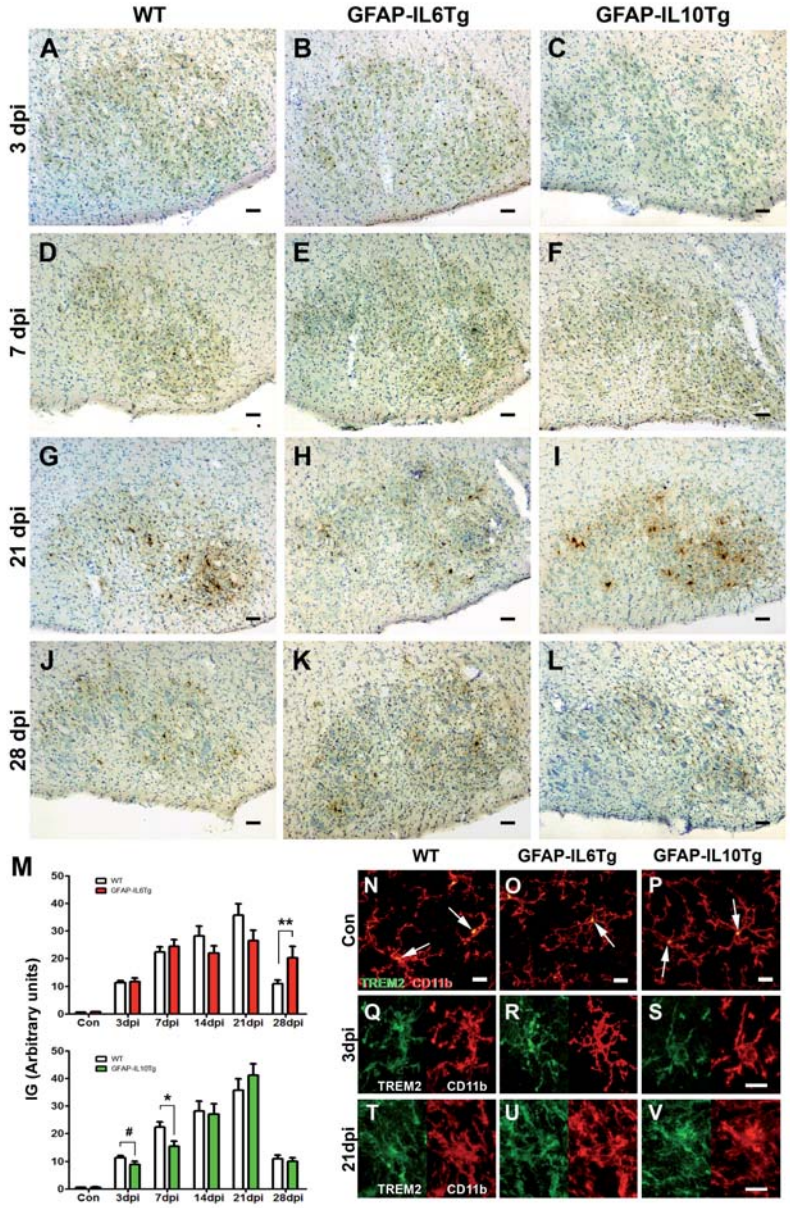

Fig. 1. TREM2 staining. (A-L) Representative microphotographs from WT, GFAP-IL6Tg and GFAP-IL10Tg mice corresponding to the ipsilateral FN at 3, 7, 21 and 28 dpi. **(M)** Graphs showing the quantification of the IG index for TREM2 of GFAP-IL6Tg (red bars) and GFAP-IL10Tg (green bars) compared with their corresponding WT (white bars).Note the lower expression of TREM2 in GFAP-IL10Tg mice compared to WT at early time-points and the higher expression observed in the GFAP-IL6Tg mice at 28 dpi. (#p≤0.09,*p≤0.05,**p≤0.01). **(N-V)** Double immunohistochemistry showing microglial cells expressing TREM2 (green) and CD11b (red). Note that in the contralateral side, TREM2 is confined around the nucleus of some of the CD11b+ cells (N-P, arrows), whereas at 3 (Q-S) and 21 dpi (T-V) is detected throughout the cytoplasm of CD11b+ cells. Scale bar (A-L) = 50μm. Scale bar (N-V) =10μm.

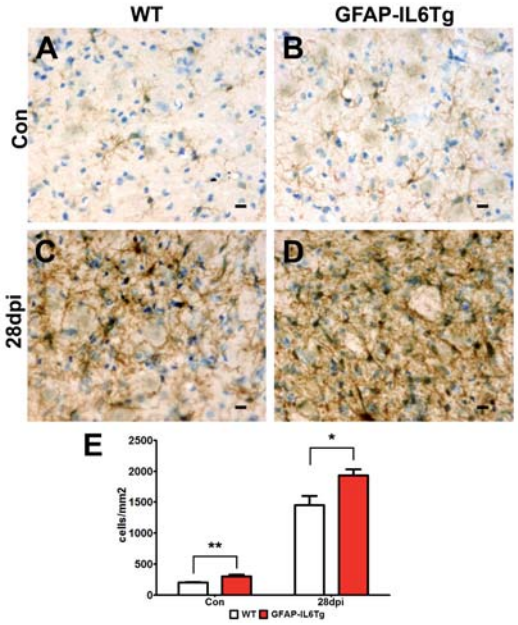

Fig. 2. Microglial density. (A-D) Representative microphotographs corresponding to the contralateral and the ipsilateral FN at 28 dpi in WT and GFAP-IL6Tg. **(E)** Graph showing the density of Iba1 positive cells in both the contralateral and the ipsilateral FN. Note that, Iba1 positive cell density is higher in GFAP-IL6Tg mice when compared to the WT in both the contralateral and the ipsilateral FN at 28 dpi (*p≤0.05,**p≤0.01). Scale bar (A-D) =10μm.

with previous published results (Almolda et al. 2014b). After 28 dpi, although there is a remarkable increase in the number of microglial cells in both groups compared with their contralateral side. GFAP-IL6Tg mice have increased number of microglial cells when compared to WT (Figure 2, C-E).

3.3 Altered microglial phagocytic markers in GFAP-IL6Tg and GFAP-IL10Tg mice

To assess the effects of astrocyte-targeted IL-6 and IL-10 on the phagocytic function of microglia along the different time-points after FNA (3, 7, 14, 21 and 28 dpi), the staining of the Fc gamma Receptor III (CD16) and Fc gamma Receptor II (CD32), linked to the phagocytic phenotype of microglial cells (Goodridge et al. 2012; Okun et al. 2010; Ulvestad et al. 1994); and CD68, a lysosomal marker related with phagocytic activity were analyzed (Travaglione et al. 2002; Holness and Simmons 1993). Our previously published results demonstrated an altered pattern of CD16/32 expression on microglial cells from GFAP-IL10Tg mice, with higher levels of CD16/32 at early time-points (3 and 7 dpi) and an abrupt decrease at 21 dpi, which correlates with a higher neuronal survival (Villacampa et al. 2015). In the present study, we assessed whether CD16/32 expression was also altered in GFAP-IL6Tg mice. No CD16/32 staining was detected in the contralateral side of either WT or GFAP-IL6Tg animals (Fig. 3I). CD16/32 started to be detected at 3 dpi in activated-ramified microglial cells of the lesioned FN, without differences between WT and GFAP-IL6Tg mice (Fig. 3A-B, M-N), and slightly increased in a similar way in both groups at 7 dpi. At 14 dpi, whereas in WT animals CD16/32 remained similar to the previous time-point, GFAP-IL6Tg experienced a higher increase (Fig. 3C-D, I). In both groups, CD16/32 staining was observed in both activated parenchymal microglia and clustering microglia (Fig. 3O-P). At 21 dpi, WT mice maintained high CD16/32 staining with distribution similar to 14 dpi, whereas in GFAP-IL6Tg animals this staining decreased abruptly in parenchymal microglia and only

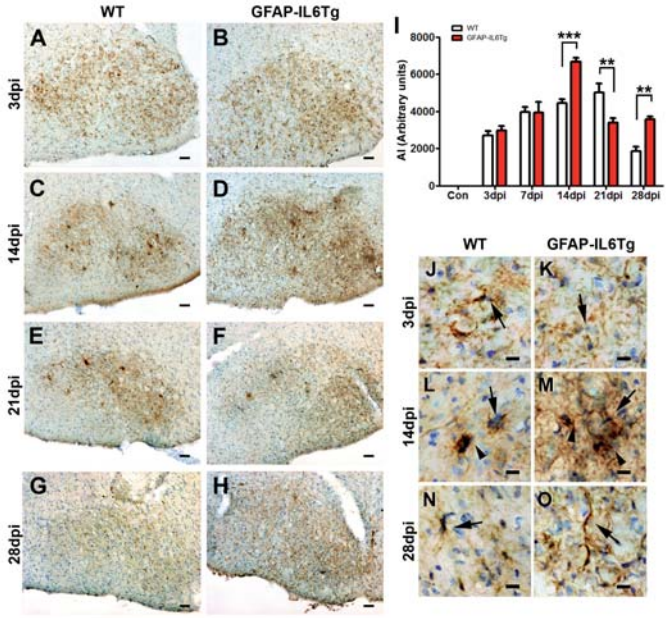

Fig. 3. CD16/32 staining. (A-H) Representative microphotographs corresponding to the ipsilateral FN at 3, 14, 21 and 28 dpi in WT and GFAP-IL6Tg mice. **(I)** Graph showing the quantification of the AI index for CD16/32. Note the differences in CD16/32 staining between WT (white bars) and GFAP-IL6Tg mice (red bars) in the later time-points after FNA.(**p≤0.01,***p≤0.001).**(J-O)** High magnification photographs showing the morphology of CD16/32+ cells (arrows) in the ipsilateral FN at 3, 14 and 28 dpi. Note that at 14 dpi, high CD16/32 staining was found in microglial clusters (O-P, arrowheads). Scale bar (A-H) = 50μm. Scale bar (J-O) =10μm.

few microglial clusters with high CD16/32 expression were observed (Fig. 3E-F, I). At 28 dpi, while WT mice experienced a pronounced reduction in CD16/32 staining, levels in GFAP-IL6Tg mice remained similar to the observed in the previous time-point and significantly higher than in WT(Fig. 3G-H, I). In both groups, at this time-point, staining was found mainly in parenchymal microglia but not in clusters. While in WT animals CD16/32+ microglia adopted a ramified/deactivated morphology, in GFAP-IL6Tg, activated microglia remained in contact with FMN, presenting a thickened soma and shorter processes (Fig. 3Q-R). As CD16/32 can be upregulated in the presence of leaked immunoglobulins to the nervous tissue (Lisi et al. 2011; Takai 2005; Nimmerjahn and Ravetch 2010), we also studied the integrity of the BBB by detection of mouse immunoglobulin (Ig) G. None of the three experimental groups presented staining against mouse IgG in neither the contralateral nor the ipsilateral FN (data not shown).

Due to the differences observed in the phagocytic marker CD16/32 in GFAP-IL6Tg and GFAP-IL10Tg mice, the next question we addressed was whether the expression of CD68 was also altered in transgenic animals after FNA. Throughout all the contralateral FN of WT, GFAP-IL6Tg and GFAP-IL10Tg mice, staining of CD68 was restricted to the soma of microglial cells, but not observed in the cellular ramifications (Fig. 4A-C, M). After FNA, a progressive increase of CD68 staining was observed in the soma and ramifications of activated microglial cells in WT, GFAP-IL6Tg and GFAP-IL10Tg mice from 3 dpi to 7 dpi (Fig. 4M). GFAP-IL10Tg presented less CD68 at 3 dpi and 7 dpi when compared to WT, whereas only at 7 dpi, GFAP-IL6Tg mice had higher expression than WT (Fig. 4D-F, M). At this time-point, CD68+ microglial cells exhibited an activated appearance, characterized by retracted processes and enlarged cell body, and approached to the FMN, without significant differences in terms of morphology in none of the groups (Fig. 4N-P). At 14 and 21 dpi, CD68 staining remained with similar levels to those found at 7 dpi and

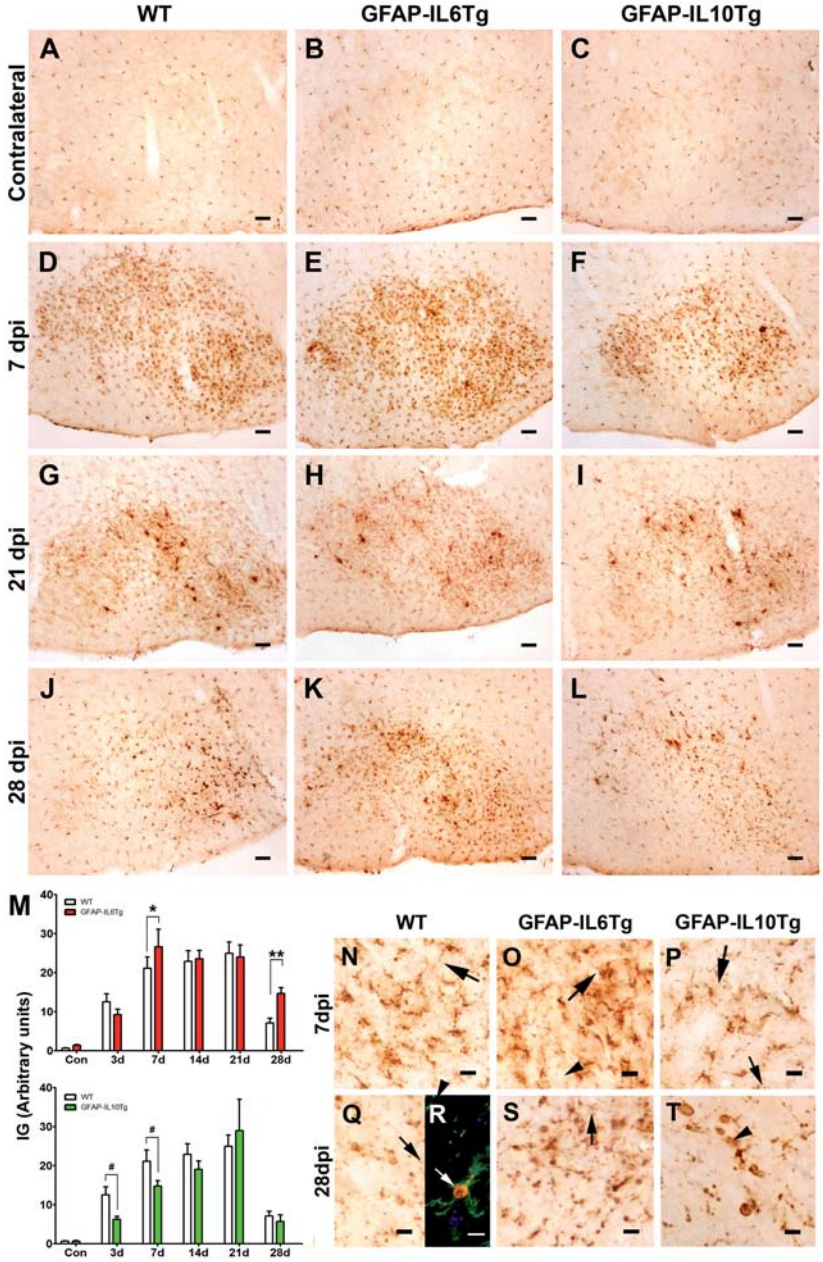

Fig. 4. CD68 staining. (A-L) Representative microphotographs corresponding to the contralateral side (Con) (A-C) and the ipsilateral FN at 7, 21 and 28 dpi (D-L) in WT, GFAP-IL6Tg and GFAP-IL10Tg mice. **(M)** Graphs showing the time course of CD68 (IG) on the ipsilateral FN of GFAP-IL6Tg (red bars) and GFAP-IL10Tg mice (green bars) compared to the WT (white bars). Note that at 7 dpi and 28 dpi CD68 is higher in GFAP-IL6Tg mice (#p≤0.09,*p≤0.05,**p≤0.01). **(N-T)** High magnification photographs showing the morphology of CD68+ cells in the ipsilateral FN at 7 and 28 dpi. At 28 dpi (Q-T), two different morphologies are noticed: ramified (black arrows) and rounded (black arrowheads) in all groups. (R) Double immunohistochemistry combining CD68 (red) with Iba1 (green) indicates that rounded CD68 staining (white arrow) is localized around the microglial nucleus. Scale bar (A-L) =10m. 50μm. Scale bar (N-T) =10μm.

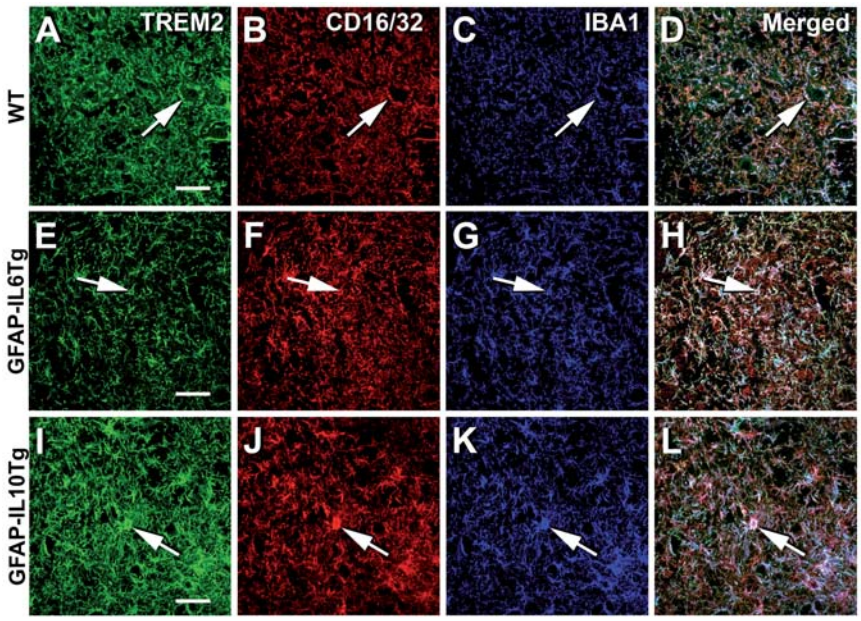

Fig. 5. TREM2+ cells expressing CD16/32. Triple immunofluorescence combining TREM2 (green), CD16/32 (red) and Iba1 (blue) in WT (A-D), GFAP-IL6Tg (E-H) and GFAP-IL10Tg (I-L) at 21 dpi. Triple colocalization can be seen in purple in merged images (D,H and L). Note that all TREM2+ cells co-express Iba1 and CD16/32 in all groups (arrows). Scale bar = 50μm.

detected in both parenchymal and clustering microglial cells, yet, the higher intensity of CD68 staining was observed within the clusters (Fig. 4G-I). No differences in CD68 staining were detected among WT, GFAP-IL6Tg and GFAP-IL10Tg mice at these time-points (Fig. 4M). When analyzed at 28 dpi, CD68 staining experienced a decrease when compared with the two previous time-points in all groups, though, this decrease was more pronounced in both WT and GFAP-IL10Tg than in GFAP-IL6Tg mice (Fig. 4J-L, M). Also in all groups, at 28 dpi, CD68 staining showed two different distributions: throughout the cytoplasm of parenchymal ramified microglial cells and forming small circular shapes (Fig. 4Q, S and T). Double immunohistochemistry with Iba1 confirmed that this circular CD68+ staining was confined around the nucleus of ramified microglial cells in all groups (Fig. 4R).

3.4 Characterization of TREM2+ cells

Due to the differences observed in the different markers of phagocytosis, we studied the co-expression of TREM2 and either CD16/32 or CD68 in Iba1+ microglial cells. In all groups of animals, TREM2 always colocalized with both Iba1 and CD16/32 (Fig. 5). However, when co-expression of TREM2 and CD68 was assessed two subpopulations of Iba1+ microglial cells appeared; one being TREM2+ and less intense for CD68 staining, and the other TREM2+ and $CD68^{high}$. Remarkably, TREM2+/$CD68^{high}$ cells were found predominantly being part of the clusters, whereas, TREM2+/$CD68^{low}$ cells appeared to be more ramified and not in close relationship with microglial clusters (Fig. 6). Those two differentiated subpopulations were observed in the three groups of animals. With the purpose to analyze the functional state of TREM2, the expression of its co-receptor DAP12 on microglial cells was studied along all time-points after FNA by using triple immunohistochemistry of TREM2, DAP12 and CD11b (Fig 7). We found that TREM2 was co-expressed along with DAP12 at all time-points and in all groups of animals analyzed. Besides, DAP12 staining was more intense in the time-points where TREM2 staining was elevated and, as observed for TREM2, it was found in both parenchymal ramified and clustering microglia.

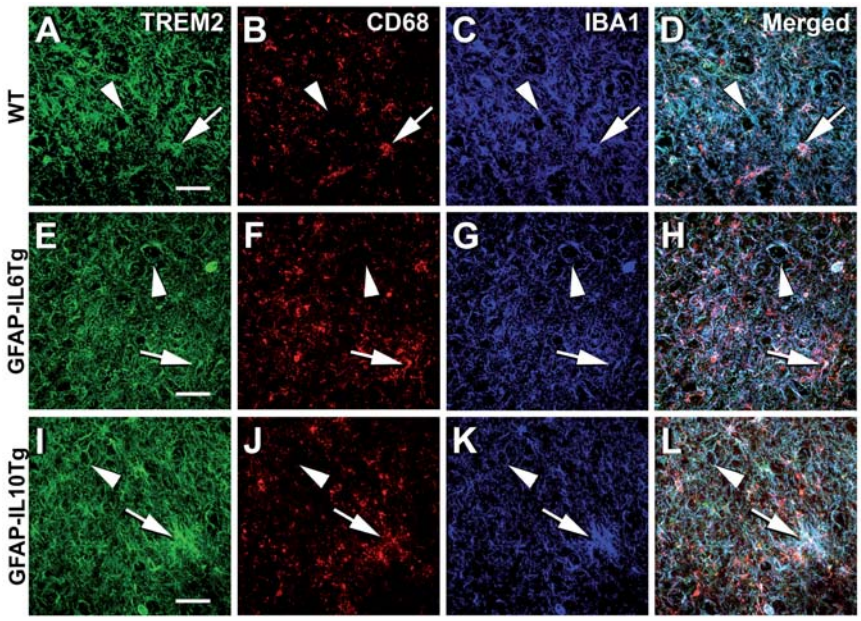

Fig. 6. TREM2+ cells expressing CD68. Triple immunofluorescence combining TREM2 (green), CD68 (red) and Iba1 (blue) in WT (A-D), GFAP-IL6Tg (E-H) and GFAP-IL10Tg (I-L) at 21 dpi. Triple colocalization can be seen in purple in merged images (D, H and L). Note that in all groups there are two subpopulations of TREM2+ cells: TREM2+/CD68^{high} cells (arrows) and TREM2+/CD68^{low} (arrowheads). Scale bar = 50μm.

4 Discussion

In this study, we demonstrated for the first time that TREM2 expression is increased in microglia after peripheral nerve injury, showing a progressive upregulation along the different time-points post-axotomy with the highest level at 21 dpi. In addition, we also demonstrated that the pattern of expression of TREM2 and other molecules related to the phagocytic capacity of microglial cells, such as CD16/32 and CD68, are influenced by the local CNS-production of IL-6 and IL-10. Transgenic production of IL-6 has a higher impact on later time-points after axotomy, making levels of the mentioned molecules to remain high; whereas the effects of transgenic production of IL-10 were more evident at early time-points, inducing lower levels of expression and a delay in the peak of CD68 and TREM2 expression.

4.1 TREM2 is involved in peripheral nerve injury

TREM2 is a receptor found in the membrane of myeloid immune cells such as macrophages, dendritic cells, osteoclasts and microglia (Colonna 2003b). Under basal conditions, TREM2 expression has been reported in microglial cells both in vitro and in vivo during development and in the adult (Chertoff et al. 2013; Schmid et al. 2002), showing a highly heterogeneous distribution across different brain regions (Schmid et al. 2002). In agreement, we observed a constitutive TREM2 expression in microglial cells of the non-lesioned FN in WT mice.

In CNS homeostatic conditions, TREM2 participate in the constant phagocytic clearance of cell debris by microglia, without triggering inflammatory responses (Neumann et al. 2009). Dysfunction of the pair TREM2/DAP12 leads to chronic neurodegenerative Nasu-Hakola disease (Kiialainen et al. 2005; Paloneva et al. 2001) and some missense TREM2 mutations increase risk of developing Alzheimers disease (Guerreiro et al. 2013; Jonsson et al. 2013). Considering the importance of TREM2 for the correct CNS function, it has been commonly linked with a neuroprotective role. Nonetheless, studies assessing the role of TREM2 after

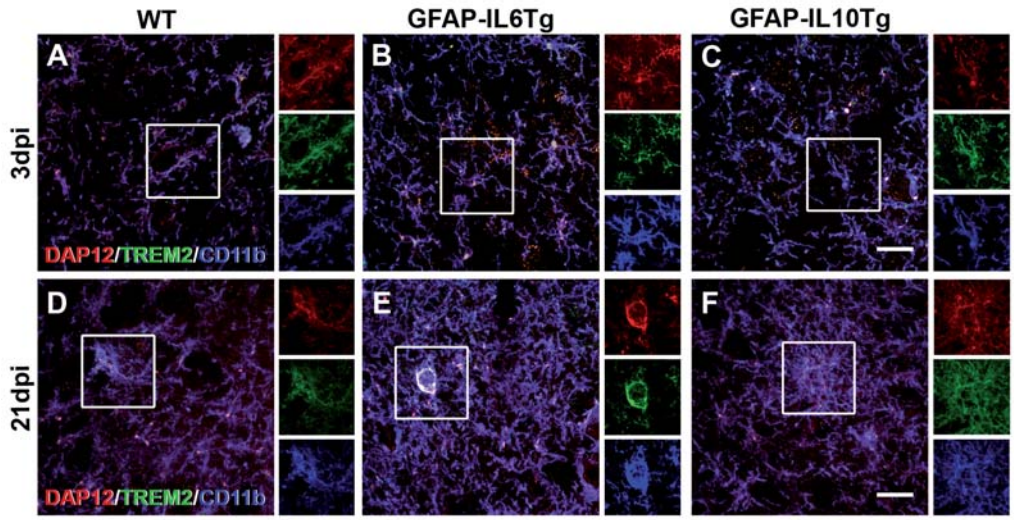

Fig. 7. Functional state of TREM2. Triple immunofluorescence combining DAP12 (red), TREM2 (green) and CD11b (blue) in WT (A and D), GFAP-IL6Tg (B and E) and GFAP-IL10Tg (C and F) mice at 3 dpi and 21 dpi. Triple colocalization can be seen in purple. Note that all TREM2+ cells co-express DAP12 and CD11b in all groups. The squares delimit the place of high magnification photographs. Scale bar = 10μm.

a variety of CNS challenges brought to light some controversy. For example, silencing microglial TREM2 exacerbated spatial cognitive deficits and tau pathology (Jiang et al. 2015). Moreover, overexpression of TREM2 rescued the symptoms (Jiang et al. 2016b) in P301S tau transgenic mice. However, the same group revealed no improvement after TREM2 overexpression in a mouse model of Alzheimers disease (Jiang et al. 2016a). Likewise, although a role in dampening inflammation is mainly assigned to TREM2 (Turnbull et al. 2006; Painter et al. 2015; Lue et al. 2015), TREM2-KO mice had attenuated inflammatory response following stroke (Sieber et al. 2013) and reduced recruited macrophages, concomitant with decreased production of inflammatory cytokines after TBI (Saber et al. 2016). However, little is known about the expression of TREM2 after peripheral nerve axotomy.

Our results clearly demonstrated that TREM2 was induced in activated microglial cells after FNA and it followed a pattern that coincides with the start, the maximum and the resolution phases of the inflammatory process triggered by axotomy. TREM2 expression starts at 3 dpi, peaks around 14-21 dpi, coinciding with the maximum number of FMN death, and decreases at 28 dpi, when surviving neurons engaged axonal regeneration and microglial activation started to decrease (Raivich et al. 1998; Moran and Graeber 2004). As FMN undergo quick changes after the mechanical transection of their axon (Aldskogius 2011; Tetzlaff et al. 2006), it could be expected that an endogenous signal in these damaged FMN triggered TREM2 increase as soon as 3 dpi. In fact, although its ligand is still undefined, TREM2 is thought by some authors as a microglial sensor (Wang et al. 2015) that interact with apoptotic neurons (Hsieh et al. 2009), probably by recognition of a wide amount of anionic lipids (Wang et al. 2015), such as phosphatidylserine, which are exposed to the membrane of damaged neurons (Ravichandran et al. 2011; Petitto et al. 2003). In our study, we found the highest level of TREM2 when peak of neuronal death occurs, and highly expressed in microglial clusters. Since these microglial formations have been proposed as places of phagocytosis of neuronal debris after FNA (Raivich et al. 1998; Moran and Graeber 2004), our findings are in agreement with the general view of TREM2 as a receptor that act as an eat-me signal during phagocytosis (Neumann et al. 2009). Supporting this theory, in this study we also report a more intense expression of CD16/32 and CD68, molecules mainly associated with a phagocytic function, in the microglial clusters at these same time-points.

Importantly, we also showed TREM2 expression in activated microglia along all time-points after peripheral nerve injury; suggesting that in addition to its role in phagocytosis, TREM2 may have another roles in microglia still not well known. In fact, some authors have proposed TREM2 as a general molecule of microglial activation (Schmid et al. 2002), playing other putative functions such as sensor of damage (Wang et al. 2015) and control of both microglial migration (Takahashi et al. 2005) and survival (Wang et al. 2015).

Even if TREM2 was expressed throughout all the time-points after FNA, its functional state might varied along the evolution of the lesion. To discard this possibility, we studied the dynamic of DAP12, an adaptor protein required to trigger TREM2-induced signaling (Bouchon et al. 2001; Lanier and Bakker 2000; Colonna 2003a; Kiialainen et al. 2005), in microglia by triple immunolabeling with TREM2 and Iba1. We demonstrated colocalization of both TREM2 and DAP12 molecules in microglial cells of the axotomized FN in all time-points analyzed, implying a functionally active TREM2 receptor along the evolution of the lesion.

4.2 Production of IL-6 and IL-10 influenced microglial phagocytic capacity and TREM2 expression after FNA

Previous results in our laboratory demonstrated that local production of IL-6 and IL-10 induced important alterations in the pattern of the microglial response associated to FNA, which correlated with modifications in the survival/death ratio of FMN: GFAP-IL6Tg mice presented higher FMN death (Almolda et al. 2014b) and GFAP-IL10Tg mice had improved FMN survival (Villacampa et al. 2015). In the present study, we clearly showed that local production of IL-6 and IL-10 affected the phagocytic capacity of microglia by changing the expression pattern of CD16/32, CD68 and TREM2. While GFAP-IL10Tg mice showed more CD16/32 from 3 to 7 dpi; GFAP-IL6Tg mice experienced a peak in CD16/32 at 14dpi, preceding the time with higher neuronal death; followed by a drop at 21 dpi. In both animals, an upturn in the expression of CD16/32 occurred at 28 dpi, when the resolution of the lesion is expected and a down-regulation of the general microglial activation markers occurs in WT animals (Almolda et al. 2014b). These results make it difficult to assign an absolute or harmful role to the expression of CD16/32 after FNA. Thus, to a better description and understanding of the phagocytic phenotype of microglia, we analyzed the expression of CD68. In GFAP-IL6Tg, we found alterations at 7 dpi and later time-points after axotomy suggesting that increased functional phagocytosis is taking place and is sustained by IL-6 over time. In contrast, the effect of transgenic production of IL-10 was more evident at early time-points, inducing lower levels of CD68 expression. A decrease in CD68 expression may be related with less presence of cellular debris expected in GFAP-IL10Tg mice since neuronal survival is promoted.

In our paradigm, we observed that, in the non-lesioned FN, TREM2 staining was similarly detected around the nucleus of microglial cells of WT, GFAP-IL6Tg and GFAP-IL10Tg. Instead, FNA induced a substantial upregulation of microglial TREM2 and DAP12 expression in all groups. As TREM2 is classically considered as an eat-me signal, our initial hypothesis was that, when compared with WT animals, the group with higher neuronal death, i.e. GFAP-IL6Tg mice would present an increase in TREM2 expression around 14-21 dpi, and the group with lower numbers of dying cells, the GFAP-IL10Tg mice, would present a decrease in the expression of this receptor. However, our results show no modifications of either TREM2 or DAP12 expression at these time-points in any of the transgenic groups.

One possibility to explain this controversy is that, as discussed before, the function of TREM2 may not be only related with the phagocytic function but rather have another roles in the microglial response (Takahashi et al. 2005; Wang et al. 2015). In fact, a role of TREM2 in promoting microglia survival makes sense (Wang et al. 2015), as GFAP-IL6Tg mice have increased TREM2 expression that correlated with higher microglial density at 28 dpi, time-point when a significant reduction in microglia numbers by programmed cell death after FNA is expected (Jones et al. 1997). In addition, considering TREM2 as microglial sensor of

danger signals in neurons (Wang et al. 2015), the lower expression at early time-points and the delay in the peak observed in GFAP-IL10Tg animals could mean that FMN presented less danger signals, as IL10 is able to maintain neuronal survival (Zhou et al. 2009; Sharma et al. 2011). In the same way, the higher and sustained levels observed in GFAP-IL6Tg at later time-points would be indicative of a worse evolution of the long-term neuronal death in these animals.

Another possibility to explain this lack of differences during the maximum peak of neuronal death, is that even though TREM2 and DAP12 are similarly expressed in transgenic animals and WT, the specific intracellular signaling triggered by this receptor in the three groups of animals may be different and lead to different outcomes after the lesion. In fact, although the mechanisms are still unclear, recent evidence suggested that, depending on the intracellular cascade triggered, TREM2 could have both activating and inhibitory roles in microglia (Hu et al. 2014). Thus, a consensus immunoreceptor tyrosine-based inhibition motifs (ITIM)sequence, leading to inhibitory signaling, seems to be embedded in the ITAM sequence of DAP12 (Barrow and Trowsdale 2006). When this ITIM sequence recruits inhibitory phosphatases, like SHIP-1, the attenuation of the activation signal of DAP12 takes place (Peng et al. 2010) and then the function of TREM2 seems to diminish (Barrow and Trowsdale 2006; Malik et al. 2015). However, no studies about the co-expression of SHIP-1 phosphatase and TREM2 receptor in activated microglia are available in the literature, making difficult to hypothesize whether this intracellular signaling will be involved in this specific paradigm and whether it will be altered under the influence of a specific anti-inflammatory or pro-inflammatory milieu.

5 Concluding remarks

In conclusion, this is the first description of TREM2 induction in microglial cells after FNA, demonstrating its presence along the evolution of the lesion, in correlation with the activation pattern of microglia, and suggesting their possible role not only in phagocytosis but also in another functions, such as sensing neuronal damage and regulating microglial survival. In addition, we showed how local production of IL-10 and IL-6 influence the phagocytic phenotype of microglia promoting changes in TREM2, CD16/32 and CD68 expression along the different time-points after FNA. Altogether, our observations indicated that TREM2 is clearly altered in activated microglial cells in both transgenic mice after FNA, leading us to postulate that pro- and anti-inflammatory microenvironments may influence the expression of this eat me signal after a peripheral nerve injury.

Acknowledgments. The authors would like to thank Miguel A. Martil and Isabella Appiah for their outstanding technical help and Núria Barba for her help on confocal microscopy. This work was supported by the Spanish Ministry of Science and Innovation (BFU2011-27400) and (BFU2014-55459-P) to BCL and NHMRC project grant 632754 to ILC.

References

1. Aldskogius H (2011) Mechanisms and consequences of microglial responses to peripheral axotomy. Frontiers in bioscience 3:857-868. doi:192
2. Almolda B, de Labra C, Barrera I, Gruart A, Delgado-Garcia JM, Villacampa N, Vilella A, Hofer MJ, Hidalgo J, Campbell IL, Gonzalez B, Castellano B (2014a) Alterations in microglial phenotype and hippocampal neuronal function in transgenic mice with astrocyte-targeted production of interleukin-10. Brain Behav Immun. doi:S0889-1591(14)00512-1
3. Almolda B, Villacampa N, Manders P, Hidalgo J, Campbell IL, Gonzalez B, Castellano B (2014) Effects of astrocyte-targeted production of interleukin-6 in the mouse on the host response to nerve injury. Glia 62 (7):1142-1161. doi:10.1002/glia.22668
4. Aloisi F (2001) Immune function of microglia. Glia 36 (2):165-179. doi:10.1002/glia.1106
5. Barrow AD, Trowsdale J (2006) You say ITAM and I say ITIM, let's call the whole thing off: the ambiguity of immunoreceptor signalling. European journal of immunology 36 (7):1646-1653. doi:10.1002/eji.200636195
6. Bianchin MM, Capella HM, Chaves DL, Steindel M, Grisard EC, Ganev GG, da Silva Junior JP, Neto Evaldo S, Poffo MA, Walz R, Carlotti Junior CG, Sakamoto AC (2004) Nasu-Hakola disease (polycystic lipomembranous osteodysplasia with sclerosing leukoencephalopathy–PLOSL): a dementia associated with bone cystic lesions. From clinical to genetic and molecular aspects. Cellular and molecular neurobiology 24 (1):1-24
7. Bisht K, Sharma KP, Lecours C, Gabriela Sanchez M, El Hajj H, Milior G, Olmos-Alonso A, Gomez-Nicola D, Luheshi G, Vallieres L, Branchi I, Maggi L, Limatola C, Butovsky O, Tremblay ME (2016) Dark microglia: A new phenotype predominantly associated with pathological states. Glia. doi:10.1002/glia.22966
8. Bouchon A, Hernandez-Munain C, Cella M, Colonna M (2001) A DAP12-mediated pathway regulates expression of CC chemokine receptor 7 and maturation of human dendritic cells. J Exp Med 194 (8):1111-1122
9. Cady J, Koval ED, Benitez BA, Zaidman C, Jockel-Balsarotti J, Allred P, Baloh RH, Ravits J, Simpson E, Appel SH, Pestronk A, Goate AM, Miller TM, Cruchaga C, Harms MB (2014) TREM2 variant p.R47H as a risk factor for sporadic amyotrophic lateral sclerosis. JAMA neurology 71 (4):449-453. doi:10.1001/jamaneurol.2013.6237
10. Campbell IL, Abraham CR, Masliah E, Kemper P, Inglis JD, Oldstone MB, Mucke L (1993) Neurologic disease induced in transgenic mice by cerebral overexpression of interleukin 6. Proc Natl Acad Sci U S A 90 (21):10061-10065
11. Cantoni C, Bollman B, Licastro D, Xie M, Mikesell R, Schmidt R, Yuede CM, Galimberti D, Olivecrona G, Klein RS, Cross AH, Otero K, Piccio L (2015) TREM2 regulates microglial cell activation in response to demyelination in vivo. Acta neuropathologica 129 (3):429-447. doi:10.1007/s00401-015-1388-1
12. Chertoff M, Shrivastava K, Gonzalez B, Acarin L, Gimenez-Llort L (2013) Differential modulation of TREM2 protein during postnatal brain development in mice. PloS one 8 (8):e72083. doi:10.1371/journal.pone.0072083
13. Colonna M (2003a) DAP12 signaling: from immune cells to bone modeling and brain myelination. The Journal of clinical investigation 111 (3):313-314. doi:10.1172/JCI17745
14. Colonna M (2003b) TREMs in the immune system and beyond. Nature reviews Immunology 3 (6):445-453. doi:10.1038/nri1106
15. Davalos D, Grutzendler J, Yang G, Kim JV, Zuo Y, Jung S, Littman DR, Dustin ML, Gan WB (2005) ATP mediates rapid microglial response to local brain injury in vivo. Nat Neurosci 8 (6):752-758. doi:nn1472 10.1038/nn1472
16. Goodridge HS, Underhill DM, Touret N (2012) Mechanisms of Fc receptor and dectin-1 activation for phagocytosis. Traffic 13 (8):1062-1071. doi:10.1111/j.1600-0854.2012.01382.x
17. Guerreiro R, Wojtas A, Bras J, Carrasquillo M, Rogaeva E, Majounie E, Cruchaga C, Sassi C, Kauwe JS, Younkin S, Hazrati L, Collinge J, Pocock J, Lashley T, Williams J, Lambert JC, Amouyel P, Goate A, Rademakers R, Morgan K, Powell J, St George-Hyslop P, Singleton A, Hardy J, Alzheimer Genetic Analysis G (2013) TREM2 variants in Alzheimer's disease. N Engl J Med 368 (2):117-127. doi:10.1056/NEJMoa1211851
18. Holness CL, Simmons DL (1993) Molecular cloning of CD68, a human macrophage marker related to lysosomal glycoproteins. Blood 81 (6):1607-1613
19. Hsieh CL, Koike M, Spusta SC, Niemi EC, Yenari M, Nakamura MC, Seaman WE (2009) A role for TREM2 ligands in the phagocytosis of apoptotic neuronal cells by microglia. Journal of neurochemistry 109 (4):1144-1156. doi:10.1111/j.1471-4159.2009.06042.x

20. Hu N, Tan MS, Yu JT, Sun L, Tan L, Wang YL, Jiang T, Tan L (2014) Increased expression of TREM2 in peripheral blood of Alzheimer's disease patients. Journal of Alzheimer's disease : JAD 38 (3):497-501. doi:10.3233/JAD-130854
21. Jiang T, Tan L, Zhu XC, Zhou JS, Cao L, Tan MS, Wang HF, Chen Q, Zhang YD, Yu JT (2015) Silencing of TREM2 exacerbates tau pathology, neurodegenerative changes, and spatial learning deficits in P301S tau transgenic mice. Neurobiol Aging 36 (12):3176-3186. doi:10.1016/j.neurobiolaging.2015.08.019
22. Jiang T, Wan Y, Zhang YD, Zhou JS, Gao Q, Zhu XC, Shi JQ, Lu H, Tan L, Yu JT (2016a) TREM2 Overexpression has No Improvement on Neuropathology and Cognitive Impairment in Aging APPswe/PS1dE9 Mice. Mol Neurobiol. doi:10.1007/s12035-016-9704-x
23. Jiang T, Yu JT, Zhu XC, Tan L (2013) TREM2 in Alzheimer's disease. Molecular neurobiology 48 (1):180-185. doi:10.1007/s12035-013-8424-8
24. Jiang T, Zhang YD, Chen Q, Gao Q, Zhu XC, Zhou JS, Shi JQ, Lu H, Tan L, Yu JT (2016b) TREM2 modifies microglial phenotype and provides neuroprotection in P301S tau transgenic mice. Neuropharmacology 105:196-206. doi:10.1016/j.neuropharm.2016.01.028
25. Jones LL, Banati RB, Graeber MB, Bonfanti L, Raivich G, Kreutzberg GW (1997) Population control of microglia: does apoptosis play a role? Journal of neurocytology 26 (11):755-770
26. Jonsson T, Stefansson H, Steinberg S, Jonsdottir I, Jonsson PV, Snaedal J, Bjornsson S, Huttenlocher J, Levey AI, Lah JJ, Rujescu D, Hampel H, Giegling I, Andreassen OA, Engedal K, Ulstein I, Djurovic S, Ibrahim-Verbaas C, Hofman A, Ikram MA, van Duijn CM, Thorsteinsdottir U, Kong A, Stefansson K (2013) Variant of TREM2 associated with the risk of Alzheimer's disease. N Engl J Med 368 (2):107-116. doi:10.1056/NEJMoa1211103
27. Kawabori M, Hokari M, Zheng Z, Kim JY, Calosing C, Hsieh CL, Nakamura MC, Yenari MA (2013) Triggering Receptor Expressed on Myeloid Cells-2 Correlates to Hypothermic Neuroprotection in Ischemic Stroke. Therapeutic hypothermia and temperature management 3 (4):189-198. doi:10.1089/ther.2013.0020
28. Kawabori M, Kacimi R, Kauppinen T, Calosing C, Kim JY, Hsieh CL, Nakamura MC, Yenari MA (2015) Triggering receptor expressed on myeloid cells 2 (TREM2) deficiency attenuates phagocytic activities of microglia and exacerbates ischemic damage in experimental stroke. The Journal of neuroscience : the official journal of the Society for Neuroscience 35 (8):3384-3396. doi:10.1523/JNEUROSCI.2620-14.2015
29. Kettenmann H, Hanisch UK, Noda M, Verkhratsky A (2011) Physiology of microglia. Physiol Rev 91 (2):461-553. doi:91/2/461 10.1152/physrev.00011.2010
30. Kettenmann H, Kirchhoff F, Verkhratsky A (2013) Microglia: new roles for the synaptic stripper. Neuron 77 (1):10-18. doi:S0896-6273(12)01162-2
31. Kierdorf K, Prinz M (2013) Factors regulating microglia activation. Front Cell Neurosci 7:44. doi:10.3389/fncel.2013.00044
32. Kiialainen A, Hovanes K, Paloneva J, Kopra O, Peltonen L (2005) Dap12 and Trem2, molecules involved in innate immunity and neurodegeneration, are co-expressed in the CNS. Neurobiology of disease 18 (2):314-322. doi:10.1016/j.nbd.2004.09.007
33. Kim SU, de Vellis J (2005) Microglia in health and disease. J Neurosci Res 81 (3):302-313. doi:10.1002/jnr.20562
34. Kleinberger G, Yamanishi Y, Suarez-Calvet M, Czirr E, Lohmann E, Cuyvers E, Struyfs H, Pettkus N, Wenninger-Weinzierl A, Mazaheri F, Tahirovic S, Lleo A, Alcolea D, Fortea J, Willem M, Lammich S, Molinuevo JL, Sanchez-Valle R, Antonell A, Ramirez A, Heneka MT, Sleegers K, van der Zee J, Martin JJ, Engelborghs S, Demirtas-Tatlidede A, Zetterberg H, Van Broeckhoven C, Gurvit H, Wyss-Coray T, Hardy J, Colonna M, Haass C (2014) TREM2 mutations implicated in neurodegeneration impair cell surface transport and phagocytosis. Science translational medicine 6 (243):243ra286. doi:10.1126/scitranslmed.3009093
35. Lanier LL, Bakker AB (2000) The ITAM-bearing transmembrane adaptor DAP12 in lymphoid and myeloid cell function. Immunology today 21 (12):611-614
36. Linnartz B, Neumann H (2013) Microglial activatory (immunoreceptor tyrosine-based activation motif)- and inhibitory (immunoreceptor tyrosine-based inhibition motif)-signaling receptors for recognition of the neuronal glycocalyx. Glia 61 (1):37-46. doi:10.1002/glia.22359
37. Lisi S, Sisto M, Lofrumento DD, D'Amore S, D'Amore M (2011) Advances in the understanding of the Fc gamma receptors-mediated autoantibodies uptake. Clinical and experimental medicine 11 (1):1-10. doi:10.1007/s10238-010-0098-1
38. Lue LF, Schmitz C, Walker DG (2015) What happens to microglial TREM2 in Alzheimer's disease: Immunoregulatory turned into immunopathogenic? Neuroscience 302:138-150. doi:10.1016/j.neuroscience.2014.09.050

39. Malik M, Parikh I, Vasquez JB, Smith C, Tai L, Bu G, LaDu MJ, Fardo DW, Rebeck GW, Estus S (2015) Genetics ignite focus on microglial inflammation in Alzheimer's disease. Molecular neurodegeneration 10:52. doi:10.1186/s13024-015-0048-1
40. Moller JC, Klein MA, Haas S, Jones LL, Kreutzberg GW, Raivich G (1996) Regulation of thrombospondin in the regenerating mouse facial motor nucleus. Glia 17 (2):121-132. doi:10.1002/(SICI)1098-1136(199606)
41. Moran LB, Graeber MB (2004) The facial nerve axotomy model. Brain Res Brain Res Rev 44 (2-3):154-178. doi:10.1016/j.brainresrev.2003.11.004
42. Nakajima K, Kohsaka S (2004) Microglia: neuroprotective and neurotrophic cells in the central nervous system. Curr Drug Targets Cardiovasc Haematol Disord 4 (1):65-84
43. Napoli I, Neumann H (2009) Microglial clearance function in health and disease. Neuroscience 158 (3):1030-1038. doi:S0306-4522(08)00972-X
44. Neumann H, Kotter MR, Franklin RJ (2009) Debris clearance by microglia: an essential link between degeneration and regeneration. Brain : a journal of neurology 132 (Pt 2):288-295. doi:awn109
45. Neumann H, Takahashi K (2007) Essential role of the microglial triggering receptor expressed on myeloid cells-2 (TREM2) for central nervous tissue immune homeostasis. Journal of neuroimmunology 184 (1-2):92-99. doi:10.1016/j.jneuroim.2006.11.032
46. Nimmerjahn A, Kirchhoff F, Helmchen F (2005) Resting microglial cells are highly dynamic surveillants of brain parenchyma in vivo. Science 308 (5726):1314-1318. doi:1110647
47. Nimmerjahn F, Ravetch JV (2010) Antibody-mediated modulation of immune responses. Immunological reviews 236:265-275. doi:10.1111/j.1600-065X.2010.00910.x
48. Okun E, Mattson MP, Arumugam TV (2010) Involvement of Fc receptors in disorders of the central nervous system. Neuromolecular medicine 12 (2):164-178. doi:10.1007/s12017-009-8099-5
49. Painter MM, Atagi Y, Liu CC, Rademakers R, Xu H, Fryer JD, Bu G (2015) TREM2 in CNS homeostasis and neurodegenerative disease. Molecular neurodegeneration 10:43. doi:10.1186/s13024-015-0040-9
50. Paloneva J, Autti T, Raininko R, Partanen J, Salonen O, Puranen M, Hakola P, Haltia M (2001) CNS manifestations of Nasu-Hakola disease: a frontal dementia with bone cysts. Neurology 56 (11):1552-1558
51. Peng Q, Malhotra S, Torchia JA, Kerr WG, Coggeshall KM, Humphrey MB (2010) TREM2- and DAP12-dependent activation of PI3K requires DAP10 and is inhibited by SHIP1. Science signaling 3 (122):ra38. doi:10.1126/scisignal.2000500
52. Petitto JM, Huang Z, Lo J, Streit WJ (2003) IL-2 gene knockout affects T lymphocyte trafficking and the microglial response to regenerating facial motor neurons. J Neuroimmunol 134 (1-2):95-103. doi:S0165572802004228
53. Piccio L, Buonsanti C, Cella M, Tassi I, Schmidt RE, Fenoglio C, Rinker J, 2nd, Naismith RT, Panina-Bordignon P, Passini N, Galimberti D, Scarpini E, Colonna M, Cross AH (2008) Identification of soluble TREM-2 in the cerebrospinal fluid and its association with multiple sclerosis and CNS inflammation. Brain : a journal of neurology 131 (Pt 11):3081-3091. doi:10.1093/brain/awn217
54. Piccio L, Buonsanti C, Mariani M, Cella M, Gilfillan S, Cross AH, Colonna M, Panina-Bordignon P (2007) Blockade of TREM-2 exacerbates experimental autoimmune encephalomyelitis. European journal of immunology 37 (5):1290-1301. doi:10.1002/eji.200636837
55. Polazzi E, Monti B (2010) Microglia and neuroprotection: from in vitro studies to therapeutic applications. Prog Neurobiol 92 (3):293-315. doi:S0301-0082(10)00130-9
56. Poliani PL, Wang Y, Fontana E, Robinette ML, Yamanishi Y, Gilfillan S, Colonna M (2015) TREM2 sustains microglial expansion during aging and response to demyelination. The Journal of clinical investigation 125 (5):2161-2170. doi:10.1172/JCI77983
57. Raivich G, Jones LL, Kloss CU, Werner A, Neumann H, Kreutzberg GW (1998) Immune surveillance in the injured nervous system: T-lymphocytes invade the axotomized mouse facial motor nucleus and aggregate around sites of neuronal degeneration. The Journal of neuroscience : the official journal of the Society for Neuroscience 18 (15):5804-5816
58. Ravichandran V, Major EO, Ibe C, Monaco MC, Girisetty MK, Hewlett IK (2011) Susceptibility of human primary neuronal cells to xenotropic murine leukemia virus-related (XMRV) virus infection. Virology journal 8:443. doi:10.1186/1743-422X-8-443
59. Rohn TT (2013) The triggering receptor expressed on myeloid cells 2: "TREM-ming" the inflammatory component associated with Alzheimer's disease. Oxidative medicine and cellular longevity 2013:860959. doi:10.1155/2013/860959

60. Saber M, Kokiko-Cochran ON, Puntambekar S, Lathia J, Lamb BT (2016) TREM2 deficiency alters acute macrophage distribution and improves recovery after TBI. J Neurotrauma. doi:10.1089/neu.2016.4401
61. Schmid CD, Sautkulis LN, Danielson PE, Cooper J, Hasel KW, Hilbush BS, Sutcliffe JG, Carson MJ (2002) Heterogeneous expression of the triggering receptor expressed on myeloid cells-2 on adult murine microglia. Journal of neurochemistry 83 (6):1309-1320
62. Sessa G, Podini P, Mariani M, Meroni A, Spreafico R, Sinigaglia F, Colonna M, Panina P, Meldolesi J (2004) Distribution and signaling of TREM2/DAP12, the receptor system mutated in human polycystic lipomembraneous osteodysplasia with sclerosing leukoencephalopathy dementia. The European journal of neuroscience 20 (10):2617-2628. doi:10.1111/j.1460-9568.2004.03729.x
63. Sharma S, Yang B, Xi X, Grotta JC, Aronowski J, Savitz SI (2011) IL-10 directly protects cortical neurons by activating PI-3 kinase and STAT-3 pathways. Brain Res 1373:189-194. doi:S0006-8993(10)02609-0
64. Sieber MW, Jaenisch N, Brehm M, Guenther M, Linnartz-Gerlach B, Neumann H, Witte OW, Frahm C (2013) Attenuated inflammatory response in triggering receptor expressed on myeloid cells 2 (TREM2) knock-out mice following stroke. PloS one 8 (1):e52982. doi:10.1371/journal.pone.0052982
65. Suzumura A (2013) Neuron-microglia interaction in neuroinflammation. Curr Protein Pept Sci 14 (1):16-20.
66. Takahashi K, Prinz M, Stagi M, Chechneva O, Neumann H (2007) TREM2-transduced myeloid precursors mediate nervous tissue debris clearance and facilitate recovery in an animal model of multiple sclerosis. PLoS medicine 4 (4):e124. doi:10.1371/journal.pmed.0040124
67. Takahashi K, Rochford CD, Neumann H (2005) Clearance of apoptotic neurons without inflammation by microglial triggering receptor expressed on myeloid cells-2. The Journal of experimental medicine 201 (4):647-657. doi:10.1084/jem.20041611
68. Takai T (2005) Fc receptors and their role in immune regulation and autoimmunity. Journal of clinical immunology 25 (1):1-18. doi:10.1007/s10875-005-0353-8
69. Tetzlaff JE, Huppenbauer CB, Tanzer L, Alexander TD, Jones KJ (2006) Motoneuron injury and repair: New perspectives on gonadal steroids as neurotherapeutics. Journal of molecular neuroscience : MN 28 (1):53-64. doi:10.1385/JMN:30:3:341
70. Thelen M, Razquin C, Hernandez I, Gorostidi A, Sanchez-Valle R, Ortega-Cubero S, Wolfsgruber S, Drichel D, Fliessbach K, Duenkel T, Damian M, Heilmann S, Slotosch A, Lennarz M, Seijo-Martinez M, Rene R, Kornhuber J, Peters O, Luckhaus C, Jahn H, Hull M, Ruther E, Wiltfang J, Lorenzo E, Gascon J, Lleo A, Llado A, Campdelacreu J, Moreno F, Ahmadzadehfar H, Dementia Genetics Spanish C, Fortea J, Indakoetxea B, Heneka MT, Wetter A, Pastor MA, Riverol M, Becker T, Frolich L, Tarraga L, Boada M, Wagner M, Jessen F, Maier W, Clarimon J, Lopez de Munain A, Ruiz A, Pastor P, Ramirez A (2014) Investigation of the role of rare TREM2 variants in frontotemporal dementia subtypes. Neurobiology of aging 35 (11):2657 e2613-2659. doi:10.1016/j.neurobiolaging.2014.06.018
71. Thrash JC, Torbett BE, Carson MJ (2009) Developmental regulation of TREM2 and DAP12 expression in the murine CNS: implications for Nasu-Hakola disease. Neurochemical research 34 (1):38-45. doi:10.1007/s11064-008-9657-1
72. Travaglione S, Falzano L, Fabbri A, Stringaro A, Fais S, Fiorentini C (2002) Epithelial cells and expression of the phagocytic marker CD68: scavenging of apoptotic bodies following Rho activation. Toxicology in vitro : an international journal published in association with BIBRA 16 (4):405-411
73. Tremblay ME (2011) The role of microglia at synapses in the healthy CNS: novel insights from recent imaging studies. Neuron glia biology 7 (1):67-76. doi:10.1017/S1740925X12000038
74. Tremblay ME, Majewska AK (2011) A role for microglia in synaptic plasticity? Communicative and integrative biology 4 (2):220-222. doi:10.4161/cib.4.2.14506
75. Turnbull IR, Gilfillan S, Cella M, Aoshi T, Miller M, Piccio L, Hernandez M, Colonna M (2006) Cutting edge: TREM-2 attenuates macrophage activation. J Immunol 177 (6):3520-3524
76. Ulland TK, Wang Y, Colonna M (2016) Regulation of microglial survival and proliferation in health and diseases. Seminars in immunology. doi:10.1016/j.smim.2016.03.011
77. Ulvestad E, Williams K, Matre R, Nyland H, Olivier A, Antel J (1994) Fc receptors for IgG on cultured human microglia mediate cytotoxicity and phagocytosis of antibody-coated targets. Journal of neuropathology and experimental neurology 53 (1):27-36
78. Villacampa N, Almolda B, Vilella A, Campbell IL, Gonzalez B, Castellano B (2015) Astrocyte-targeted production of IL-10 induces changes in microglial reactivity and reduces motor neuron death after facial nerve axotomy. Glia 63 (7):1166-1184. doi:10.1002/glia.22807

79. Wake H, Moorhouse AJ, Jinno S, Kohsaka S, Nabekura J (2009) Resting microglia directly monitor the functional state of synapses in vivo and determine the fate of ischemic terminals. The Journal of neuroscience : the official journal of the Society for Neuroscience 29 (13):3974-3980. doi:29/13/3974
80. Wang Y, Cella M, Mallinson K, Ulrich JD, Young KL, Robinette ML, Gilfillan S, Krishnan GM, Sudhakar S, Zinselmeyer BH, Holtzman DM, Cirrito JR, Colonna M (2015) TREM2 lipid sensing sustains the microglial response in an Alzheimer's disease model. Cell 160 (6):1061-1071. doi:10.1016/j.cell.2015.01.049
81. Zhou Z, Peng X, Insolera R, Fink DJ, Mata M (2009) IL-10 promotes neuronal survival following spinal cord injury. Exp Neurol 220 (1):183-190. doi:S0014-4886(09)00357-4
82. Zhu C, Herrmann US, Li B, Abakumova I, Moos R, Schwarz P, Rushing EJ, Colonna M, Aguzzi A (2015) Triggering receptor expressed on myeloid cells-2 is involved in prion-induced microglial activation but does not contribute to prion pathogenesis in mouse brains. Neurobiology of aging 36 (5):1994-2003. doi:10.1016/j.neurobiolaging.2015.02.019

ANNEX II. Supplementary figures

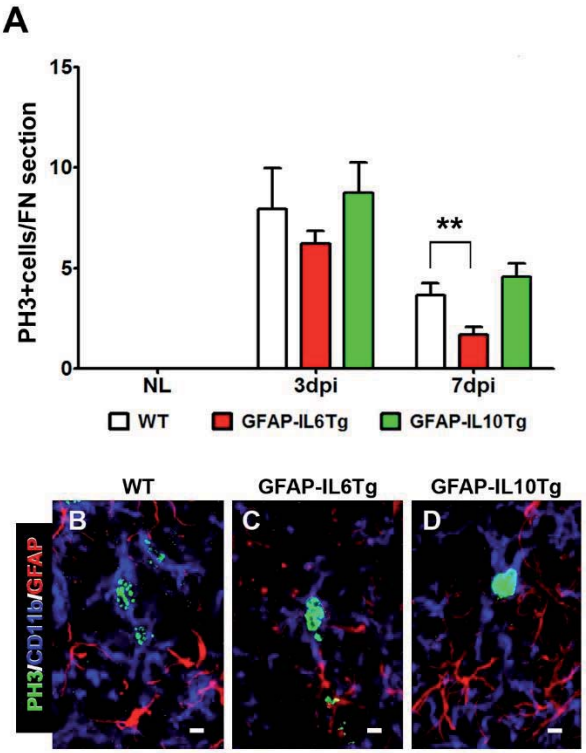

Supplementary Figure 1. Microglial cell proliferation after FNA. (A) Graph showing the quantification of phosphohistone 3 (PH3)+ cells per FN section in the non-lesioned (NL) and at 3 and 7 dpi in WT (white bars), GFAP-IL6Tg (red bars) and GFAP-IL10Tg (green bars). Note that GFAP-IL6Tg mice showed a significant reduction in the number of PH3+ cells at 7 dpi. (**p<0.005; ***p<0.001). **(B-D)** Triple immunohistochemistry combining PH3 (green), CD11b (blue) and GFAP (red) in WT (B), GFAP-IL6Tg (C) and GFAP-IL10Tg animals (D). Note that PH3 staining was found exclusively in the nucleus of microglia in all three experimental groups. Scale bar= 5 μm. For methodologic details, please see Annex 8.III.

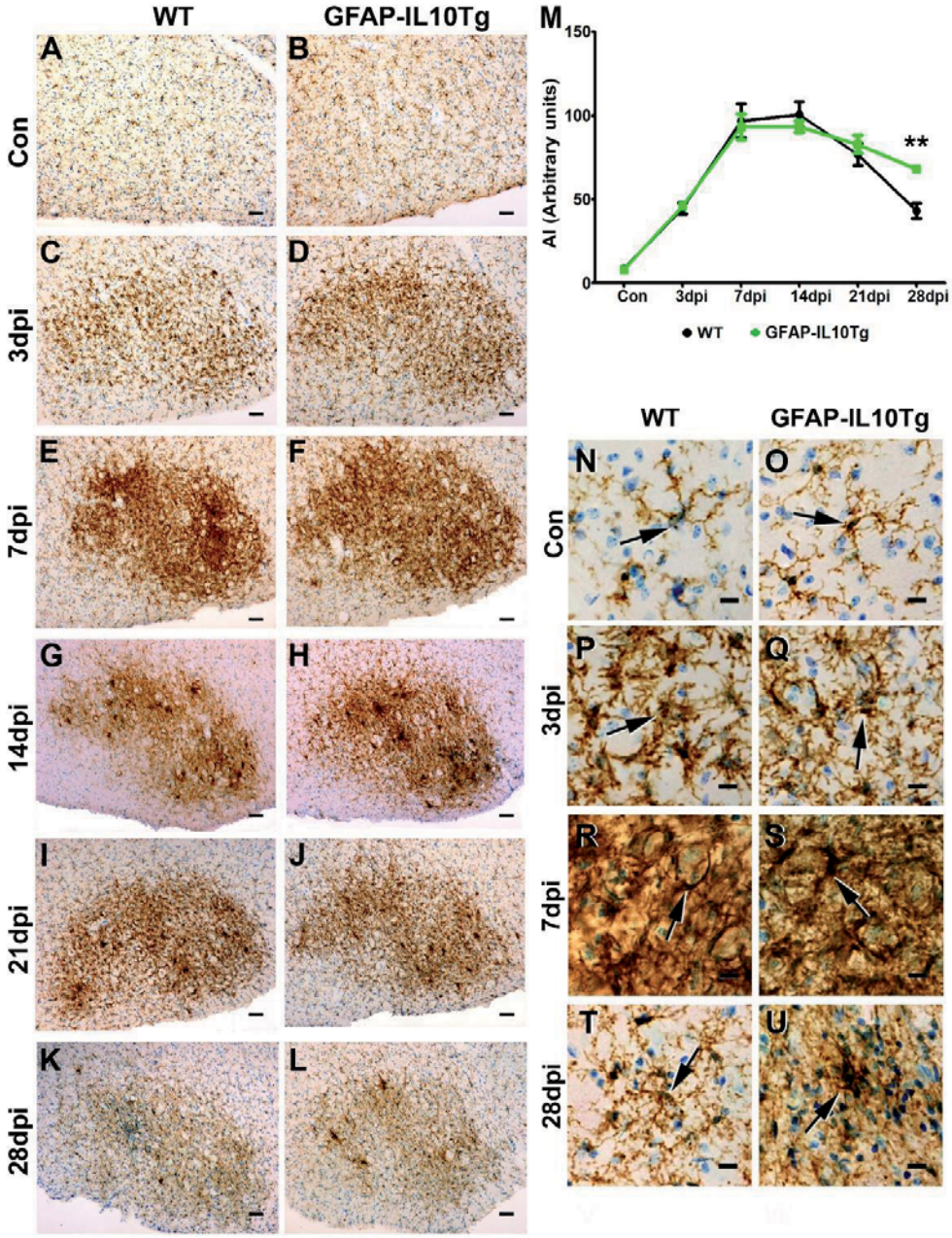

Supplementary Figure 2. CD11b expression In GFAP-IL10Tg mice. (A-L) Representative images showing the expression of CD11b in the contralateral (Con; A and B) and the ipsilateral sides of both WT (C, E, G, I and K) and GFAP-IL10Tg animals (D, F, H, J and L) at the different survival times analyzed. **M)** Histogram showing the AI index (% Area covered by the immunolabeling x Mean grey value mean) of CD11b staining in WT and GFAP-IL10Tg animals along the evolution of FNA. Note that at 28 dpi the AI index is higher in GFAP-IL10Tg animals (**p< 0.005). **(N-U)** High magnification images in the contralateral (N and O) and the ipsilateral side of axotomized animals (P-U) showing the morphology and spatial location of CD11b+ cells: ramified microglial-like cells in the non-lesioned FN (arrows in N and O) and activated cells at 3 dpi (arrows in P and Q), 7 dpi (arrows in R and S) and 28 dpi (arrows in T and U). Scale bar (A-L) = 50 μm; (N-U) = 10 μm.

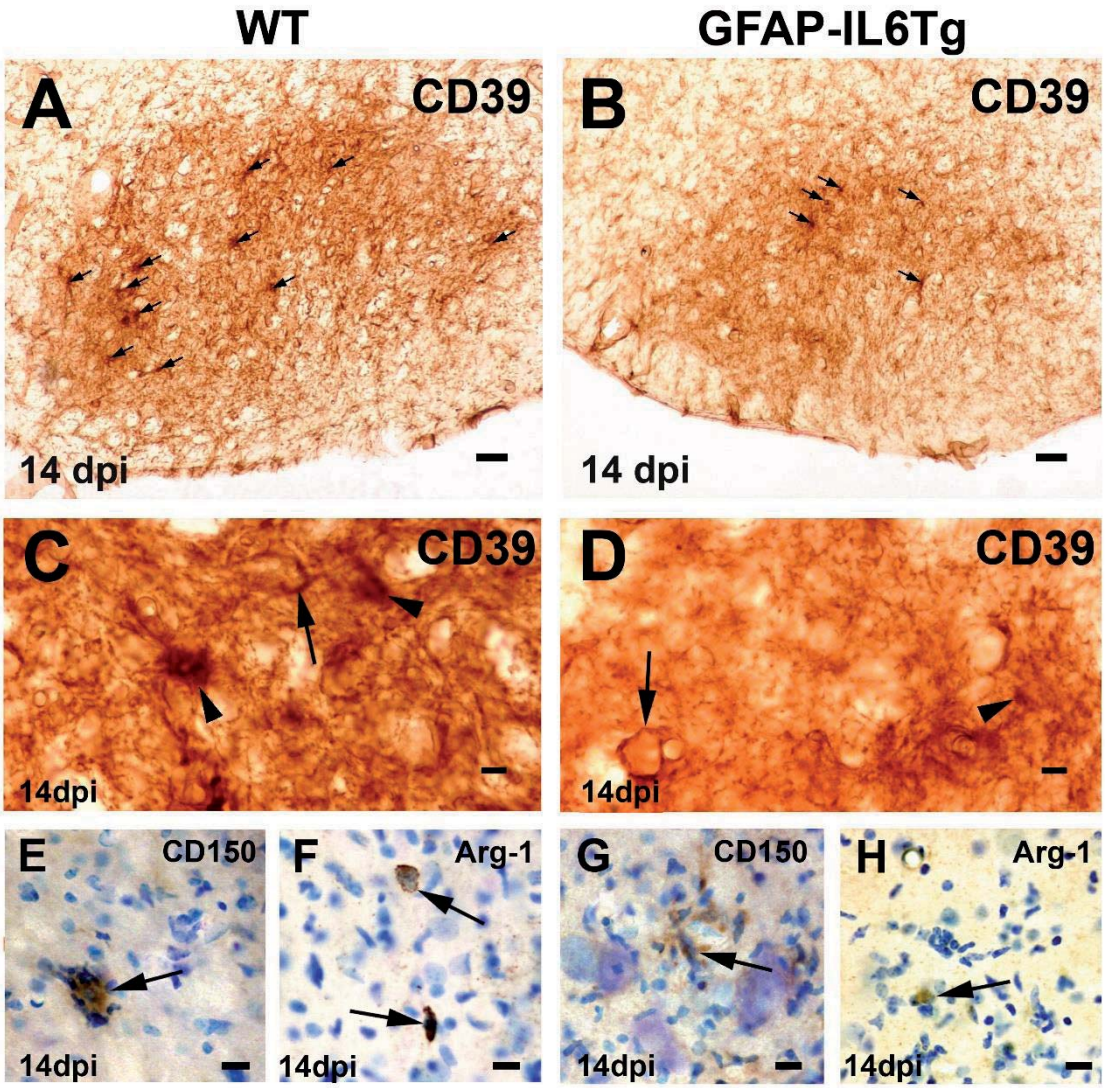

Supplementary Figure 3. Expression of alternative activation markers in GFAP-IL6Tg mice. (A and B) Representative microphotographs corresponding to the ipsilateral side of the FN stained with CD39 in WT (A) and GFAP-IL6Tg mice (B) at 14 dpi. Note that GFAP-IL6Tg mice had less density of CD39+ clusters (arrows). **(C and D)** High magnification photographs showing CD39 staining in microglial clusters (arrowheads) and in elongated microglial cells wrapping FMN (arrows) at 14 dpi in both WT and GFAP-IL6Tg mice. **(E and G)** High magnification photographs showing CD150 staining in relation to microglial clusters (arrows) at 14 dpi in both WT (E) and GFAP-IL6Tg (G). **(F and H)** High magnification photographs showing Arginase-1 (Arg-1) + cells (arrows) at 14 dpi in both WT (F) and GFAP-IL6Tg (H). Scale bar (A-B)= 50μm; (C-H)=10μm.

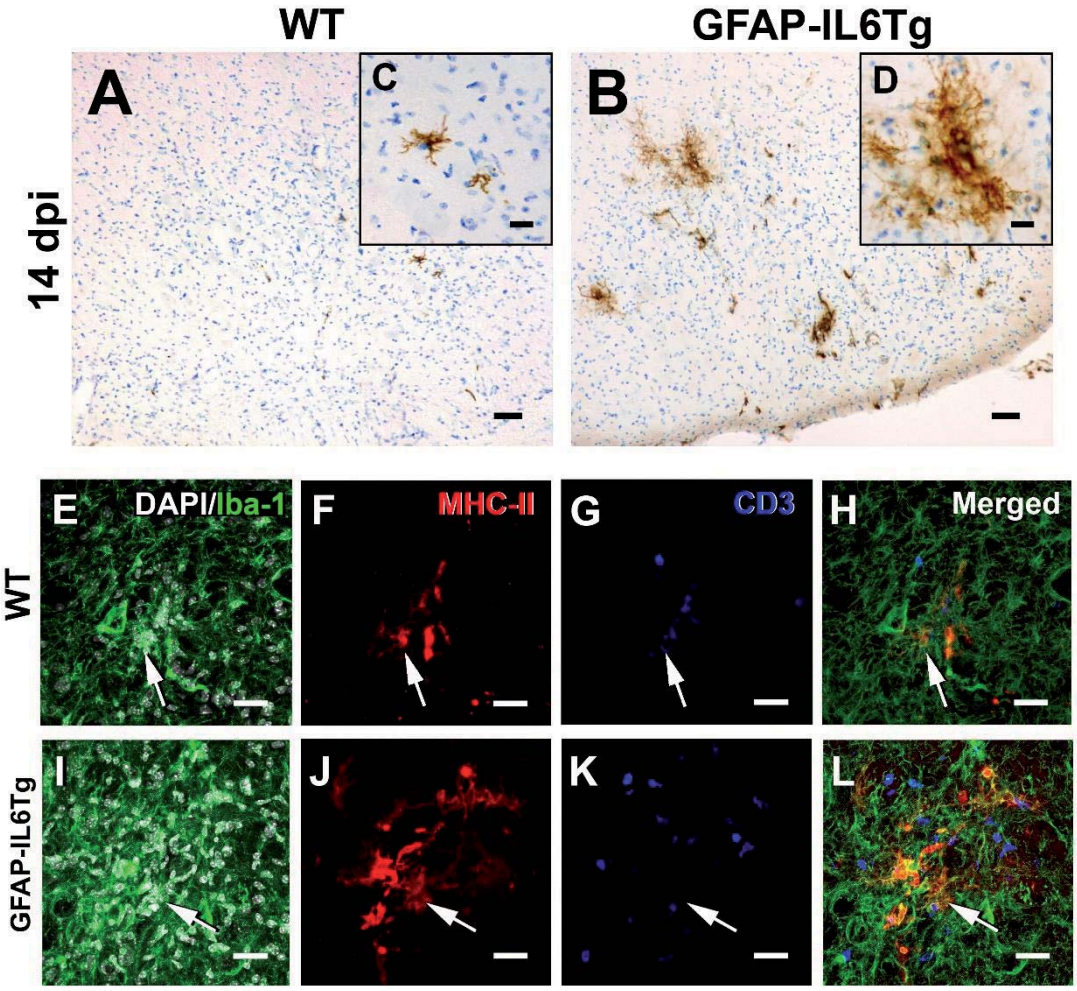

Supplementary Figure 4. MHC-II expression in GFAP-IL6Tg mice. (A and B) Representative microphotographs corresponding to the ipsilateral side of the FN in WT and GFAP-IL6Tg mice at 14 dpi. (C and D) High magnification photographs showing the characteristic ramified morphology of MHC-II+ cells found in WT and GFAP-IL6Tg mice. **(E-L)** Triple immunohistochemistry combining Iba1 (green), MHC-II (red) and CD3 (blue). Cell nuclei were stained with DAPI (white). Merged images (H and L) showed colocalization of MHC-II and Iba-1. Arrows point to an Iba1+ microglial cluster in WT (E-H) and GFAP-IL6Tg mice (I-J) containing MHC-II+ cells (F and J). Note that CD3+ cells are close to the microglial cluster (G and K). Scale bar (A and B)= 50μm; (Squares in A and B)= 10μm; (C-J)= 25μm.

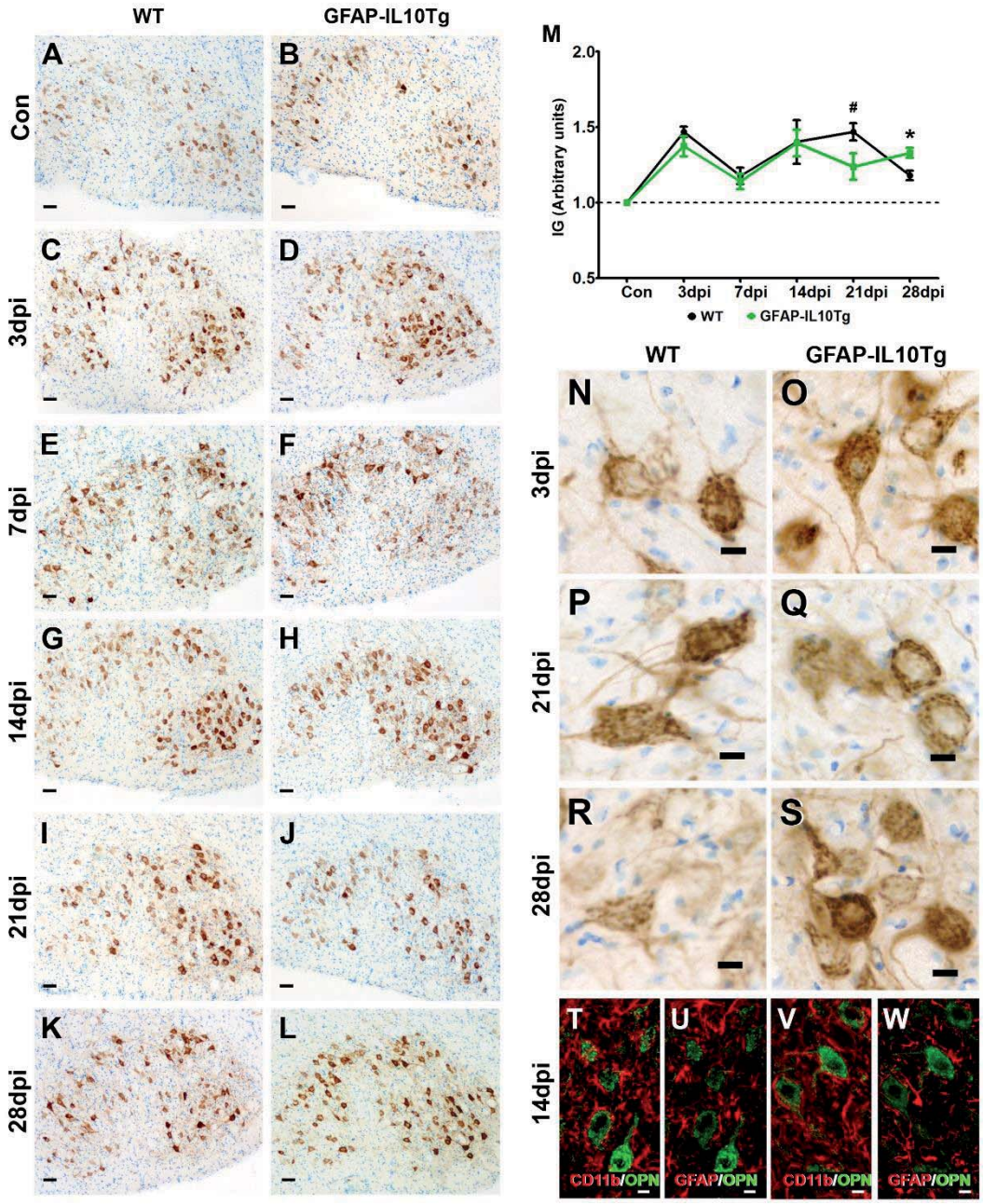

Supplementary Figure 5. Osteopontin expression in GFAP-IL10Tg animals. (A-L) Representative microphotographs showing the expression of osteopontin (OPN) in the contralateral (Con; A and B) and the ipsilateral sides of FN in both WT (C, E, G, I and K) and GFAP-IL10Tg animals (D, F, H, J and L) at the different survival times after FNA. **(M)** Graph showing the time course of OPN intensity grade (IG) on the ipsilateral FN of WT and GFAP-IL10Tg animals in comparison to their corresponding contralateral. Note that, in GFAP-IL10Tg mice, the OPN IG is significantly lower at 21 dpi but higher at 28 dpi than WT (#p< 0.08; *p<0.05). **(N-S)** High-magnification images showing the morphology and distribution of OPN+ cells in the ipsilateral side of axotomized animals at 3 dpi (N and O), 21 dpi (P and Q) and 28dpi (R and S). OPN staining is observed in association with cytoplasm of FMN and neuronal projections. **(T-W)** Double immunofluorescence showed no co-localization between OPN (green) and either CD11b (red in T and V) or GFAP (red in U and W) in neither WT (T and U) nor GFAP-IL10Tg animals (V and W). Scale bar (A-L) = 50 µm; (N-W) = 10 µm.

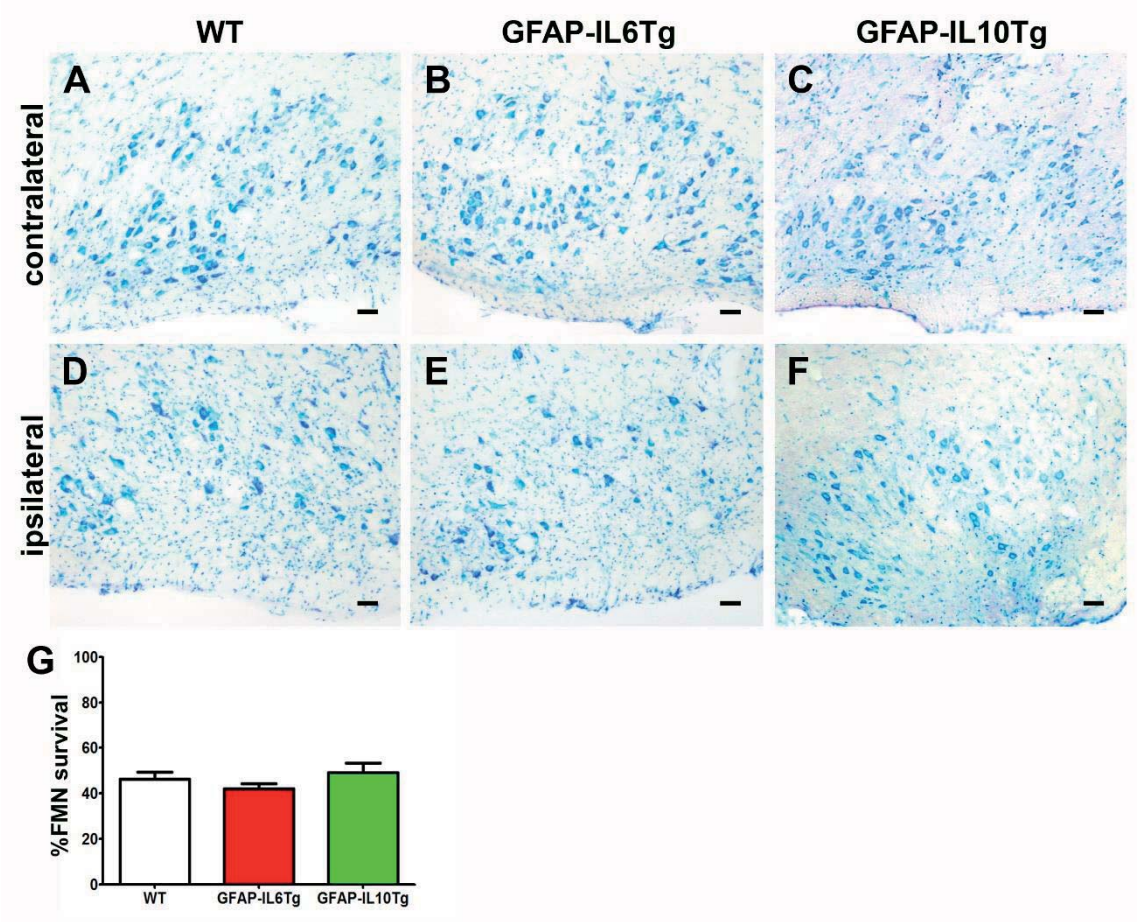

Supplementary Figure 6. Long-term neuronal survival. (A-F) Representative microphotographs of Toluidine blue staining showing the center of the contralateral (A-C) and the ipsilateral sides (D-F) of the FN of WT (A and D), GFAP-IL6Tg (B and E) and GFAP-IL10Tg mice (C and F) at 42 dpi. Note the important reduction in the number of FMN at 42 dpi in the ipsilateral side of all groups of animals. **(G)** Graph showing the percentage of FMN survival at 42 dpi. Note that long-term neuronal survival after FNA is similar in WT (white bar, 46,26%), GFAP-IL6Tg (red bar, 42,11%) and GFAP-IL10Tg mice (green bar, 48,98%). Scale bar= 50µm.

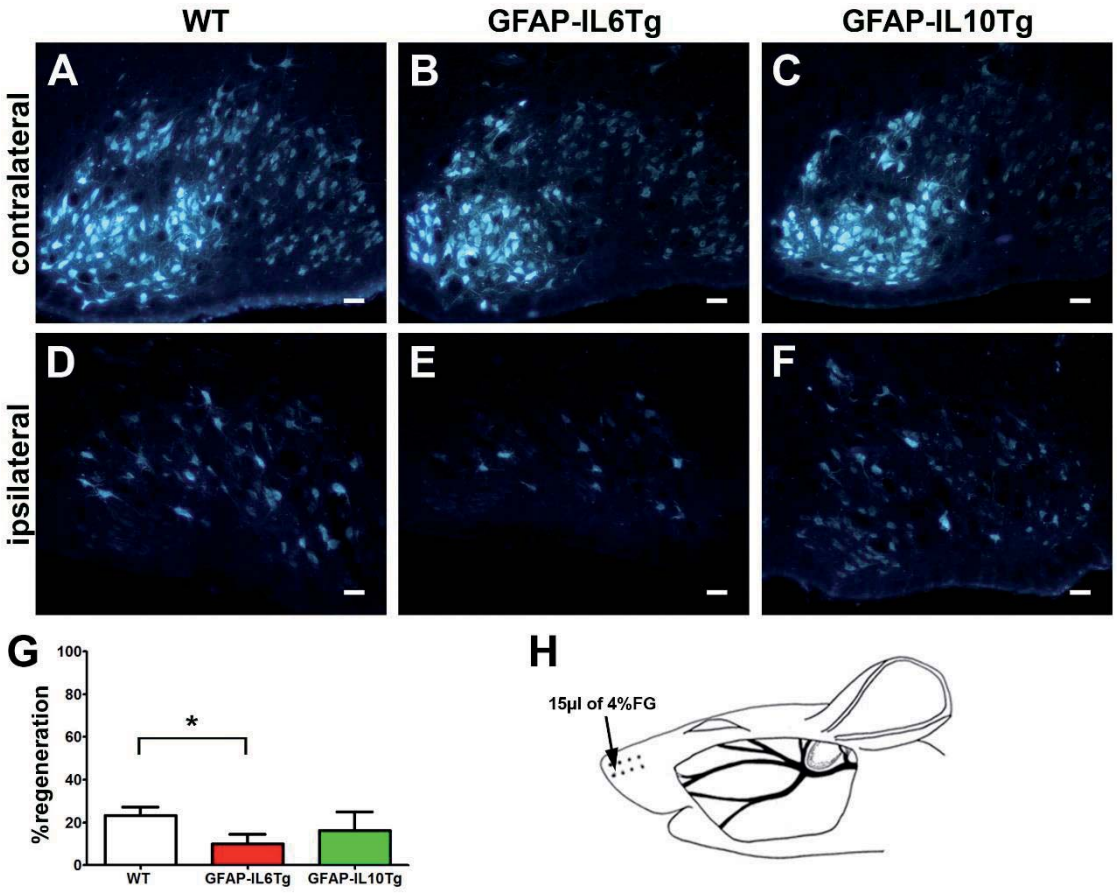

Supplementary Figure 7. Nerve regeneration. (A-F) Representative microphotographs showing Fluorogold (FG)+ FMN in the contralateral (A-C) and the ipsilateral sides (D-F) of the FN of WT (A and D), GFAP-IL6Tg (B and E) and GFAP-IL10Tg mice (C and F) at 42 dpi. Note the substantial reduction in the number of FG+ FMN in the ipsilateral side of the FN in the three experimental groups. **(G)** Graph showing the percentage of regenerating FMN at 42 dpi. Nerve regeneration was similar between WT (white bar, 23,22%) and GFAP-IL10Tg (green bar, 16,20%) but notably lower in GFAP-IL6Tg mice (redbar, 9,93%). (*p<0.05). Scale bar= 50µm. **(H)** Schematic representation showing the main branches of the facial nerve and the injection site of the retrograde fluorescent marker Fluorogold® (FG). For methodologic details, please see Annex 8.III.

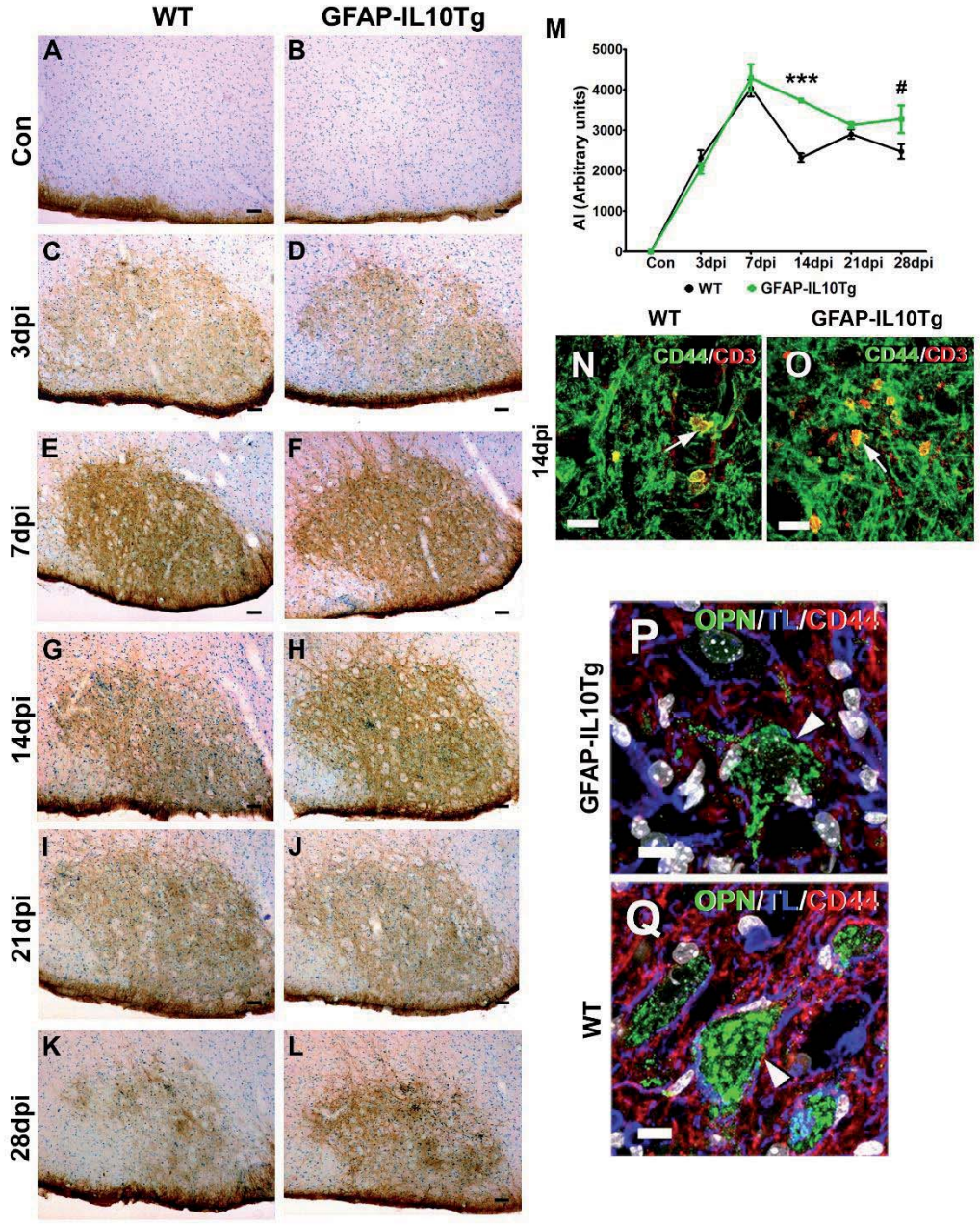

Supplementary Figure 8. CD44 expression in GFAP-IL10Tg animals. (A-L) Representative images showing the expression of CD44 in the contralateral (Con; A and B) and the ipsilateral sides of FN in both WT (C, E, G, I and K) and GFAP-IL10Tg animals (D, F, H, J and L) at the different survival times after FNA. **(M)** Graph showing the time course of AI index for CD44 on the ipsilateral FN of WT and GFAP-IL10Tg animals in comparison to their corresponding contralateral. Note that at 14 and 28 dpi the AI index is significantly higher in GFAP-IL10Tg animals than in WT (***p< 0.0001; #p<0.06) **(N-Q)** Double and triple immunofluorescence combining CD44 with CD3 (N and O), and with OPN and tomato lectin (TL) (P and Q), demonstrate co-localization of CD44 with CD3+ lymphocytes (arrows in N and O), but not with either OPN or TL in both WT (N and P) and GFAP-IL10Tg animals (O and Q). Note that the number of CD3+ cells co-expressing CD44 are more abundant in GFAP-IL10Tg mice. Also, some CD44+ processes are found surrounding neuronal OPN and covered by TL+ ramifications in both WT and GFAP-IL10Tg animals (arrowheads in P and Q). Scale bar (A-L) = 50 µm; (N-Q) = 10 µm.

Annex III. Supplementary Methodology

Phosphohistone-3 triple immunohistochemistry

For the characterization of cells expressing phosphohistone-3 (PH3) triple-immunolabellings combining PH3, CD11b and GFAP were performed. Briefly, free-floating sections were washed with 1% TBS Triton X-100 and incubated in the appropriate blocking solution at RT for 1h followed by overnight incubation at 4°C and 1h at RT with the specific primary antibody combinations: rabbit anti-PH3 (1:300; 06-570; Millipore), rat anti-CD11b (1:1000; MCA74GA; AbD Serotec) and mouse anti-GFAP (1:6000; 63893, Sigma). After several washes with 1% TBS Triton X-100, sections in each combination were incubated for 1h at RT with the corresponding secondary antibodies: Alexa Fluor® 488 conjugated anti-rabbit (1:1000; A21206; Molecular Probes), Alexa Fluor® 647 conjugated anti-rat (1:1000; A21247; Molecular Probes) and Alexa Fluor® 488-conjugated anti-mouse secondary antibody(1:1000; A31570; Molecular Probes). Before being coverslipped with Fluorescence Mounting Medium (S-3023; Dako), triple labeled sections were nuclei stained with 4′,6-diamidino-2-phenylindole (DAPI; 1:10000; D9542; Sigma Aldrich). Colocalization was analyzed with a Zeiss LSM 700 confocal microscope.

Retrograde fiber tracing

Thirty-five days after facial nerve axotomy, a set of animals were anaesthetized as described (Villacampa et al 2015) and injected with Fluoro-Gold (FG) (39286; Sigma-Aldrich), a retrograde fluorescent tracer. A total of 15µl of a 4% FG solution dissolved in distilled water was injected between the first and the second row of vibrissae using a 100µl Hamilton syringe. The FG injection was applied in both unoperated (contralateral) and axotomized (ipsilateral) side. A week after the injection, animals were deeply anaesthetized with a solution of xylazine (20mg/kg) and ketamine (80mg/kg) injected intraperitoneally (0.015ml/g) and perfused intracardially with 4% paraformaldehyde in 0.1 M phosphate buffer (pH 7.4). Brains were removed and post-fixed in the same fixative for 4h at 4°C and, after rinsing in phosphate buffer, cryopreserved for 48h in a 30% sucrose solution and frozen with 2-methylbutane solution (Sigma-Aldrich). Consecutive coronal sections (30-µm-thick) of the brainstem containing the facial nucleus (FN) were obtained using a CM3050s Leica cryostat and collected on gelatin-coated slides. The contralateral and the ipsilateral side of every section through the facial nucleus (30-40 sections) were examined and photographed using a DXM1200 Nikon digital camera joined to a Nikon Eclipse E600 microscope using a filter for FG (excitation: 330-380 nm, long pass filter: 420 nm). All somata of FG positive facial motoneurons (FMN) were counted using Image J software (National Institutes of Health, USA).

Annex IV. Participation in scientific meetings

In national meetings

Villacampa, N.; Almolda, B.; Hofer, M.; Campbell, IL.; González, B.; Castellano, B.
Effects of astrocytic-targeted IL-10 overexpression on neuronal survival and nerve regeneration after facial nerve axotomy
V Meeting Spanish Glial Net (RGE)
Málaga, Spain. December, 2010.
PARTICIPATION: ORAL

Villacampa, N.; Almolda, B.; Campbell, IL.; González, B.; Castellano, B.
Changes in microglial activation correlate with increased neuronal survival and lymphocyte infiltration after facial nerve axotomy in astrocyte-targeted IL-10 transgenic mice
IV Scientific Symposia Integrative Neurbiology
Barcelona, Spain. April, 2014.
PARTICIPATION: ORAL

In international meetings

Villacampa, N.; Almolda, B.; Hofer, M.; Campbell, IL.; González, B.; Castellano, B.
Effects of astrocytes-targeted IL-10 overexpression on microgial activation and long-term survival after facial nerve axotomy
COST Meeting Action BM603 Inflammation in Brain Disease
Dublin, Ireland. June, 2011
PARTICIPATION: POSTER

Villacampa, N.; Almolda, B.; Hofer, M.; Campbell, IL.; González, B.; Castellano, B.
Astrocyte-targeted IL-10 production increases the expression of MHC-II after facial nerve axotomy
X European Meeting on Glial Cell Function in Health and Disease.
Prague, Czech Republic. September, 2011
PARTICIPATION: POSTER

Almolda, B.; Villacampa, N.; Manders, P.; Hidalgo, J.; Campbell, IL.; González, B. and Castellano, B.
Effects of astrocyte-targeted IL-6 production in the paradigm of facial nerve axotomy
X European Meeting on Glial Cell Function in Health and Disease.
Prague, Czech Republic. September, 2011
PARTICIPATION: POSTER

Villacampa, N.; Almolda, B.; Hofer, M.; Campbell, IL.; González, B. and Castellano, B.
Decrease in Osteopontin expression correlates with reduction in neuronal degeneration after facial nerve axotomy in astrocyte targeted-IL10 transgenic mice
Symposium Frontiers of Glial Research, a satellite event of the FENS forum
Barcelona, Spain, July 2012
PARTICIPATION: POSTER

Villacampa, N.; Almolda, B.; Hofer, M.; Campbell, IL.; González, B. and Castellano, B.
Astrocyte-targeted IL-10 production has a beneficial effect on short-term neuronal survival after facial nerve axotomy.
11th International Society of Neuroimmunology, Boston, US, November 2012
PARTICIPATION: POSTER

Villacampa, N.; Almolda, B.; Hofer, M.; Hidalgo, J.; Campbell, IL.; González, B. and Castellano, B.
Effects of CNS-targeted IL-6 or IL10 production on Microglial Activation and Motor Neuron Degeneration After Facial Nerve Axotomy

3rd Venusberg Meeting on Neuroinflammation
Bonn, Germany, February 2013
PARTICIPATION: POSTER

Villacampa, N.; Almolda, B.; Hofer, M.; Hidalgo, J.; Campbell, IL.; González, B. and Castellano, B.
Effects of CNS-targeted IL-6 or IL10 production on Microglial Activation and Motor Neuron Degeneration After Facial Nerve Axotomy
ISN Satellite: Understanding Glial Cells Functions in the Normal and Injured CNS
Mérida, México, April 2013
PARTICIPATION: ORAL

Villacampa, N.; Almolda, B.; Hofer, M.; Hidalgo, J.; Campbell, IL.; González, B. and Castellano, B.
Effects of CNS-targeted IL-6 or IL10 production on Microglial Activation and Motor Neuron Degeneration After Facial Nerve Axotomy
ISN-ASN Biannual Meeting
Cancún, México, April 2013
PARTICIPATION: POSTER

Villacampa, N.; Almolda, B.; Hofer, M.; Hidalgo, J.; Campbell, IL.; González, B. and Castellano, B.
Effects of CNS-targeted IL-6 or IL10 production on Microglial Activation and Motor Neuron Degeneration After Facial Nerve Axotomy
XI European Meeting on Glial Cell Function in Health and Disease
Berlin, Germany, July 2013
PARTICIPATION: POSTER

Villacampa, N.; Almolda, B.; Vilella A.; Campbell, IL.; González, B. and Castellano, B.
Changes in microglial activation correlate with increased neuronal survival and lymphocyte infiltration after facial nerve axotomy in astrocyte-targeted IL-10 transgenic mice
2014 Conference on Glial Biology in Medicine, UAB
Birmingham, Alabama, US, October 2014
PARTICIPATION: POSTER

Villacampa, N.; Almolda, B.; Vilella A.; Campbell, IL.; González, B. and Castellano, B.
Astrocyte-targeted production of IL-10 induces changes in microglial reactivity and reduces motor neuron death after facial nerve axotomy
Cytokines Downunder 2014
Melbourne, VIC, Australia, October 2014
PARTICIPATION: POSTER

Villacampa, N.; Almolda, B.; Campbell, IL.; González, B. and Castellano, B.
CNS-targeted IL-6 production leads to higher recruitment of pro-inflammatory T-helper cells after facial nerve axotomy
12th International Society of NeuroImmunology Meeting
Mainz, Germany, November 2014
PARTICIPATION: ORAL

Villacampa, N.; Almolda, B.; Campbell, IL.; González, B. and Castellano, B.
Differential Expression of TREM2 in Transgenic Mice with CNS-targeted IL-6 or IL-10 production Correlates with Opposing effects on Neurodegeneration after Facial Nerve Axotomy
XII European Meeting on Glial Cell Function in Health and Disease
Bilbao, Spain, July 2015
PARTICIPATION: POSTER